Gondwana Research 80 (2020) 202–227

Contents lists available at ScienceDirect

Gondwana Research

journal homepage: www.elsevier.com/locate/gr

GR Focus Review

Lithospheric evolution of the Pre- and Early Andean convergent margin, Chile

Verónica Oliveros [a,*], Paulina Vásquez [b], Christian Creixell [b], Friedrich Lucassen [c], Mihai N. Ducea [d,e], Isabella Ciocca [a], Javiera González [a], Mauricio Espinoza [a], Esteban Salazar [b], Felipe Coloma [b], Simone A. Kasemann [c]

[a] Departamento Ciencias de la Tierra, Universidad de Concepción, Casilla 160-C, Concepción, Chile
[b] Servicio Nacional de Geología y Minería, Av. Santa María 104, Santiago, Chile
[c] Faculty of Geosciences and MARUM-Center for Marine Environmental Sciences, University of Bremen, Leobener Strasse, 28359 Bremen, Germany
[d] Department of Geosciences, University of Arizona, Tucson, AZ 85721, USA
[e] Faculty of Geology and Geophysics, University of Bucharest, 010041 Bucharest, Romania

ARTICLE INFO

Article history:
Received 29 March 2019
Received in revised form 20 November 2019
Accepted 30 November 2019
Available online 10 December 2019

Editor: M. Santosh

ABSTRACT

The proto-Andean and Early Andean evolution of the southwestern Gondwana margin comprises three stages that differ in their magmatic evolution and deformational style: the Gondwana cycle (~330–280 Ma), the Pre-Andean stage (~280–210 Ma) and the Early Andean Cycle (210–100 Ma). These stages have been traditionally interpreted as the upper crustal response to changes in the tectonic setting which include: Cordilleran-style continental arc (Gondwana cycle), orogenic collapse and possibly slab break-off that led to continental rifting and extensive crustal melting (Pre-Andean stage), and subsequent subduction re-initiation in oceanic arc-style context (Early Andean cycle).

The petrological and geochemical characteristics of Carboniferous to Jurassic igneous rocks from this region however do not support the described model. Elemental and Sr-Nd-Pb isotopic data of 86 samples, along with a compilation of ~1230 samples from the literature suggest that subduction was the most likely process by which the magmatic record was generated. Sub-alkaline affinities, LILE enrichment over HFSE, Nb—Ta troughs, porphyritic textures and hornblende- and biotite-bearing lithologies are present in all studied units, whereas isotopes suggest that magma sources are a mixture of depleted mantle and variable contribution from the continental crust. Even though the aforementioned features are common to all igneous rocks, some changes point to a decline in the contribution of crustal/lithospheric sources to the magmatism with time. Thus, SiO_2, La_N/Yb_N and $^{87}Sr/^{86}Sr_{initial}$ exhibit a systematic decrease from ~285 to 150 Ma, whereas the $\varepsilon Nd_{initial}$ parameter increases in the same period.

These changes were accompanied by the shift from dominant compressional (Carboniferous-Early Permian) to transtentional (Middle Permian-Jurassic) stresses in the upper crust, suggesting that the margin went from advancing to retreating due to Pangea reorganization and break-up. Following a potential flat slab event, slab roll-back may have induced extension in the upper crust and lithospheric loss as a consequence of delamination or thermal erosion.

Contents

* Corresponding author.
E-mail address: voliveros@udec.cl (V. Oliveros).

https://doi.org/10.1016/j.gr.2019.11.002
1342-937X/

1. Introduction

The continental margin of southwestern South America has been periodically active since the Early Paleozoic, as early as the Cambrian (Escayola et al., 2007), but certainly since the Early Carboniferous (e.g. Bahlburg et al., 2009; Charrier et al., 2007, 2014; Mpodozis and Ramos, 1989; Willner et al., 2008). Two orogenic cycles, the Early Carboniferous-Early Permian Gondwana cycle and the Jurassic to recent Andean cycle, both separated by the Pre-Andean stage, from the Middle Permian to Late Triassic (Charrier et al., 2007) have been widely proposed in the southern central Andes of north and central Chile between the Pacific coast and the border region to Argentina (e.g. Coira et al., 1982; Ruiz et al., 1965; Vicente, 1975). Published research indicates that both cycles differ mostly in their magmatic products and tectonic regime. While the Gondwanan cycle involves, beside the mantle source, relevant amounts of crustal additions to arc magmatism in a compressive tectonic setting (e.g. Hervé et al., 2014; Lucassen et al., 1999; Mpodozis and Ramos, 1989), the Andean Cycle is dominated by mantle additions to magmatism (Lucassen et al., 2006; Oliveros et al., 2007; Rossel et al., 2013) in a variable tectonic setting, from dominantly extensional/transtensional in the Jurassic-early Cretaceous, to compressive and transpressive since the Late Cretaceous (Arriagada et al., 2006; Charrier et al., 2014; Pichowiak et al., 1990; Scheuber et al., 1994). In this region, as often is the case with subduction-related magmatic arcs elsewhere in the geologic archive, the main set of tools used for identifying past tectonics environments comes primarily from the geochemistry of magmatic rocks themselves.

This study focuses on the tectonic and magmatic evolution associated to the period in between the two orogenic cycles, from Middle Permian to Late Triassic times, which is still a subject of debate. The time span of this stage is bracketed in between the initial phases of the Choiyoi magmatism, at ~285 Ma (Sato et al., 2015), and the beginning of the Andean subduction at the Triassic-Jurassic boundary (Charrier et al., 2007). The classic interpretation of the Choiyoi magmatism and its tectonic setting includes orogenic collapse that triggered extensive crustal anatexis followed by continental rifting, possibly slab break-off and the termination of subduction (Kleiman and Japas, 2009; Mpodozis and Ramos, 1989), a model that has also been proposed for northern Chile and Perú (Mišković and Schaltegger, 2009; Mpodozis and Kay, 1992). However, many recent studies have highlighted the lack of geochemical and petrological signatures of such tectonic configuration in the Permian and Triassic geological record (e.g. Coloma et al., 2017; Del Rey et al., 2016, 2019; Espinoza et al., 2019; González et al., 2018; Rocher et al., 2015). In addition to that, there is no tectono-magmatic model that accounts for the geodynamics mechanisms by which the subduction would have resumed along the margin in the Early Jurassic, perhaps due to the fact that the lithological units of this time span do not correspond to what would be expected for a subduction initiation setting (e.g. forearc ophiolites with chemical evolution from tholeiitic basalt to high-Mg andesites and boninites, Stern et al., 2012; Whattam and Stern, 2011). Thus, whereas the processes of Early Andean subduction are fairly well understood (Lucassen et al., 2006; Oliveros et al., 2007; Pichowiak et al., 1990), the inferred onset of this subduction process is much less clear. On the other hand, recent global reconstructions of plate motion back to the Devonian, suggest that Southwestern Gondwana would have been a convergent margin from the Carboniferous to the Jurassic, and would have maintained this character after supercontinent break-up (Müller et al., 2016; Riel et al., 2018; Young et al., 2019). A reappraisal of the classic model for the Late Paleozoic-Early Mesozoic evolution of the margin seems thus necessary at this point.

The modern forearc region of north-central Chile (22°-30°S) preserves the geological record from three stages mentioned above (Gondwana cycle, Pre-Andean stage and Andean cycle) (Fig. 1). Remarkably large volumes of volcanic, plutonic and sedimentary rocks of Carboniferous to Early Cretaceous ages are exceptionally well exposed due to prevalent arid to semiarid climatic conditions. Consequently, this area is suitable for a large temporal scale study of the magmatic evolution of the continental margin, in order to get a more detailed image of the tectonic regime associated to the transition between the Gondwana and Andean cycles.

In this work, we present newly acquired elemental and Sr-Nd-Pb isotopic data for volcanic and plutonic rocks of mainly Triassic age cropping out in northern Chile between 25° and 30° S, along with a comprehensive compilation of stratigraphic data and structural relationship of the geological units of this period. The geochemical data are contrasted to a database of ~1050 geological samples from igneous units of Carboniferous to Jurassic age, cropping out between 18° and 40°S in Chile and western Argentina (Fig. 1), in order to unravel the tectonic evolution of the continental lithosphere during this time span.

2. Geological setting

The Andean region in northern Chile, between 22° and 30°S features three important morphostructural units where Paleozoic and Mesozoic units crop out: the Coastal Cordillera, Frontal Cordillera (27°30′ - 30°'00′ S) and Domeyko Cordillera (22°00′ – 27°30′S) (Figs. 2,3). In the Frontal Cordillera, large portions of crystalline Paleozoic to Triassic rocks, mostly fragments of magmatic arcs, are exposed. Their current exposure was controlled by a thick-skinned deformation style which occurred in response to crustal shortening during the Eocene and Miocene compressional events (Cembrano et al., 2002; Fosdick et al., 2015; Lossada et al., 2017) (Fig. 2). The cover of these crystalline rocks consists mostly of Triassic to Late Jurassic inverted backarc basins (Oliveros et al., 2012), Neogene, arc-related, volcanic sequences (Bissig et al., 2003; Kay and Mpodozis, 2001) and sedimentary filling of foreland basins in the Argentinian side (Fosdick et al., 2015).

2.1. Gondwana cycle (Late Carboniferous to ~285 Ma)

The representative units of this orogenic cycle between 22° and 30°S are distributed along two parallel N-S oriented belts: 1) voluminous plutonic complexes with minor metamorphic and volcanic rocks in the Frontal and Domeyko Cordilleras to the east, 2) and metamorphic

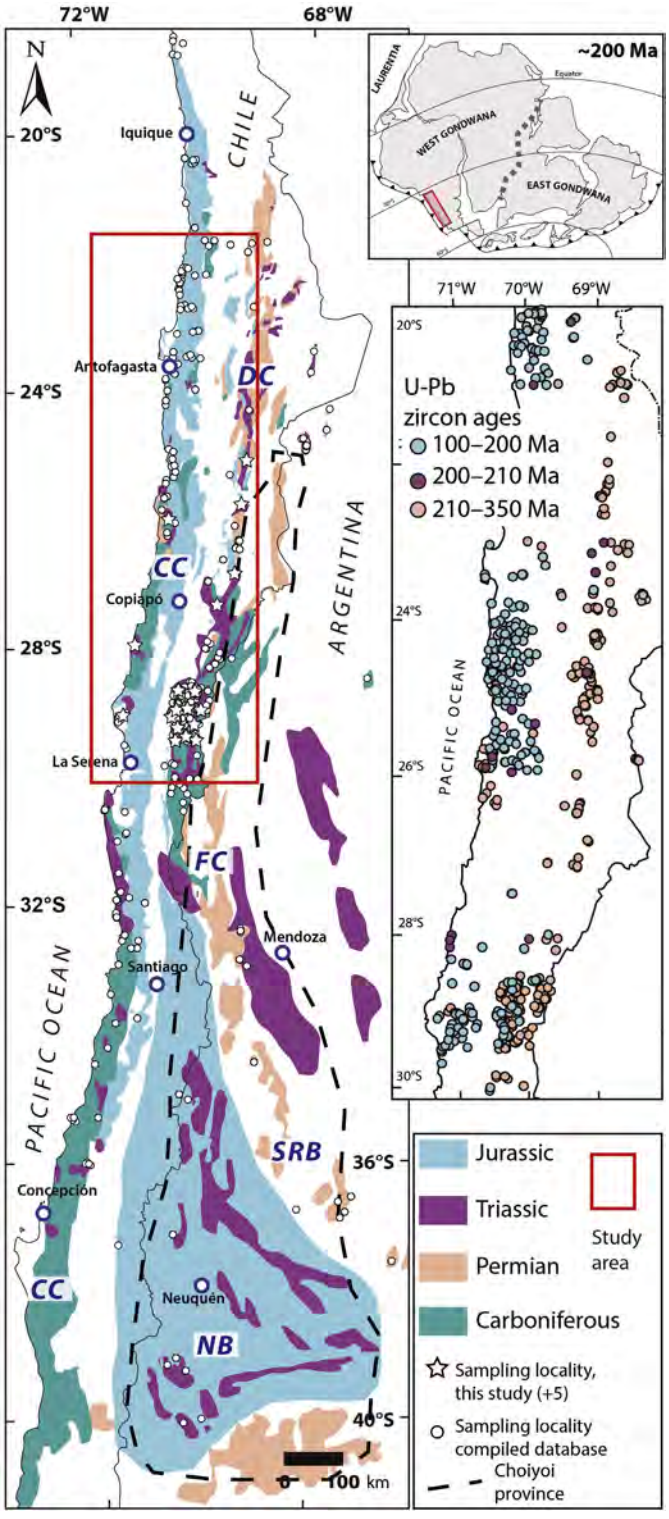

Fig. 1. Schematic distribution of the Late Paleozoic to Jurassic units cropping out in Chile and Western Argentina between 20° and 40°S and sample locations. In the case of Jurassic deposits of the Neuquén Basin, they are represented as the proposed full extension of the basin during the Jurassic (Howell et al., 2005). DC: Domeyko Cordillera; FC: Frontal Cordillera; SRB: San Rafael Block and NB: Neuquén Basin. White stars indicate locations with 5 or more samples analyzed for this study (see Tables 2 and 3 for specific locations). White dots show locations of samples from the compiled database of published works (Supplementary Material). The limits of the Choiyoi province are after Kleiman and Japas (2009) and Spalletti and Limarino (2017), and include only Middle Permian to Early Triassic rocks. Compilation of the U—Pb zircon ages in the study area is from the Chilean National Geological and Mining survey (SERNAGEOMIN) and its program for the updating of the geological cartography in northern Chile.

complexes in the Coastal Cordillera to the west (Fig. 1). In the eastern belt, restricted patches of Devonian to Early Carboniferous metasedimentary and metavolcanic complexes (Fig. 3, Cornejo et al., 2009; Maksaev et al., 2014; Tomlison et al., 1999) are exposed as tectonic slices controlled by Incaic transpressive/reverse structural systems around 26° S, and similar to the south, between 28° and 30° S (Nasi et al., 1990; Ribba et al., 1988; Salazar and Coloma, 2016), or as roof-pendant on Late Paleozoic granitoids (e.g. El Cepo Metamorphic Complex, 30°S, Murillo et al., 2017; Ortiz and Merino, 2015). These granitoids are in turn the most voluminous constituents of the Frontal and Domeyko Cordilleras. They are represented by dominantly metaluminous and calk-alcaline diorites to granites with ages ranging from the Late Carboniferous (330 Ma) to the Cisuralian (260 Ma) (Hervé et al., 2014; Maksaev et al., 2014; Ortiz and Merino, 2015; Pankhurst et al., 1996; Salazar et al., 2013). Volumetrically minor volcanic sequences of the same age have also been recognized in the study area, corresponding to the Cerro Bayo Formation and the lower part of the La Tabla Formation (Maksaev et al., 2014; Salazar et al., 2013).

These rocks are partly coeval with Late Paleozoic forearc sedimentary sequences and metamorphic complexes that are currently exposed along the coast south between 26° and 29°S, (Fig. 3)(Bell, 1987; Creixell et al., 2016; Fuentes et al., 2019) and their equivalents around 31°S (Choapa Metamorphic Complex, Arrayán and Huentelauquén formations; Rebolledo and Charrier, 1994; Thiele and Hervé, 1984; Willner et al., 2008). These rocks are representative of an accretionary prism (Bell, 1987) that was active during the Late Carboniferous-Early Permian, when subduction resumed along the western margin of Gondwana after the Devonian (Mpodozis and Ramos, 1989; Pankhurst et al., 2015). In the study area, the Carboniferous to Cisuralian Permian granitoids and volcanic rocks that crop at the Frontal and Domeyko Cordilleras in the study area represent the magmatic arc (Mpodozis and Kay, 1992; Hervé et al., 2014; del Rey et al., 2016). Similarly, the Carboniferous plutons cropping out in the Coastal Cordillera south between 32° and 38°S, are also interpreted as the Gondwana magmatic arc (Deckart et al., 2014). This cycle ended with the development of the San Rafael orogenic phase, a compressive event that would have propagated deformation inland as fold-and-thrust belts during the Early Permian at least between 35° and 30°S (Rapalini and Astini, 2005; Kleiman and Japas, 2009) but also in northermost Chile at 23°-22°S (Tomlinson et al., 2012). It has been proposed that this orogenic phase may have been due to the collision of a continental terrain (Mpodozis and Kay, 1992) but more recently has been attributed to the processes of non-collisional orogens such as slab shallowing or flat-slab subduction (Martínez, 2004; Kleiman and Japas, 2009; Ramos and Folguera, 2009; Tomlinson et al., 2012; Del Rey et al., 2016, 2019).

2.2. Pre-Andean stage (~285 Ma to Rhaetian)

In the Frontal and Domeyko Cordilleras between 24° and 30°S, Permian pyroclastic and effusive rocks along with plutonic complexes of intermediate to acidic composition are the youngest Paleozoic units cropping out (Fig. 2). Among the volcanic units, the La Tabla and Guanaco Sonso formations are the thickest and more widespread sequences. Both units extend beyond the Permian boundaries: the lower sequences of the la Tabla Formation are Carboniferous in age and the upper strata of the Guanaco Sonso Formation overlap in time with the Early Triassic plutons and sedimentary units (Fig. 3). Cisuralian to Lopingian intrusives also crop out in this area and are spatially related to the coeval volcanic rocks (Brown, 1991; Ortiz and Merino, 2015; Salazar and Coloma, 2016).

Triassic magmatic rocks make up most of the volume of the eastern part of the Frontal Cordillera in the Chilean side south of 28° S (Fig. 2). Lower-Middle Triassic intrusive rocks ranging from diorite to granites in composition crop out between 28° and 30°S in the Frontal Cordillera with the most representative unit being the Chollay Plutonic Complex (Fig. 3). These plutonic complexes are covered by Permian and Late

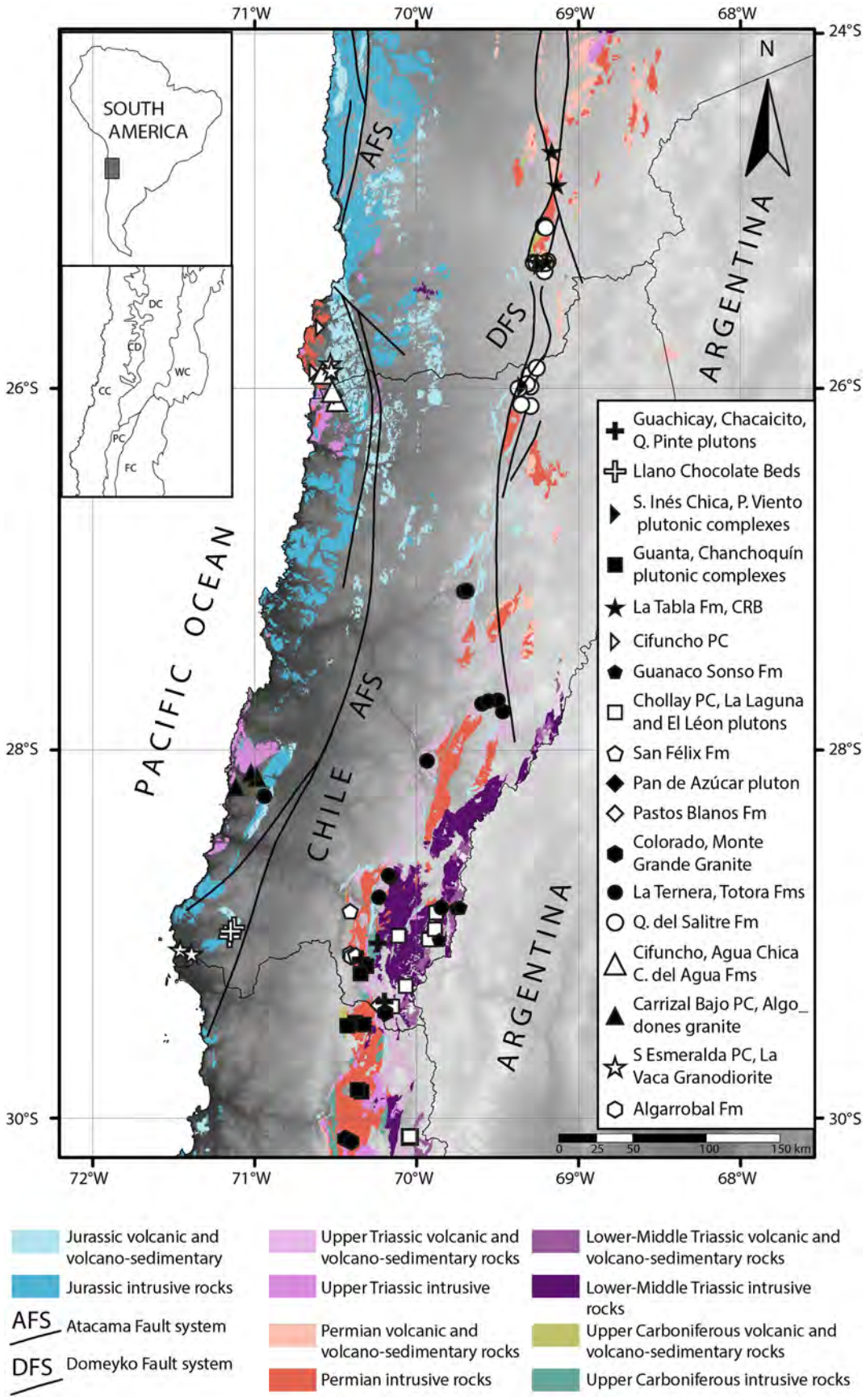

Fig. 2. Simplified geological map showing the distribution of Upper Carboniferous to Jurassic volcano-sedimentary and intrusive rocks in northern Chile between 22° and 30°S, and limits of the main morphotectonic units in Chile and Argentina at the same latitudes (inset).. CC: Coastal Cordillera, DC: Domeyko Cordillera, CD: Central Depression, PC: Principal Cordillera, WC: Western Cordillera, FC: Frontal Cordillera, PC: plutonic complex, CRB: Cerro Ratones Beds.

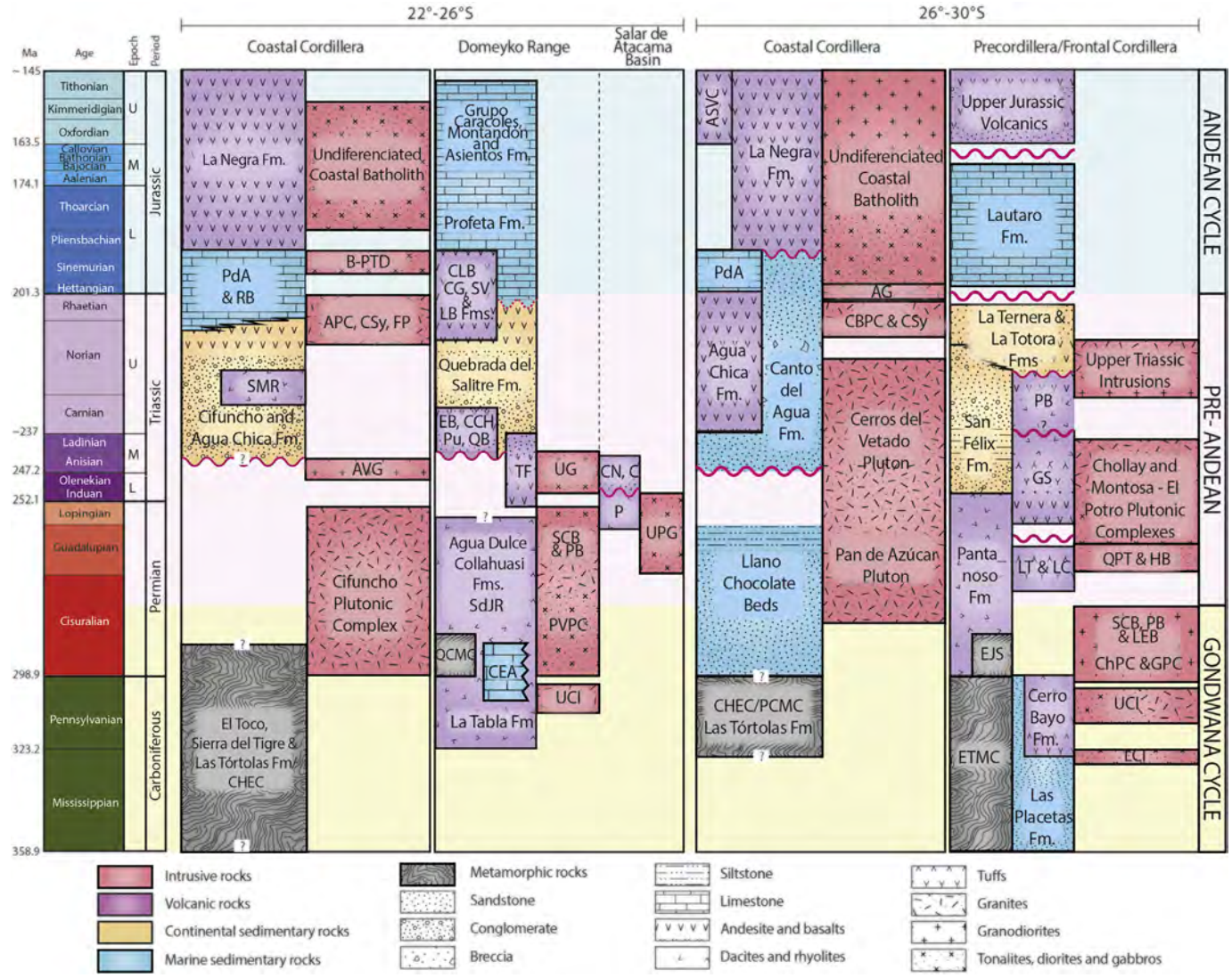

Fig. 3. Chronostratigraphic scheme of the relevant units in northern Chile between 22° and 30°S.CHEC: Chañaral Epimetamorphic Complex, QCMC: Quebrada del Carrizo Metamorphic Complex; PCMC: Punta de Choros Metamorphic Complex; CMR: Sierra Miranda Rhyolites; PdA: Pan de Azúcar Fm; RB: Rencoret beds; APC: Anchuña Plutonic Complex; FP: Flamenco Pluton; CSy: Capitana Syenogranites; B-PTD: Bolfin-Punta Tetas Metadiorites; AVG: Agua Verde Granodiorite; CLB: Cerro La Ballena Fm; CG: Cerro Guanaco Fm; SV: Sierra de Varas Fm; LL: Las Lomas; EB: El Bordo Beds, CCH: Cerros de Chuquicamata; Pu: Pular Fm; TF: Tuina Fm; SdJR: Sierra del Jardín Rhyolites; CEA: Cerro El Árbol Fm; UG: Undiferentiated granitoids; SCB: Sierra del Castillo Batholith; PB: Pedernales Batholith; PVPC: Punta del Viento Plutonic Complex; UCI: Upper Carboniferous intrusives; CN: Cerro Negro Beds; C: Cas FM.; P: Peine Fm; AG: Algodones Granite; CBPC: Carrizal Bajo Plutonic Complex; EJS: El Jardín Schists; ETMC: El Tránsito Metamorphic Complex; PBF: Pastos Blancos Fm; GS; Guanaco Sonso Fm and Paso del Guanaco Sonso Beds; LT: La Tabla Fm; LC: Laguna Chica Fm; QPT: Quegrada del Pintado Tonalites; HB: Hielo Batholith; LEB: La Estancilla Batholith; ChPC: Chanchoquín Plutonic Complex; GPC: Guanta Plutonic Complex; LB: Las Bateas Fm, QB: Quebrada Blanca Fm; ASVC: Agua Salada Volcanic Complex; LCI: Lower Carboniferous intrusives. Upper Jurassic Volcanics include the volcano-sedimentary units: Lagunillas, Algarrobal and Sierra Fraga formations, and Quebrada Vicuñita BedsStratigraphic series and their numerical ages are from Cohen et al. (2017).

Triassic, that include pyroclastic, hypabyssal and effusive rocks of ages between 233 and 219 Ma (Maksaev et al., 2014; Ortiz and Merino, 2015). Upper Triassic plutons are also found in the Frontal Codillera, although they are volumetrically much more restricted than the older intrusives. These units are composed of monzo and syenogranite of ca. 225–220 Ma in age (Nasi et al., 1990) and intermediate to acidic, cordierite-bearing, small plutons of ca 217–214 Ma in age (Hervé et al., 2014; Nasi et al., 1990). Lower-Middle Triassic volcanic rocks crop out in the eastern flank of the Domeyko Cordillera, in the vicinity of the Salar de Atacama (~23°40′S, 68°W) (Breitkreuz et al., 1989). The youngest Late Triassic volcanic units correspond to basic to intermediate lava sequences and related volcanosedimentary rocks of Norian-Rhaetian (Domeyko Cordillera) or Carnian-Norian (Frontal Cordillera) age, which were deposited directly over Late Paleozoic to Early-Middle Triassic plutonic rocks (Martínez et al., 2015; Salazar et al., 2013).

Along the Coastal Cordillera, the record of Cisuralian to Triassic rocks is restricted. Around 25°30′-26°S there are two plutonic complexes of Permian age (Cifuncho and Pan de Azúcar, Figs. 2,3), composed of granodiorite to syenogranite intrusives, which are the sole Late Paleozoic plutonic rocks documented so far for the coast of northern Chile (Brown, 1991). Scarce outcrops of Late Triassic plutons are also recognized along the coast, that in some cases were emplaced along associated synplutonic normal faults (Grocott et al., 2009). Volcanic and volcanoclastic sequences are even less common, with some limited outcrops of Cisuralian age at ~28°S and of Upper Triassic age at ~28°S and ~25°30′S (Cifuncho and Agua Chica formations; Contreras et al., 2013; Welkner et al., 2006).

The Cisuralian to Lower Triassic igneous rocks, in particular those cropping out in the Frontal and Domeyko Cordilleras, are thought to be the products of an anorogenic magmatism resulted from extensive crustal melting, (Parada et al. 1982; Mpodozis and Kay, 1992) and

have been interpreted as the equivalent to the Choiyoi Group in Argentina based in their similar age range, from 285 Ma to 245 Ma (Maksaev et al., 2014; Sato et al., 2015). The Middle to Late Triassic volcanic sequences are often reported as bimodal basaltic-rhyolite suites (Cornejo and Mpodozis, 1996; Parada et al., 1999; Morata et al., 2000) and have been interpreted as products of continental rift magmatism with mantle sources (Kay and Ramos, 1990) and related to the development of NW-oriented large-scale rift basins in a passive margin (e.g.: Ichigualasto, Cuyo and San Félix basins, Charrier et al., 2007). On the other hand, some authors have interpreted the Guadalupian to Rhaetian magmatism (del Rey et al., 2016; Coloma et al., 2017; González et al., 2018), the Middle-Late Triassic basins in Chile (Espinoza et al., 2019; Salazar et al., 2019), and also the Choiyoi magmatism (Rocher et al. 2016), as subduction-related.

The dominant structural style during the entire Pre-Andean stage would have been extensional, with the development of large volcanic calderas controlled by normal faults and abundant dyke swarms in the Permiam and Triassic magmatism (Giambiagi and Martinez, 2008; González et al., 2018; Llambías and Sato, 1995; Salazar and Coloma, 2016). A major deformational phase (Huárpica) that separates the

Table 1
Lithologies, alteration degree and age range for the studied units. Listed lithologies correspond only to analyzed samples and not to the entire petrographic range of each unit, see Petrography section for a more detailed description of all lithological types. Alteration degree was estimated through petrographic analysis of each sample and it is represented by the total volume of alteration minerals in each sample (Supplementary Material 1; Coloma et al., 2017; Ortiz and Merino, 2015). Age data from the literature for the studied samples are listed in Supplementary Material 2.

	Unit	Samples	Lithologies	Alteration degree	Age range
Gonwdana cycle	Chacaicito Pluton	RCM-077q	Syenogranite	0.12	329–324 Ma[a]
	Quebrada Pinte Diorite	MCM-168 Bq	Diorite	0.07	324 Ma[a]
	Guachicay Pluton	MCM-159q	Tonalite	0.09	303 Ma[a]
	Llano de Chocolate Beds	CPV-12-12, CPV-12-105, CPV-12-127	Rhyolite, Dacite, Rhyolitic tuff	0.24–0.8	318–285 Ma[b]
	Punta del Viento Plutonic Complex	CPV-15-365	Granite	0.18	295–277 Ma[c]
	Chanchoquín and Guanta Plutonic Complexes	MCM-129q, RCM-133q, O7–13, O7–15, MCM-205q, MCM-280q, RCM-015q	Quartz Monzodiorite, Tonalite, Granodiorite, Syenogranite	0.00–0.16	296–285 Ma[d]
	La Tabla Formation, Cerro Rincones Beds	CPV-14-176, CPV-14-249, CPV-14-263, CPV-15-353	Rhyolitic tuff, Dacite	0.11–0.26	294–289 Ma[c]
	Cifuncho Plutonic Complex	CPV-14-180A, CPV-14-191	Monzogranite	0.08–0.09	284–256 Ma[e]
	Sierra de Doña Inés Chica Plutonic Complex	CPV-15-320	Quartz Monzodiorite	0.28	280–255 Ma[f]
	Guanaco Sonso Formation	SCL-28q, SCL-96q, RCM-150q	Dacitic tuff, Rhyolitic tuff	0.13–0.35	265–240 Ma[d]
	La Laguna Gabbro	O7-10, O7-11	Gabbro	0.01–0.02	255 Ma[g]
	Chollay Plutonic Complex	SCL-02q, SCL-09q, MCM-010q, MCM-022q, MCM-265q, RCM-040q	Granodiorite, Tonalite, Syenogranite, Monzogranite	0.015–0.17	247–237 Ma[d]
	San Felix Formation	CPV-12-38, CPV-12-49b	Lithic tuff	0.5–0.7	254–212 Ma[h]
	Pan de Azúcar Pluton	CPV-14-192	Granite	0.13	230 Ma[i]
	Pastos Blancos Formation	RCM-78q	Andesite	0.33	231–216 Ma[a]
	Colorado Syenogranite	RCM-61q	Syenogranite	0.05–0.09	229–219 Ma[d]
	La Totora Formation	CPV-12-23, CPV-12-24, CPV-12-60, SCL-26q	Basalt, Andesite, Rhyolithic tuff	0.15–0.49	221–210 Ma[d,j]
	Montegrande Granite	O7-06, O7-07	Granite, Granodiorite	0.01	215 Ma[k]
Pre-Andean stage	Canto del Agua Formation	CPV-12-90	Lithic tuff	0.4	212.6 Ma[h]
	La Ternera Formation	CPV-15-271, CPV-15-274, CPV-15-278, CPV-15-279, CPV-15-280, CPV-15-281, CPV-15-284, CPV-15-285, CPV-15-287, CPV-15-410	Basalt, Basaltic Andesite, Andesite, Andesitic Tuff, Dacitic tuff, Lithic tuff	0.28–0.51	220–199 Ma[l,m]
	Quebrada del Salitre Formation	CPV-14-245, CPV-14-247, CPV-14-253, CPV-14-256, CPV-15-303, CPV-15-310, CPV-15-311, CPV-15-312, CPV-15-314, CPV-15-319, CPV-15-322, CPV-15-330, CPV-15-332, CPV-15-337, CPV-15-359, CPV-15-386	Basalt, Basaltic Andesite, Andesite, Dacite, Rhyolite, Andesitic breccia, Lithic tuff	0.17–0.60 mean = 0.32	212 Ma[c]
	Cifuncho Formation	CPV-14-184, CPV-14-187, CPV-14-190	Andesite, Dacite	0.16–0.32	212–205 Ma[e]
	Carrizal Bajo Complex	CPV-12-91A, CPV-12-91B, CPV-12-93	Diorite, Tonalite, Granodiorite	0.05–0.23	208–206 Ma[n]
	Agua Chica Formation	CPV-14-194, CPV-14-198	Andesite, Dacitic tuff	0.3–0.4	200 Ma[o]
	Algodones Granite	CPV-12-92	Diorite	0.4	203–199 Ma[n]
Early Andean cycle	Sierra Esmeralda Plutonic Complex	CPV-14-181B, CPV-14-182B	Tonalite, Monzodiorite	0.14–0.32	194 Ma[e]
	La Vaca Granodiorite	CPV-12-01, CPV-12-03	Granodiorite, Dike (andesite)	0.02–0.13	193–191 Ma[p]
	Algarrobal Formation	CPV-12-26B, CPV-12-28x, CPV-12-30x	Basaltic andesite, Andesite	0.2–0.3	152–137 Ma[a]

[a] Ortiz and Merino (2015).
[b] Creixell et al. (2016).
[3] Venegas et al. (2013).
[d] Salazar et al. (2013).
[5] Contreras e al. (2013).
[6] Cornejo et al. (1993).
[g] Hervé et al. (2014).
[8] Vallejos (2012).
[9] Berg and Baumann (1985).
[j] Maksaev et al. (2014).
[k] Coloma et al. (2017).
[l] Espinoza et al. (2015).
[m] Peña et al. (2013).
[14] Arévalo and Welkner (2008).
[o] Espinoza et al. (2015).
[16] Creixell et al. (2012).

Choiyoi magmatism from Middle Triassic rocks is interpreted as an extensional event (Sato et al., 2015 and references therein). During the Triassic, the development of NW-oriented rift basins is well documented, both in the continental foreland (Ichigualasto and Cuyo basins) and margin (Profeta, La Ternera, San Félix basins) (Charrier et al., 2007; Giambiagi et al., 2008; Salazar et al., 2019; Espinoza et al., 2019).

2.3. Early Andean cycle (Jurassic)

The early stage of the Andean subduction system or Andean orogeny is represented in northern Chile by the Coastal Batholith, which is mostly composed by intermediate plutons that span the entire Jurassic period. Whereas the intrusive units constitute the roots of the magmatic arc, the Jurassic La Negra Formation and its equivalents along the Coastal Cordillera represent the penecontemporaneous volcanic products (Kramer et al., 2005; Oliveros et al., 2006). In the Frontal and Domeyko Cordillera, Jurassic marine and volcanic sequences are interpreted as the back-arc basin and associated back-arc volcanism to the early Andean subduction system, respectively (Ardill et al., 1998; Oliveros et al., 2012; Prinz et al., 1994; Rossel et al., 2013).

Even though the Early Andean arc was emplaced over Paleozoic continental crust, due to the rather primitive nature (calc-alkaline to tholeiitic affinities) of its magmatism and its tectonic and palaeogepgraphic configuration (intra-arc and back-arc basins), it has been compared to modern oceanic-type subductions systems or island arcs (Lucassen et al., 2006; Rossel et al., 2013) rather to typical continental arcs. An extensional strucutral setting would have been dominated the margin during the Early Andean cycle, due to the oblique subduction of the Phoenix plate, that induced stress partition on the upper plate developing transtensional sinistral systems (Grocott and Taylor, 2002; Scheuber and Gonzalez, 1999).

3. Samples and methods

86 samples of volcanic and plutonic rocks from units cropping out in the Coastal, Domeyko and Frontal Cordilleras of northern Chile (25°S-30°S) and ranging in age from Upper Carboniferous to Upper Jurassic (Table 1) were selected for petrographical and geochemical analysis. In total, 65 samples were analyzed for major and trace elements (Table 2): 48 by total fusion XRF and ICP-MS, at the Activation Laboratories, Ontario, Canada, and 17 by ICP-MS at the Laboratory of the National Geological and Mining Survey (SERNAGEOMIN), Chile. 69 samples were analyzed for whole rock Sr-Nd-Pb isotopic composition (Table 3): 27 at the Geosciences Department, University of Arizona, USA by TIMS (Sr—Nd isotopes) and MC-ICP-MS (Pb isotopes) (following the procedures outlined in Drew et al., 2009 and Otamendi et al., 2009), and 42 at the Isotope Geochemistry laboratory of the MARUM Center, University of Bremen, Germany.

Due to the high alteration degree that affects the vast majority of the Paleozoic and Mesozoic Andean rocks, collecting fresh samples in the field is not a feasible task and it is only possible to remove weathered surfaces and/or to gather relatively fresh rock chips. Therefore, the samples selected for geochemical analyses were crushed to <5 mm fraction and cleansed, small fresh fragments, representative of the entire lithology, were handpicked under binocular lens in order to avoid altered areas of the rock. The selected fragments were powdered under 50 μm for further chemical treatment prior to the elemental and isotopic analyses. Details of geochemical procedures are in the Supplementary Material.

A database of 1237 samples from the Andean region of Chile and western Argentine between 18°00′ and 40°00′S has been compiled (Supplementary Material 3) in order to compare the magmatism represented by the samples analyzed in this work to the Carboniferous-Jurassic magmatism along the entire western Gondwana margin. The amount of information for the samples in the database is variable but at least it includes precise location in UTM coordinates, age or age range and major elements composition. For the majority of the samples (75%) petrography (lithological classification) and trace elements are also reported and Sr, Nd and Pb isotope composition is available for the 23%, 19% and 13% of samples, respectively.

4. Petrography

A detailed list of the petrographic results for the analyzed samples can be found in the Supplementary Material 1. All collected samples are altered to some extent and exhibit variable proportions of hydrothermal or very low-grade metamorphic minerals such as chlorite (−smectite), sericite, calcite, epidote, clays, Fe-oxihydrates and quartz. Much less common is the occurrence of biotite, actinolite or opaque minerals. These secondary minerals may fill amygdules or veinlets, replace igneous crystals, volcanic glass or small crystal within the groundmass. Details of secondary mineral phases are listed in the Supplementary Material 1.

4.1. Gondwana cycle

The older units are Carboniferous small plutons that crop out in the Frontal Cordillera (29°00′-29°30′): Chacaicito, Quebrada Pinte and Guachicay. Guachicay pluton is a leucocratic, coarse grained, biotite -and minor muscovite- tonalite; Quebrada Pinte diorites correspond to melanocratic, coarse grained amphibole diorites and quartz diorites with penetrative planar fabric and Chacaicito pluton is composed of leucocratic, coarse grained biotite syenogranites (Ortiz and Merino, 2015). Cisuralian plutons (>285 Ma) are volumetrically more significant in the Frontal and Domeyko Cordilleras, sampled units correspond to: the Punta del Viento Plutonic Complex (25°00′-26°00′), a leucocratic quartz monzonite with scarce clinopyroxene; the Chanchoquín Plutonic Complex (28°30′-29°15′S) and Guanta Unit (29°15–31°S) are leucocratic, medium to coarse grained quartz monzodiorite, tonalite, granodiorite and syenogranite with biotite and minor amphibole or muscovite; and the Cifuncho Plutonic Complex (27°00′-28°15′S) a leucocratic, medium grained biotite monzogranite with scarce amphibole. The Llano de Chocolate beds (28°45′-29°05′S) crop out in the Coastal Cordillera and are the only volcanic unit assigned to this cycle that was sampled. Rocks are porphyritic ryholites and dacites, with plagioclase, quartz and minor alkali-feldspar phenocrysts, felsitic groundmass and devitrified glass.

4.2. Pre-Andean stage

The Guadalupian to Rhaetian intrusives are voluminous in the Frontal Cordillera and much less represented in the Coastal Cordillera. In the former, sampled units from older to younger, correspond to: the La Laguna Gabbro (30°05′S); the Chollay Plutonic Complex (28°30′-29°30′S) leucocratic medium to fine grained biotite-amphibole tonalite and quartz mozodiorite, leucocratic, medium grained biotite-muscovite granodiorite and monzo and syenogranite; the Sierra de Doña Inés Chica Plutonic Complex (26°00′-26°30′) a medium to coarse grained, leucocratic, hornblende and biotite granodiorite; the Colorado Syenogranite (28°45′-30°15′S), a leucocratic, coarse to medium to grained, biotite syenogranite; and the Montegrande Granite (30°05′S), an inequigranular, leucocratic, biotite granite with minor intersticial amphibole and clinopyroxene. In the Coastal Cordillera, samples correspond to the Pan de Azúcar pluton (26°00′-26°20′S), a leucocratic, coarse grained muscovite granite; the Carrizal Bajo Plutonic Complex (28°00′S), medium to fine grained, equigranular biotite tonalites and granodiorites and amphibole tonalite; and Algodones Granite (28°00′), a medium grained quartz diorite, with clinopyroxene and biotite.

Volcanic and volcanosedimentary units crop out mainly in Frontal and Domeyko Cordilleras, with less voluminous sequences in the Coastal Cordillera. In general, these units exhibit variable petrographic compositions, ranging from basalt to rhyolite, but with

Table 2
Major and trace (ICP-MS analysis) element composition of the studied samples. Coordinates for each sample are in UTM WGS84 datum. Negative figures indicate element concentrations below the detection limit, with the absolute value as the half of the respective detection limit. La_N/Yb_N and Eu/Eu^* parameters are normalized to the chondritic values of Sun and McDonough (1989). FUS-ICP: Lithium Metaborate/Tetraborate Fusion; TD: Total Digestion. FUS-ICP-MS, TD-ICP-MS analyses are from Actlabs and ICP-MS analyses are from the Chemistry Laboratory of the Chilean Geological and Mining Survey.

Dy	Ho	Er	Tm	Yb	Lu	La/YbN	Eu/Eu*	Y	Sc	Hf	Nb	Ta	Th	Zn	Co	Ni	Ba	Cr	V	Cu
9.65	2.01	5.77	0.80	5.37	0.78	1.08	0.80	58.34	20.79	5.74	7.38	0.38	2.6	83.1	31.9	52.6	107.1	34.0	67.9	41.8
4.77	0.97	2.86	0.40	2.74	0.40	6.92	0.67	30.12	11.54	0.81	12.68	0.80	9.0	67.0	16.2	18.7	425.9	30.4	158.7	21.8
4.31	0.89	2.57	0.35	2.41	0.35	1.89	0.70	18.69	18.70	3.58	5.74	0.42	4.7	112.2	26.3	19.7	359.9	4.8	19.9	17.1
4.35	0.88	2.49	0.33	2.27	0.33	1.87	0.99	25.39	12.27	3.16	4.14	0.23	1.3	80.6	39.8	155.8	266.9	458.2	185.5	10.2
3.98	0.81	2.37	0.33	2.28	0.34	5.40	0.80	26.71	7.65	3.64	6.81	0.43	8.4	37.8	8.8	7.9	367.1	17.3	41.9	2.9
5.94	1.25	3.65	0.52	3.54	0.50	4.28	0.27	39.53	2.65	2.86	7.96	0.68	12.5	29.8	1.1	6.8	241.8	10.8	9.8	9.7
3.40	0.71	2.08	0.35	2.39	0.38	7.95	0.84	19.90	6.00	3.60	6.30	0.99	11.0	40.0	35.0	−10.0	937.0	−10.0	32.0	20.0
5.15	1.00	2.83	0.43	2.83	0.43	6.69	0.42	27.70	7.00	3.50	7.80	1.42	12.7	40.0	34.0	−10.0	329.0	−10.0	24.0	−5.0
3.58	0.76	2.31	0.39	2.67	0.42	1.53	1.00	21.70	12.00	2.70	2.40	0.29	1.5	40.0	17.0	−10.0	71.0	−10.0	124.0	10.0
2.77	0.58	1.76	0.27	1.78	0.28	4.79	1.03	16.10	12.00	3.10	2.90	0.35	2.9	50.0	27.0	30.0	161.0	40.0	105.0	60.0
2.55	0.54	1.59	0.25	1.81	0.28	4.68	0.89	15.30	8.00	2.80	2.90	0.39	3.2	80.0	23.0	−10.0	371.0	30.0	66.0	−5.0
2.57	0.52	1.52	0.24	1.59	0.24	5.20	0.92	14.20	9.00	2.60	2.70	0.37	3.1	50.0	25.0	−10.0	171.0	−10.0	53.0	−5.0
2.83	0.56	1.65	0.25	1.77	0.28	4.52	0.95	15.50	9.00	2.90	3.00	0.37	3.2	60.0	17.0	−10.0	246.0	20.0	79.0	−5.0
5.87	1.10	2.98	0.42	2.74	0.41	8.93	0.45	30.70	10.00	5.00	8.50	1.04	15.3	60.0	29.0	−10.0	498.0	−10.0	48.0	20.0
3.58	0.67	1.89	0.30	1.97	0.29	3.32	0.33	18.60	4.00	1.70	3.00	0.89	5.9	30.0	43.0	−10.0	223.0	−10.0	11.0	−5.0
2.82	0.56	1.51	0.21	1.35	0.21	6.07	0.74	15.50	12.00	2.80	2.10	0.39	3.3	50.0	29.0	−10.0	101.0	60.0	84.0	−5.0
2.84	0.58	1.69	0.26	1.79	0.28	5.25	0.91	15.10	14.00	3.40	3.90	0.38	4.4	80.0	22.0	30.0	80.0	40.0	85.0	10.0
2.93	0.59	1.73	0.24	1.47	0.23	3.28	1.04	14.00	22.00	2.30	3.70	0.29	1.4	124.0	39.8	81.0	70.0	127.0	148.0	39.5
2.36	0.46	1.33	0.20	1.25	0.20	4.91	0.83	12.80	8.00	3.20	7.00	0.86	6.0	30.1	19.5	75.0	163.0	21.0	64.0	27.9
9.25	1.91	5.93	0.91	6.10	0.91	4.16	0.44	49.30	10.00	7.60	12.50	1.40	17.6	3.5	0.8	33.0	1000.0	10.0	7.0	1.9
3.40	0.68	1.88	0.26	1.70	0.27	4.00	1.10	17.40	24.00	2.60	3.90	0.29	1.9	97.4	29.0	64.0	152.0	144.0	173.0	14.5
4.31	0.91	2.72	0.40	2.52	0.41	2.72	0.99	21.70	28.00	3.20	7.30	0.55	1.9	196.0	58.0	98.0	181.0	165.0	182.0	8.6
4.68	0.98	2.89	0.43	3.08	0.51	6.47	0.78	26.60	7.00	6.00	8.70	0.82	12.3	2.7	4.5	38.0	913.0	8.0	36.0	13.6
4.64	0.86	2.43	0.34	2.18	0.31	7.06	1.02	16.10	22.00	4.10	8.10	0.63	1.6	117.0	22.7	81.0	163.0	104.0	174.0	77.8
5.65	1.10	3.16	0.45	2.96	0.45	4.55	0.92	23.20	19.00	5.30	6.50	0.58	2.4	4.2	6.1	44.0	153.0	5.0	119.0	25.5
6.05	1.17	3.15	0.46	2.94	0.44	3.42	1.02	22.20	26.00	4.50	4.70	0.43	1.2	19.8	23.1	144.0	131.0	29.0	199.0	20.9
5.34	0.89	2.43	0.38	2.76	0.43	8.43	0.47	19.70	6.00	5.70	9.00	0.88	9.0	2.7	0.4	20.0	382.0	9.0	−2.5	12.3
9.98	2.01	5.98	0.91	6.07	0.92	4.26	0.75	44.20	7.00	10.00	13.40	1.22	9.5	3.6	1.0	3.0	47.0	10.0	42.0	2.5
7.49	1.49	4.48	0.68	4.69	0.71	1.83	0.61	31.80	14.00	7.80	11.80	1.06	10.6	6.9	2.6	50.0	1140.0	14.0	37.0	4.4
4.53	0.91	2.58	0.39	2.41	0.37	2.76	1.06	18.40	30.00	3.60	2.90	0.33	1.0	103.0	34.2	121.0	135.0	116.0	203.0	44.2
2.87	0.56	1.53	0.23	1.38	0.20	2.65	0.97	10.90	12.00	1.90	3.10	0.36	1.0	72.2	21.1	37.0	79.0	112.0	153.0	53.8
4.22	0.82	2.37	0.33	2.26	0.34	7.70	0.80	16.70	12.00	5.30	9.40	0.81	4.1	28.7	16.1	88.0	456.0	32.0	94.0	5.4
5.86	1.21	3.33	0.47	3.06	0.48	3.79	0.93	31.70	27.00	5.70	10.10	0.71	2.3	36.1	26.0	73.0	1110.0	58.0	212.0	76.4
5.78	1.24	3.91	0.60	4.09	0.67	3.34	0.37	35.40	4.00	6.30	9.00	1.13	11.9	1.7	0.3	18.0	1100.0	11.0	−2.5	11.4
6.14	1.19	3.36	0.48	3.24	0.51	2.59	1.00	32.30	40.00	4.90	10.50	0.77	1.0	158.0	47.8	94.0	451.0	188.0	260.0	6.0
4.47	0.87	2.60	0.39	2.55	0.40	6.43	0.76	23.00	15.00	6.10	11.30	0.95	5.7	43.9	15.5	1920.0	537.0	53.0	98.0	17.6
12.60	2.46	7.20	1.04	6.84	1.10	5.72	0.49	69.10	7.00	9.70	12.60	1.46	14.1	2.0	0.9	55.0	390.0	7.0	6.0	3.9
4.00	0.80	2.23	0.34	2.17	0.36	5.56	0.82	22.10	15.00	4.60	9.10	0.83	5.6	45.8	14.2	49.0	148.0	38.0	90.0	27.1
3.72	0.76	2.25	0.33	2.20	0.37	7.58	0.75	20.40	12.00	7.90	11.60	1.03	14.1	9.9	11.9	65.0	702.0	13.0	75.0	18.5
4.22	0.85	2.33	0.34	2.25	0.36	1.98	1.00	15.10	27.00	3.10	5.00	0.39	0.6	166.0	40.5	66.0	93.0	300.0	175.0	50.7
2.64	0.51	1.45	0.22	1.51	0.23	12.85	0.79	12.80	8.00	3.50	6.10	0.68	4.8	14.3	8.0	139.0	1440.0	20.0	59.0	16.5
2.19	0.42	1.24	0.19	1.27	0.20	11.39	0.85	11.60	6.00	3.30	5.40	0.62	3.6	7.0	2.6	215.0	1900.0	18.0	29.0	28.7
3.83	0.75	2.14	0.32	2.01	0.32	4.94	0.89	14.70	16.00	4.20	9.70	0.73	2.5	14.5	15.1	202.0	2030.0	11.0	94.0	9.1
2.48	0.47	1.45	0.23	1.55	0.25	2.33	0.89	3.70	7.00	3.10	5.40	0.54	3.7	17.1	9.2	35.0	156.0	25.0	40.0	5.0
3.77	0.73	1.98	0.30	1.92	0.28	3.78	1.02	16.00	21.00	2.60	8.10	0.69	1.2	60.8	39.1	63.0	160.0	132.0	155.0	98.9
9.77	1.97	6.09	0.98	6.66	1.01	3.88	0.27	20.40	4.00	3.70	8.20	1.54	14.8	2.2	−0.1	4.0	112.0	6.0	−2.5	5.8
4.39	0.85	2.35	0.35	2.22	0.34	3.33	1.03	18.40	25.00	3.30	8.40	0.65	1.3	117.0	30.7	78.0	97.0	106.0	174.0	34.1
4.20	0.79	2.24	0.35	2.28	0.35	7.28	0.91	16.10	15.00	5.20	8.80	0.81	3.6	35.8	16.7	194.0	374.0	31.0	100.0	14.9
8.58	1.73	5.12	0.80	5.40	0.79	4.98	0.24	50.00	8.00	6.60	13.70	1.02	14.4	−15.0	−0.5	−10.0	575.0	−10.0	146.0	−5.0
2.68	0.50	1.50	0.21	1.40	0.20	7.33	0.99	14.90	15.00	2.60	5.00	0.37	3.2	70.0	20.0	30.0	411.0	−10.0	7.0	40.0
4.23	0.87	2.64	0.45	3.08	0.49	4.05	0.39	23.50	5.00	3.20	8.50	1.08	13.0	−15.0	−0.5	−10.0	659.0	−10.0	7.0	−5.0
3.19	0.67	1.91	0.28	2.00	0.28	11.45	0.73	29.37	8.17	2.68	9.45	1.06	13.4	48.9	6.2	1.3	776.2	9.5	41.5	−2.5
4.06	0.89	2.68	0.41	2.99	0.43	8.20	0.62	32.39	10.13	2.28	13.00	1.13	15.7	33.6	3.6	2.5	879.4	15.6	21.6	−2.5
1.20	0.25	0.49	0.11	0.43	0.11	40.20	1.05	21.86	6.40	1.22	7.53	0.45	8.2	73.6	7.0	17.5	984.0	17.8	12.4	−2.5
3.17	0.67	1.99	0.31	2.25	0.33	5.76	0.83	34.12	5.28	1.68	5.28	0.78	10.0	40.9	5.8	19.5	1101.7	16.9	−5.0	−2.5
17.50	3.69	10.23	1.44	9.92	1.42	3.68	0.96	26.22	23.79	2.83	8.04	1.02	2.0	81.0	57.0	49.2	798.7	164.2	301.1	36.4
4.40	0.90	2.45	0.35	2.36	0.35	7.53	0.87	24.90	−5.00	3.30	−5.00	0.92	8.7	79.1	22.4	13.7	677.0	20.0	92.3	20.0
2.57	0.55	1.60	0.25	1.78	0.27	9.95	0.77	16.51	13.43	3.20	10.36	0.66	9.8	13.0	25.0	65.2	238.5	114.4	189.4	104.8
4.62	0.96	2.64	0.39	2.65	0.39	6.08	0.76	17.95	3.38	3.43	17.56	0.75	6.0	76.5	26.1	13.2	430.2	62.7	101.9	34.2
8.87	1.97	5.91	0.94	6.83	0.96	2.87	0.19	51.82	8.75	2.62	24.89	3.30	27.3	21.3	−2.5	6.1	274.1	−5.0	−5.0	11.3
6.53	1.48	4.29	0.65	4.57	0.67	2.88	0.29	48.26	8.72	0.78	7.59	0.05	17.5	45.9	−2.5	4.9	366.5	−5.0	−5.0	−2.5
2.18	0.41	1.24	0.19	1.40	0.19	6.09	0.38	41.94	11.93	2.64	10.08	1.02	9.6	44.7	4.9	−2.5	465.0	16.6	11.5	−2.5
3.34	0.75	2.08	0.32	2.17	0.33	7.85	0.79	37.84	5.96	3.98	12.14	3.20	10.7	18.5	3.3	−2.5	611.1	−5.0	−5.0	−2.5
3.82	0.86	2.56	0.40	2.83	0.42	8.43	0.49	17.68	−2.50	3.98	−2.50	1.03	14.6	32.3	−2.5	7.2	1075.2	−5.0	13.7	−2.5
4.45	0.84	2.17	0.29	2.01	0.27	7.81	0.98	16.32	−2.50	1.90	−2.50	1.22	8.9	47.1	−2.5	−2.5	514.4	−5.0	−5.0	−5.0

Sr	Zr	Rb	As	Be	Sb	Sn	U	W	Bi	Cd	Cs	Ga	Ge	In	Mo	Pb	Ag	Tl	Analytical technique (element)

187	232	20.4	−0.3	N.D.	0.39	4.67	0.75	0.17	−0.50	0.04	0.19	17.0	1.35	N.D.	0.59	2.84	0.25	N.D.	FUS-ICP-MS, TD-ICP-MS
281	8	95.4	−0.3	N.D.	0.22	4.10	1.78	1.65	−0.50	0.01	3.67	18.0	0.84	N.D.	0.54	9.89	0.02	N.D.	FUS-ICP-MS, TD-ICP-MS
362	133	24.1	15.2	N.D.	0.56	3.43	1.16	0.37	−0.50	0.02	1.17	19.2	0.92	N.D.	0.31	4.60	0.16	N.D.	FUS-ICP-MS, TD-ICP-MS
138	140	9.4	−0.3	N.D.	0.69	1.45	0.28	0.30	−0.50	0.02	1.63	15.1	1.20	N.D.	0.62	5.11	0.14	N.D.	FUS-ICP-MS, TD-ICP-MS
264	157	87.2	23.8	N.D.	4.07	2.94	2.13	0.67	1.43	0.02	4.46	17.0	0.72	N.D.	0.31	7.54	0.16	N.D.	FUS-ICP-MS, TD-ICP-MS
14	82	146.2	6.8	N.D.	0.69	14.49	3.08	2.20	1.33	0.03	3.25	13.2	0.22	N.D.	0.40	11.39	0.11	N.D.	FUS-ICP-MS, TD-ICP-MS
111	169	130.0	−2.5	2.00	−0.10	2.00	1.97	N.D.	−0.05	N.D.	2.80	16.0	1.50	−0.05	−1.00	7.00	1.00	0.52	FUS-ICP-MS, TD-ICP-MS
179	138	116.0	−2.5	2.00	−0.10	3.00	1.95	N.D.	−0.05	N.D.	5.60	18.0	2.10	−0.05	−1.00	19.00	0.80	0.52	FUS-ICP-MS, TD-ICP-MS
319	120	11.0	13.0	−0.50	1.20	−0.50	0.72	N.D.	−0.05	N.D.	6.00	17.0	2.20	−0.05	−1.00	−2.50	0.70	0.17	FUS-ICP-MS, TD-ICP-MS
319	144	73.0	−2.5	−0.50	−0.10	−0.50	0.76	N.D.	−0.05	N.D.	4.50	17.0	1.90	−0.05	−1.00	6.00	0.90	0.42	FUS-ICP-MS, TD-ICP-MS
234	142	33.0	−2.5	2.00	0.80	−0.50	0.89	N.D.	−0.05	N.D.	0.60	18.0	2.40	−0.05	−1.00	6.00	0.90	0.14	FUS-ICP-MS, TD-ICP-MS
331	128	55.0	−2.5	1.00	0.70	−0.50	0.72	N.D.	−0.05	N.D.	8.10	15.0	2.10	−0.05	−1.00	−2.50	0.80	0.23	FUS-ICP-MS, TD-ICP-MS
238	134	36.0	−2.5	1.00	−0.10	−0.50	0.92	N.D.	−0.05	N.D.	2.40	17.0	1.70	−0.05	−1.00	−2.50	0.90	0.21	FUS-ICP-MS, TD-ICP-MS
122	231	166.0	−2.5	2.00	−0.10	4.00	2.29	N.D.	0.10	N.D.	3.60	19.0	2.10	−0.05	−1.00	22.00	1.40	0.73	FUS-ICP-MS, TD-ICP-MS
46	66	211.0	−2.5	2.00	−0.10	4.00	3.30	N.D.	−0.05	N.D.	4.70	14.0	2.30	−0.05	−1.00	30.00	−0.25	0.88	FUS-ICP-MS, TD-ICP-MS
403	126	56.0	−2.5	1.00	−0.10	−0.50	0.85	N.D.	−0.05	N.D.	11.60	15.0	1.30	−0.05	−1.00	7.00	1.00	0.33	FUS-ICP-MS, TD-ICP-MS
312	159	86.0	−2.5	1.00	−0.10	−0.50	0.93	N.D.	−0.05	N.D.	14.80	19.0	1.30	−0.05	−1.00	7.00	1.00	0.32	FUS-ICP-MS, TD-ICP-MS
261	43	2.5	6.0	−0.50	2.00	0.20	0.26	1.10	−0.05	−0.05	12.70	17.0	1.60	−0.05	1.00	5.00	0.10	−0.03	FUS-ICP-MS, TD-ICP-MS
200	94	8.0	9.0	1.00	−0.10	1.10	1.47	1.30	0.50	−0.05	1.20	15.0	1.20	−0.05	0.50	7.10	−0.05	−0.03	FUS-ICP-MS, TD-ICP-MS
12	61	200.0	6.0	2.00	2.10	4.50	2.43	5.00	−0.50	−0.05	13.80	21.0	1.70	0.10	0.40	1.30	−0.05	1.27	FUS-ICP-MS, TD-ICP-MS
474	35	8.3	3.0	2.00	0.90	0.30	0.63	3.60	−0.50	−0.05	2.30	17.0	2.10	−0.05	0.10	3.20	−0.05	−0.03	FUS-ICP-MS, TD-ICP-MS
452	50	17.7	7.0	1.00	1.50	0.30	0.58	6.80	−0.50	−0.05	1.60	20.0	1.40	−0.05	−0.05	4.70	−0.05	−0.03	FUS-ICP-MS, TD-ICP-MS
296	43	94.4	9.0	2.00	0.20	2.00	1.90	3.90	0.20	0.20	3.50	17.0	1.40	−0.05	1.30	11.10	0.20	0.40	FUS-ICP-MS, TD-ICP-MS
613	60	2.3	4.0	1.00	1.20	1.20	0.48	1.90	−0.50	0.10	2.30	18.0	1.30	−0.05	0.70	11.40	0.50	0.18	FUS-ICP-MS, TD-ICP-MS
88	110	4.0	1.0	−0.50	0.60	0.90	0.55	2.70	0.10	−0.05	0.20	15.0	1.30	−0.05	0.30	5.60	0.20	0.07	FUS-ICP-MS, TD-ICP-MS
375	64	22.6	6.0	1.00	2.50	0.80	0.37	1.80	0.10	0.10	5.30	22.0	1.50	−0.05	0.20	19.40	0.20	0.11	FUS-ICP-MS, TD-ICP-MS
179	142	17.8	2.0	1.00	0.70	3.00	2.66	2.10	0.10	−0.05	0.70	13.0	1.10	−0.05	1.20	2.50	0.30	0.09	FUS-ICP-MS, TD-ICP-MS
94	333	8.9	11.0	3.00	0.80	2.50	2.37	3.40	0.10	−0.05	0.40	19.0	1.80	0.10	1.20	3.30	0.30	−0.03	FUS-ICP-MS, TD-ICP-MS
116	31	143.0	10.0	2.00	2.90	1.70	2.36	7.50	0.30	−0.05	27.60	19.0	2.40	−0.05	0.40	10.40	0.10	0.81	FUS-ICP-MS, TD-ICP-MS
187	35	12.1	1.0	1.00	0.70	0.90	0.32	1.70	0.10	−0.05	1.00	19.0	1.10	−0.05	0.10	6.90	0.10	0.11	FUS-ICP-MS, TD-ICP-MS
91	38	9.7	2.0	−0.50	0.70	0.70	0.48	2.00	0.10	−0.05	0.50	12.0	1.10	−0.05	0.20	4.40	0.30	−0.03	FUS-ICP-MS, TD-ICP-MS
265	64	56.0	2.0	2.00	0.70	0.80	1.10	2.90	0.10	−0.05	1.70	17.0	1.30	−0.05	0.20	12.80	0.20	0.13	FUS-ICP-MS, TD-ICP-MS
414	89	67.3	5.0	2.00	−0.10	0.50	0.48	−0.25	−0.05	−0.05	8.40	21.0	1.80	−0.05	0.40	7.80	0.10	0.29	FUS-ICP-MS, TD-ICP-MS
23	170	151.0	3.0	2.00	−0.10	5.10	2.77	0.60	−0.05	−0.05	3.90	18.0	2.00	−0.05	0.30	5.00	−0.05	0.80	FUS-ICP-MS, TD-ICP-MS
438	138	21.6	3.0	1.00	−0.10	0.80	0.34	−0.25	−0.05	−0.05	1.80	18.0	1.50	−0.05	0.50	6.10	−0.05	−0.03	FUS-ICP-MS, TD-ICP-MS
90	177	99.2	5.0	2.00	3.90	1.10	1.15	1.10	0.20	2.50	10.10	18.0	1.50	−0.05	0.50	14.40	0.90	1.03	FUS-ICP-MS, TD-ICP-MS
57	70	91.0	−0.5	3.00	−0.10	3.00	3.44	0.50	−0.05	0.10	3.00	21.0	1.90	0.10	0.70	15.60	0.20	0.36	FUS-ICP-MS, TD-ICP-MS
143	158	71.3	3.0	2.00	0.40	0.70	1.83	0.70	0.70	−0.05	5.30	16.0	1.10	−0.05	0.20	7.40	0.20	0.20	FUS-ICP-MS, TD-ICP-MS
272	25	85.1	4.0	2.00	−0.10	0.50	2.67	−0.25	−0.05	−0.05	2.50	16.0	1.40	−0.05	−0.05	23.40	−0.05	0.46	FUS-ICP-MS, TD-ICP-MS
140	79	8.2	12.0	−0.50	−0.10	1.40	0.35	−0.25	−0.05	−0.05	0.30	15.0	1.20	−0.05	0.60	7.70	−0.05	−0.03	FUS-ICP-MS, TD-ICP-MS
100	83	74.2	5.0	1.00	1.90	0.80	1.29	2.50	0.10	−0.05	3.30	15.0	1.40	−0.05	0.20	69.90	0.30	0.32	FUS-ICP-MS, TD-ICP-MS
48	68	69.4	3.0	−0.50	1.00	1.70	1.10	2.10	0.10	1.10	1.70	8.0	1.20	−0.05	0.40	27.00	0.40	0.86	FUS-ICP-MS, TD-ICP-MS
116	74	104.0	5.0	2.00	2.30	0.80	1.29	3.70	0.10	−0.05	4.00	14.0	1.80	−0.05	0.10	13.20	0.20	0.59	FUS-ICP-MS, TD-ICP-MS
240	77	3.3	4.0	1.00	0.90	1.20	1.17	3.80	0.10	−0.05	1.60	11.0	1.30	−0.05	0.40	3.60	0.10	0.13	FUS-ICP-MS, TD-ICP-MS
362	74	10.8	1.0	−0.50	0.90	0.70	1.43	6.60	−0.05	−0.05	3.40	17.0	1.60	−0.05	0.10	3.70	0.10	−0.03	FUS-ICP-MS, TD-ICP-MS
43	54	18.8	21.0	1.00	1.50	2.50	1.62	3.40	0.30	−0.05	0.50	13.0	1.70	−0.05	0.20	30.00	0.20	−0.03	FUS-ICP-MS, TD-ICP-MS
439	74	3.1	1.0	1.00	1.00	1.00	0.26	1.80	−0.05	−0.05	3.60	17.0	1.60	−0.05	0.10	4.20	0.10	−0.03	FUS-ICP-MS, TD-ICP-MS
306	95	30.5	1.0	1.00	0.70	0.90	0.99	3.10	0.10	−0.05	2.30	18.0	1.10	−0.05	0.20	12.40	0.30	0.07	FUS-ICP-MS, TD-ICP-MS
52	175	123.0	−2.5	3.00	0.40	3.00	3.59	1.80	0.20	N.D.	1.80	18.0	2.30	−0.05	−1.00	6.00	2.20	1.00	ICP-MS
487	112	28.0	6.0	2.00	−0.10	2.00	0.84	1.20	−0.05	N.D.	6.50	19.0	1.70	−0.05	−1.00	8.00	1.60	0.38	ICP-MS
48	110	189.0	8.0	3.00	−0.10	2.00	2.60	0.70	−0.05	N.D.	4.50	15.0	0.70	−0.05	−1.00	18.00	0.70	0.78	ICP-MS
327	154	144.8	N.D.	N.D.	N.D.	N.D.	2.11	N.D.	N.D.	N.D.	4.62	N.D.	N.D.	N.D.	N.D.	34.36	N.D.	N.D.	ICP-MS
129	119	147.2	N.D.	N.D.	N.D.	N.D.	2.64	N.D.	N.D.	N.D.	2.53	N.D.	N.D.	N.D.	N.D.	21.91	N.D.	N.D.	ICP-MS
388	111	114.8	N.D.	N.D.	N.D.	N.D.	0.81	N.D.	N.D.	N.D.	2.07	N.D.	N.D.	N.D.	N.D.	−2.50	N.D.	N.D.	ICP-MS
97	87	147.0	N.D.	N.D.	N.D.	N.D.	1.38	N.D.	N.D.	N.D.	2.50	N.D.	N.D.	N.D.	N.D.	28.47	N.D.	N.D.	ICP-MS
427	149	35.3	N.D.	N.D.	N.D.	N.D.	0.52	N.D.	N.D.	N.D.	0.51	N.D.	N.D.	N.D.	N.D.	6.81	N.D.	N.D.	ICP-MS
393	296	89.5	N.D.	N.D.	N.D.	N.D.	1.45	N.D.	N.D.	N.D.	1.87	N.D.	N.D.	N.D.	N.D.	6.97	N.D.	N.D.	ICP-MS
1024	84	12.7	N.D.	N.D.	N.D.	N.D.	1.36	N.D.	N.D.	N.D.	2.28	N.D.	N.D.	N.D.	N.D.	5.13	N.D.	N.D.	ICP-MS
381	148	58.4	N.D.	N.D.	N.D.	N.D.	1.23	N.D.	N.D.	N.D.	1.23	N.D.	N.D.	N.D.	N.D.	2.50	N.D.	N.D.	ICP-MS
−3	21	232.1	N.D.	N.D.	N.D.	N.D.	4.02	N.D.	N.D.	N.D.	3.70	N.D.	N.D.	N.D.	N.D.	12.49	N.D.	N.D.	ICP-MS
−3	46	233.8	N.D.	N.D.	N.D.	N.D.	2.49	N.D.	N.D.	N.D.	5.04	N.D.	N.D.	N.D.	N.D.	16.37	N.D.	N.D.	ICP-MS
−3	45	194.6	N.D.	N.D.	N.D.	N.D.	1.19	N.D.	N.D.	N.D.	2.88	N.D.	N.D.	N.D.	N.D.	20.86	N.D.	N.D.	ICP-MS
52	19	151.4	N.D.	N.D.	N.D.	N.D.	1.95	N.D.	N.D.	N.D.	3.99	N.D.	N.D.	N.D.	N.D.	16.60	N.D.	N.D.	ICP-MS
34	32	184.5	N.D.	N.D.	N.D.	N.D.	1.84	N.D.	N.D.	N.D.	6.95	N.D.	N.D.	N.D.	N.D.	−2.50	N.D.	N.D.	ICP-MS
653	143	86.4	N.D.	N.D.	N.D.	N.D.	1.84	N.D.	N.D.	N.D.	1.92	N.D.	N.D.	N.D.	N.D.	11.38	N.D.	N.D.	ICP-MS

prevalence of intermediate to acidic rocks particularly in the Permian units. The only exception is the Pastos Blancos Formation that in its base is composed of basaltic andesites whereas the upper part is a sequence of rhyolites and rhyolitic tuffs. The volcanic rocks are all porphyritic but some aphanitic basalts are present in the Quebrada del Salitre and La Ternera formations. Sampled units cropping out in the Frontal and Domeyko Cordillera are, from north to south: Cerro Rincones Beds and the La Tabla, Cerro Guanaco, Quebrada del Salitre, La Ternera, Guanaco Sonso, Pastos Blancos, La Totora and Algarrobal formations.

Table 3
Sr, Nd and Pb isotopic composition of the studied samples. Laboratory internal precision is 0.1% for each ratio. Initial ratio were calculated using the elemental ratios (Rb/Sr, Sm/Nd, Th/Pb and U/Pb) from Table 1 and Ortiz and Merino (2015), Salazar and Coloma (2016) and Coloma et al. (2017), decay constants $\lambda_{87Rb} = 1.42 \times 10^{-11}$ yr^{-1}, $\lambda_{147Sm} = 6.54 \times 10^{-12}$ yr^{-1}, $\lambda_{232Th} = 4.9475 \times 10^{-11}$yr^{-1}, $\lambda_{235U} = 9.8485 \times 10^{-10}$ yr^{-1}, $\lambda_{238U} = 1.5513 \times 10^{-10}$ yr^{-1}, and the ages assigned to geological units listed in Table 1 and Supplementary Material 2.

Sample	Unit	Petrography	East	North	$^{87}Sr/^{86}Sr$	±	$^{87}Rb/^{86}Sr$	±	$(^{87}Sr/^{86}Sr)_i$	$^{147}Sm/^{144}Nd$	±
CPV-12-23[a]	La Totora Formation	Andesite	376,484	6,814,323	0.705281	N.D.	0.192082	N.D.	0.704692	0.131692	N.D.
CPV-12-24[a]	La Totora Formation	Andesite	383,333	6,826,718	0.706232	N.D.	0.023013	N.D.	0.706161	0.160713	N.D.
CPV-12-38[a]	San Félix Formation	Lithic tuff	362,530	6,778,657	0.772771	N.D.	24.342171	N.D.	0.688111	0.116632	N.D.
CPV-12-49b[a]	San Félix Formation	Lithic tuff	359,174	6,805,415	0.713912	N.D.	2.564980	N.D.	0.704991	0.124326	N.D.
CPV-12-60[a]	La Totora Formation	Basalt	382,348	6,827,655	0.705249	N.D.	0.058141	N.D.	0.705071	0.122780	N.D.
CPV-12-91A[a]	Carrizal Bajo Complex	Diorite	301,526	6,884,546	0.707604	N.D.	0.463108	N.D.	0.706241	0.156654	N.D.
CPV-12-91B[a]	Carrizal Bajo Complex	Tonalite	301,526	6,884,546	0.710087	N.D.	0.941808	N.D.	0.707315	0.107727	N.D.
CPV-12-92[a]	Algodones Granite	Quartz diorite	298,038	6,887,501	0.705248	N.D.	0.184637	N.D.	0.704720	0.136342	N.D.
CPV-12-93[a]	Carrizal Bajo Complex	Granite	288,859	6,878,634	0.740676	N.D.	11.585174	N.D.	0.706572	0.148031	N.D.
SCL-02q[b]	Chollay Plutonic Complex	Monzogranite	410,948	6,804,964	0.728949	N.D.	9.526124	N.D.	0.695682	0.117300	N.D.
SCL-09q[b]	Chollay Plutonic Complex	Granodiorite	410,315	6,794,865	0.709081	N.D.	1.289932	N.D.	0.704576	0.114931	N.D.
SCL-26q[b]	La Totora Formation	Rhyolitic tuff	414,172	6,808,064	0.720557	N.D.	7.418839	N.D.	0.697566	0.107184	N.D.
O7–06[a]	Montegrande Granite	Granite	357,424	6,668,630	0.717407	N.D.	2.561413	N.D.	0.709612	0.081563	N.D.
O7–07[a]	Montegrande Granite	Granite	361,047	6,666,761	0.739412	N.D.	12.313627	N.D.	0.701936	0.095807	N.D.
O7–10[a]	La Laguna Gabbro	Gabbro	396,451	6,669,570	0.706910	N.D.	0.311530	N.D.	0.705944	0.132288	N.D.
O7–11[a]	La Laguna Gabbro	Gabbro	396,266	6,669,913	0.706784	N.D.	0.357314	N.D.	0.705676	0.132747	N.D.
O7–13[a]	Guanta Plutonic Complex	Granodiorite	368,473	6,695,942	0.707952	N.D.	0.338900	N.D.	0.706554	0.104338	N.D.
O7–15[a]	Guanta Plutonic Complex	Tonalite	366,163	6,697,056	0.709614	N.D.	0.980228	N.D.	0.705485	0.130041	N.D.
CPV-12-105[a]	Llano de Chocolate Beds	Rhyolite	286,402	6,789,103	0.717356	N.D.	3.577483	N.D.	0.701124	0.132543	N.D.
CPV-12-12[a]	Llano de Chocolate Beds	Dacite	289,084	6,794,562	0.711739	N.D.	2.100524	N.D.	0.702658	0.122331	N.D.
CPV-12-127[a]	Llano de Chocolate Beds	Rhyolitic tuff	287,052	6,792,338	0.728827	N.D.	7.104194	N.D.	0.698114	0.156505	N.D.
CPV-12-01[a]	La Vaca Granodiorite	Diabase	257,848	6,780,649	0.707362	N.D.	0.489877	N.D.	0.706108	0.173803	N.D.
CPV-12-03[a]	La Vaca Granodiorite	Granodiorite	264,762	6,778,121	0.705755	N.D.	0.712174	N.D.	0.703750	0.124258	N.D.
CPV-12-26B[a]	Algarrobal Formation	Andesite (breccia fragment)	359,110	6,779,598	0.705429	N.D.	0.252732	N.D.	0.704880	0.159827	N.D.
CPV-12-28x[a]	Algarrobal Formation	Basaltic Andesite	361,226	6,778,404	0.706023	N.D.	0.351336	N.D.	0.705260	0.153155	N.D.
CPV-12-30x[a]	Algarrobal Formation	Andesite	359,946	6,778,193	0.706584	N.D.	1.059021	N.D.	0.704285	0.134207	N.D.
CPV-12-90[a]	Canto del Agua Formation	Lithic tuff	306,157	6,873,300	0.753027	N.D.	17.254616	N.D.	0.700821	0.149829	N.D.
CPV-14-176[b]	La Tabla Formation	Rhyolitic tuff	480,403	7,272,029	0.716532	N.D.	3.391408	N.D.	0.702291	0.118763	N.D.
CPV-14-180A[b]	Cifuncho Plutonic Complex	Monzogranite	335,853	7,160,972	0.713675	N.D.	1.876045	N.D.	0.706116	0.133984	N.D.
CPV-14-181B[b]	Sierra Esmeralda Plutonic Complex	Monzodiorite	342,187	7,138,664	0.706378	N.D.	0.099754	N.D.	0.706104	0.164938	N.D.
CPV-14-182B[b]	Sierra Esmeralda Plutonic Complex	Tonalite	342,760	7,134,508	0.706446	N.D.	0.662008	N.D.	0.704624	0.135504	N.D.
CPV-14-184[b]	Cifuncho Formation	Andesite (porphyry)	340,042	7,134,594	0.706198	N.D.	0.407961	N.D.	0.704968	0.133138	N.D.
CPV-14-187[b]	Cifuncho Formation	Andesite	339,123	7,134,911	0.706049	N.D.	0.480672	N.D.	0.704613	0.130071	N.D.
CPV-14-190[b]	Cifuncho Formation	Dacite (porphyry)	337,489	7,133,332	0.705932	N.D.	0.437557	N.D.	0.704612	0.140619	N.D.
CPV-14-191[b]	Cifuncho Plutonic Complex	Monzogranite	331,989	7,133,968	0.724988	N.D.	3.943363	N.D.	0.710543	0.131223	N.D.
CPV-14-192[b]	Pan de Azúcar Pluton	Granite	344,202	7,119,705	0.764289	N.D.	13.344639	N.D.	0.712828	0.164345	N.D.
CPV-14-194[b]	Agua Chica Formation	Dacitic tuff	346,064	7,116,574	0.706659	N.D.	0.401998	N.D.	0.705516	0.134879	N.D.
CPV-14-198[b]	Agua Chica Formation	Andesite	345,848	7,117,138	0.707456	N.D.	0.797477	N.D.	0.705188	0.133824	N.D.
CPV-14-245[b]	Quebrada del Salitre Formation	Basaltic Andesite	476,322	7,196,656	0.705226	N.D.	0.027706	N.D.	0.705142	0.162681	N.D.
CPV-14-247[b]	Quebrada del Salitre Formation	Lapilli tuff	478,187	7,202,622	0.707710	N.D.	0.115730	N.D.	0.707361	0.136957	N.D.
CPV-14-249[b]	La Tabla Formation	Rhyolitic tuff	477,668	7,201,891	0.876917	N.D.	49.018932	N.D.	0.673243	0.132040	N.D.
CPV-14-253[b]	Quebrada del Salitre Formation	Basalt	476,972	7,201,597	0.707463	N.D.	0.050661	N.D.	0.707310	0.163548	N.D.
CPV-14-256[b]	Quebrada del Salitre Formation	Basaltic andesite	469,978	7,201,796	0.706121	N.D.	0.113280	N.D.	0.705746	0.156501	N.D.
CPV-14-263[b]	Cerro Rincones Beds	Dacite	480,329	7,252,855	0.712774	N.D.	0.923167	N.D.	0.708917	0.116623	N.D.
CPV-15-303[b]	Quebrada del Salitre Formation	Basaltic andesite	467,921	7,113,260	0.707072	N.D.	0.470297	N.D.	0.705654	0.153351	N.D.
CPV-15-310[b]	Quebrada del Salitre Formation	Rhyolite	462,332	7,114,194	0.783389	N.D.	19.135402	N.D.	0.725697	0.143350	N.D.
CPV-15-311[b]	Quebrada del Salitre Formation	Basalt	467,495	7,132,147	0.706261	N.D.	0.142660	N.D.	0.705788	0.158989	N.D.
CPV-15-312[b]	Quebrada del Salitre Formation	Andesite	471,764	7,136,501	0.711310	N.D.	3.190121	N.D.	0.700738	0.126051	N.D.
CPV-15-314[b]	Quebrada del Salitre Formation	Rhyolite (dome)	467,881	7,125,180	0.724584	N.D.	4.626663	N.D.	0.709251	0.133384	N.D.
CPV-15-319[b]	Quebrada del Salitre Formation	Dacite	465,751	7,126,652	0.709752	N.D.	1.442864	N.D.	0.705402	0.134681	N.D.
CPV-15-320[b]	Sierra de Doña Inés Chica Plutonic Complex	Quartz Monzodiorite	465,519	7,125,144	0.713253	N.D.	0.905693	N.D.	0.709576	0.125884	N.D.
CPV-15-322[b]	Quebrada del Salitre Formation	Andesite	460,778	7,123,934	0.708094	N.D.	0.169468	N.D.	0.707554	0.167180	N.D.
RCM-61q[b]	Colorado Syenogranite	Syenogranite	381,620	6,744,026	0.720311	N.D.	6.852070	N.D.	0.698383	0.130575	N.D.
RCM-78q[b]	Pastos Blancos Formation	Andesite	379,914	6,748,141	0.706036	N.D.	0.166319	N.D.	0.705501	0.129313	N.D.
SCL-28q[b]	Guanaco Sonso Formation	Rhyolitic tuff	423,238	6,807,445	0.744433	N.D.	11.433074	N.D.	0.703937	0.137724	N.D.
MCM-010q[b]	El León Monzogranites	Monzogranite	385,798	6,747,866	0.712216	N.D.	1.280321	N.D.	0.707621	0.116639	N.D.
MCM-022q[b]	Chollay Plutonic Complex	Syenogranite	396,485	6,760,228	0.716408	N.D.	3.312754	N.D.	0.704712	0.113900	N.D.
MCM-129q[b]	Chanchoquín Plutonic Complex	Quartz monzodiorite	368,977	6,772,428	0.713828	N.D.	0.857087	N.D.	0.710279	0.161306	N.D.
MCM-159q[b]	Upper Carboniferous Pluton	Tonalite	365,695	6,776,725	0.720205	N.D.	4.376437	N.D.	0.701297	N.D.	N.D.
MCM-168 Bq[b]	Quebrada Pinte Diorite	Diorite	375,805	6,786,355	0.706544	N.D.	0.239219	N.D.	0.705441	N.D.	N.D.
MCM-205q[b]	Guanta Plutonic Complex	Granodiorite	363,509	6,737,985	0.709394	N.D.	0.657955	N.D.	0.706667	0.126653	N.D.
MCM-265q[b]	Chollay Plutonic Complex	Monzogranite	388,323	6,790,790	0.710789	N.D.	0.035809	N.D.	0.710667	0.113489	N.D.
MCM-280q[b]	Guanta Plutonic Complex	Granodiorite	368,652	6,736,827	0.707837	N.D.	0.443607	N.D.	0.705938	0.131119	N.D.
RCM-015q[b]	Guanta Plutonic Complex	Syenogranite	358,677	6,736,102	0.756869	N.D.	269.900512	N.D.	−0.371497	0.165533	N.D.
RCM-040q[b]	Chollay Plutonic Complex	Tonalite	406,713	6,788,541	0.757628	N.D.	271.909100	N.D.	−0.150861	0.209212	N.D.
RCM-077q[b]	Chacaicito Pluton	Syenogranite	380,434	6,748,991	0.749256	N.D.	226.125420	N.D.	−0.309628	0.157639	N.D.
RCM-133q[b]	Chanchoquín Plutonic Complex	Granodiorite	365,378	6,767,843	0.710688	N.D.	8.395069	N.D.	0.675663	0.125301	N.D.
RCM-150q[b]	Guanaco Sonso Formation	Rhyolitic tuff	412,909	6,787,833	0.725080	N.D.	15.826631	N.D.	0.668254	0.108168	N.D.
SCL-96[b]	Guanaco Sonso Formation	Dacitic tuff	425,477	6,807,665	0.709549	N.D.	0.383130	N.D.	0.708193	0.143762	N.D.

$^{143}Nd/^{144}Nd$	±	εNd	$(^{143}Nd/^{144}Nd)_i$	εNd_i	$(^{206}Pb/^{204}Pb)_i$	$^{206}Pb/^{204}Pb$	$(^{207}Pb/^{204}Pb)_i$	$^{207}Pb/^{204}Pb$	$(^{208}Pb/^{204}Pb)_i$	$^{208}Pb/^{204}Pb$
0.512630	N.D.	−0.16	0.512444	1.63	18.62	18.80	15.66	15.67	38.49	38.74
0.512789	N.D.	2.95	0.512562	3.94	18.52	18.57	15.65	15.65	38.61	38.62
0.512308	N.D.	−6.44	0.512121	−3.94	18.21	19.32	15.65	15.71	37.72	39.65
0.512363	N.D.	−5.36	0.512164	−3.11	18.35	19.07	15.64	15.68	37.39	39.11
0.512605	N.D.	−0.64	0.512432	1.39	18.53	18.56	15.64	15.65	38.51	38.66
0.512218	N.D.	−8.19	0.512006	−7.14	18.77	19.17	15.76	15.78	38.78	39.40
0.512485	N.D.	−2.98	0.512339	−0.63	18.56	18.80	15.64	15.65	37.10	39.69
0.512756	N.D.	2.30	0.512577	3.85	18.69	18.96	15.69	15.70	38.57	39.08
0.512689	N.D.	0.99	0.512488	2.28	18.57	18.95	15.64	15.66	38.41	38.89
0.512498	N.D.	−2.74	0.512309	−0.25	18.13	18.75	15.55	15.58	37.89	38.67
0.512433	N.D.	−4.00	0.512248	−1.44	18.60	18.90	15.57	15.59	37.99	38.53
0.512568	N.D.	−1.36	0.512416	1.13	18.44	18.72	15.56	15.57	38.03	38.65
0.512199	N.D.	−8.56	0.512085	−5.42	18.54	18.56	15.65	15.65	38.45	38.50
0.512505	N.D.	−2.59	0.512371	0.16	18.47	18.57	15.64	15.65	38.54	38.70
0.512463	N.D.	−3.41	0.512274	−1.62	18.55	18.89	15.63	15.65	38.49	38.86
0.512482	N.D.	−3.04	0.512293	−1.26	18.65	19.03	15.74	15.76	38.65	39.10
0.512296	N.D.	−6.67	0.512098	−3.25	18.44	18.52	15.64	15.65	38.38	38.58
0.512310	N.D.	−6.40	0.512058	−3.88	18.61	18.94	15.68	15.70	38.81	39.07
0.512329	N.D.	−6.03	0.512052	−3.42	18.60	18.68	15.65	15.65	38.59	38.68
0.512325	N.D.	−6.11	0.512082	−3.22	17.77	19.81	15.60	15.71	36.88	40.34
0.512782	N.D.	2.81	0.512483	4.31	18.31	19.12	15.63	15.68	37.09	39.39
0.512955	N.D.	6.18	0.512750	6.71	18.54	19.03	15.71	15.73	38.63	39.18
0.512672	N.D.	0.66	0.512511	2.50	18.56	18.92	15.69	15.71	38.65	39.25
0.512616	N.D.	−0.43	0.512456	0.29	18.51	18.90	15.64	15.66	38.41	38.91
0.512803	N.D.	3.22	0.512650	4.07	18.61	18.69	15.68	15.69	38.60	38.73
0.512637	N.D.	−0.02	0.512503	1.20	18.56	19.00	15.65	15.67	38.48	39.04
0.512454	N.D.	−3.59	0.512245	−2.32	18.50	19.08	15.65	15.68	38.38	39.15
0.512341	N.D.	−5.79	0.512112	−2.85	18.47	19.32	15.60	15.65	37.86	39.40
0.512297	N.D.	−6.66	0.512048	−4.39	18.58	18.87	15.59	15.60	38.21	38.83
0.512775	N.D.	2.66	0.512566	3.45	18.40	18.96	15.57	15.59	38.74	39.11
0.512717	N.D.	1.54	0.512545	3.05	18.37	18.62	15.56	15.57	38.16	38.47
0.512693	N.D.	1.07	0.512508	2.79	18.30	18.61	15.53	15.55	38.03	38.40
0.512675	N.D.	0.72	0.512496	2.50	18.22	18.84	15.54	15.57	38.05	38.92
0.512683	N.D.	0.87	0.512488	2.39	18.01	18.80	15.61	15.65	37.92	38.83
0.512291	N.D.	−6.77	0.512070	−4.62	18.51	18.78	15.59	15.61	38.26	38.85
0.512354	N.D.	−5.54	0.512063	−4.42	18.44	18.74	15.57	15.59	38.16	38.33
0.512647	N.D.	0.17	0.512470	1.75	18.33	18.57	15.56	15.57	38.17	38.48
0.512557	N.D.	−1.58	0.512382	0.03	18.16	18.43	15.57	15.59	38.04	38.45
0.512677	N.D.	0.76	0.512451	1.68	18.39	18.50	15.55	15.55	38.11	38.30
0.512512	N.D.	−2.46	0.512322	−0.84	18.46	18.90	15.58	15.60	38.23	38.82
0.512322	N.D.	−6.16	0.512070	−3.76	15.58	21.65	15.45	15.76	31.34	45.60
0.512676	N.D.	0.74	0.512449	1.64	N.D.	N.D.	N.D.	N.D.	N.D.	N.D.
0.512739	N.D.	1.97	0.512500	3.17	18.34	18.62	15.55	15.57	38.15	38.46
0.512332	N.D.	−5.97	0.512108	−2.97	18.41	18.92	15.56	15.59	37.89	38.96
0.512704	N.D.	1.29	0.512491	2.46	18.39	18.52	15.55	15.56	38.16	38.36
0.512672	N.D.	0.66	0.512473	2.11	18.31	19.51	15.56	15.62	37.72	39.40
0.512814	N.D.	3.43	0.512572	4.56	18.43	18.56	15.57	15.58	38.26	38.39
0.512519	N.D.	−2.32	0.512327	−0.22	18.51	18.70	15.58	15.59	38.30	38.60
0.512614	N.D.	−0.47	0.512411	1.42	18.28	18.80	15.55	15.58	37.99	38.69
0.512638	N.D.	0.00	0.512451	1.68	18.33	18.86	15.56	15.58	38.11	38.63
0.512304	N.D.	−6.52	0.512069	−3.94	18.36	18.69	15.56	15.57	38.04	38.60
0.512930	N.D.	5.70	0.512685	6.54	18.41	18.51	15.60	15.61	38.35	38.41
0.512514	N.D.	−2.41	0.512322	−0.51	17.84	19.21	15.55	15.62	37.27	39.05
0.512438	N.D.	−3.90	0.512247	−1.95	18.36	18.60	15.57	15.58	38.15	38.44
0.512444	N.D.	−3.78	0.512220	−1.91	18.52	18.89	15.57	15.59	38.17	38.76
0.512312	N.D.	−6.36	0.512119	−3.78	18.77	18.93	15.62	15.63	38.49	38.81
0.512345	N.D.	−5.72	0.512160	−3.09	18.62	18.93	15.60	15.61	38.31	38.90
0.512116	N.D.	−10.18	0.511809	−8.87	17.54	18.49	15.53	15.58	35.31	38.45
N.D.	N.D.	0.00	N.D.	N.D.	18.45	18.60	15.58	15.59	38.12	38.47
N.D.	N.D.	0.00	N.D.	N.D.	18.29	18.54	15.57	15.58	38.06	38.37
0.512363	N.D.	−5.36	0.512121	−2.76	17.66	18.27	15.52	15.56	36.49	37.67
0.512415	N.D.	−4.35	0.512237	−1.80	18.11	18.75	15.57	15.60	37.20	38.69
0.512364	N.D.	−5.34	0.512106	−2.83	17.24	18.75	15.51	15.59	36.29	38.68
0.512343	N.D.	−5.75	0.512025	−4.59	18.09	19.05	15.55	15.60	36.65	38.77
0.512396	N.D.	−4.72	0.512074	−5.10	18.48	18.84	15.59	15.61	37.82	38.64
0.512335	N.D.	−5.91	0.511995	−4.27	18.47	18.66	15.59	15.60	38.15	38.65
0.512337	N.D.	−5.87	0.512097	−3.20	18.83	19.18	15.59	15.61	38.57	39.20
0.512410	N.D.	−4.44	0.512232	−1.59	20.56	18.69	15.66	15.57	43.43	38.59
0.512637	N.D.	−0.02	0.512403	1.66	18.65	19.05	15.60	15.62	38.14	38.78

[a] Geosciences Department, University of Arizona.
[b] Isotope Geochemistry laboratory of the MARUM Center, University of Bremen.

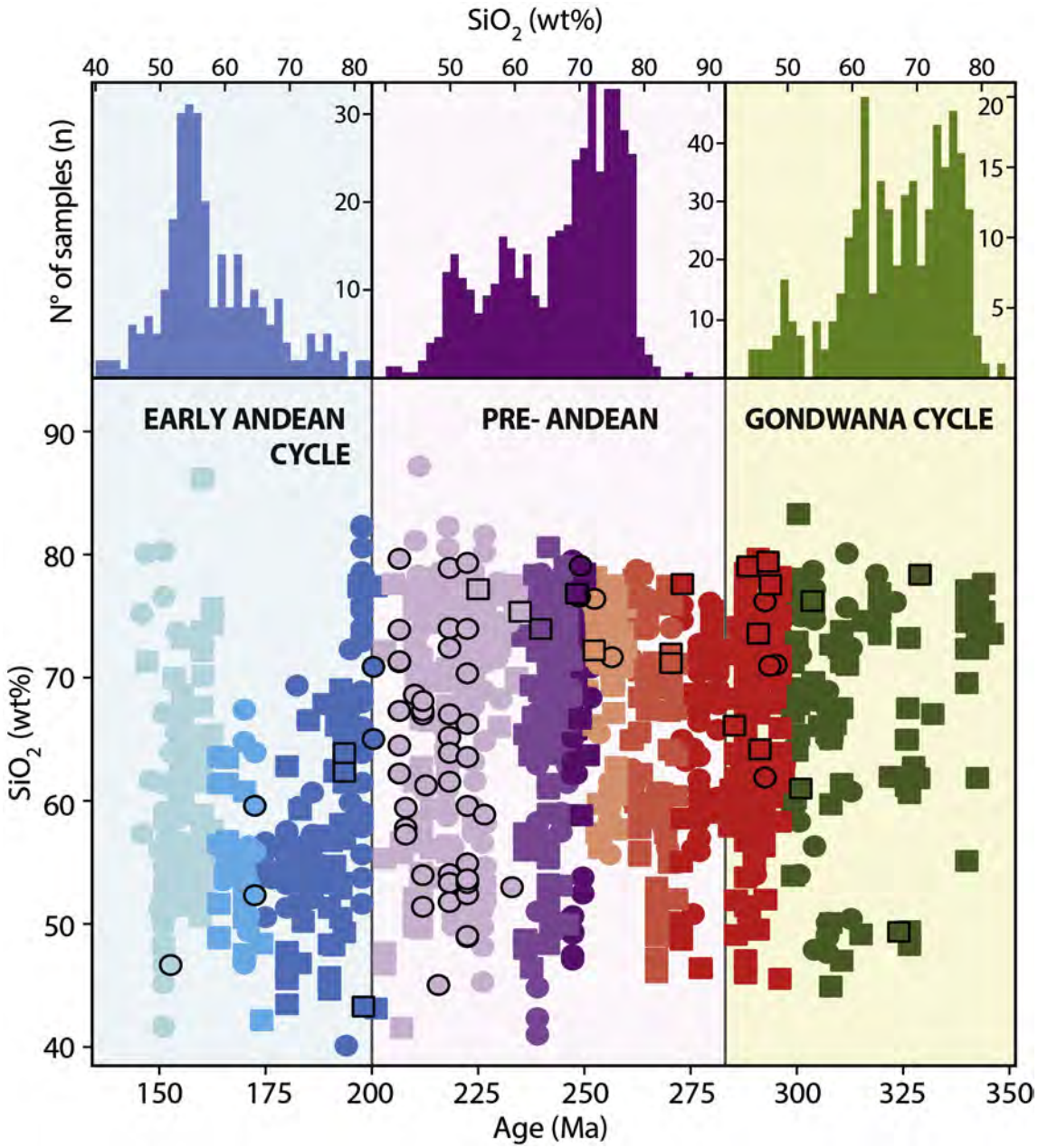

Fig. 4. SiO_2 content (wet-free basis) of samples from Carboniferous to Jurassic igneous units. Circles correspond to volcanic rocks and squares to plutonic rocks, symbols with black stroke correspond to samples analyzed for this study.

The collected samples from Permian units (La Tabla Formation, 24°′00–27°00′S; Guanaco Sonso Formation, 27°30′-31°00′S; Cerro Rincones Beds, 24°10′-24°30′S) correspond to rhyolitic tuffs and dacites with plagioclase, quartz and minor alkali feldspar phenocyrsts, felsitic groundmass or glassy matrix, and scarce acidic lithics. Samples from Cerro Guanaco Formation (24°45–25°10′S) are andesites and andesitic tuffs bearing plagioclase amphibole and opaque minerals phenocrysts, with minor clinopyroxene or biotite, and intersestal or intergranular groundmass with plagioclase microliths, altered mafics and devitrified glass.

The Quebrada del Salitre (25°15′-26°15′S) samples comprise: i) apahnitic to fine grained porphyritic basalts and basaltic andesites with ubiquitous plagioclase phenocrysts and minor olivine or in a groundmass of slightly oriented plagioclase microliths, altered mafics (clinopryroxene and olivine?) and opaque minerals; iii) porphyritic andesites and dacites with either plagioclase-clinopyroxene or plagioclase-quartz-K-feldspar-amphibole phenocrysts and intersestal or intergranular groundmass; iii) porphyritic (fine grained) rhyolites with scarce plagioclase and quartz phenocysts in a felsitic groundmass and iv) lithic and crystalline tuffs with quartz and plagioclase phenocryst and minor pyroxene or undetermined mafic minerals, andesitic to dacitic lithics in a glassy matrix.

Samples from La Ternera Formation (27°00′-28°15′S) correspond to apahnitic to fine grained porphyritic basalts with small clinopyroxene and altered olivine phenocrysts in a hialopilitic groundmass with altered mafics and opaque minerals; porphyritic basaltic andesites and andesites with plagioclase and clinopyroxene phenocrysts, in an intersestal groundmass of plagioclase microliths, variable amounts of quartz, mafics and devitrified glass. Pyroclastic and epiclastic samples in this unit correspond to lithic and crystalline tuffs with quartz, plagioclase and K-feldspar phenocrysts, andesitic to dacitic lithics in a glassy matrix. Samples from la Totora Formation (28°15′-29°15′S) correspond to aphanitic or fine

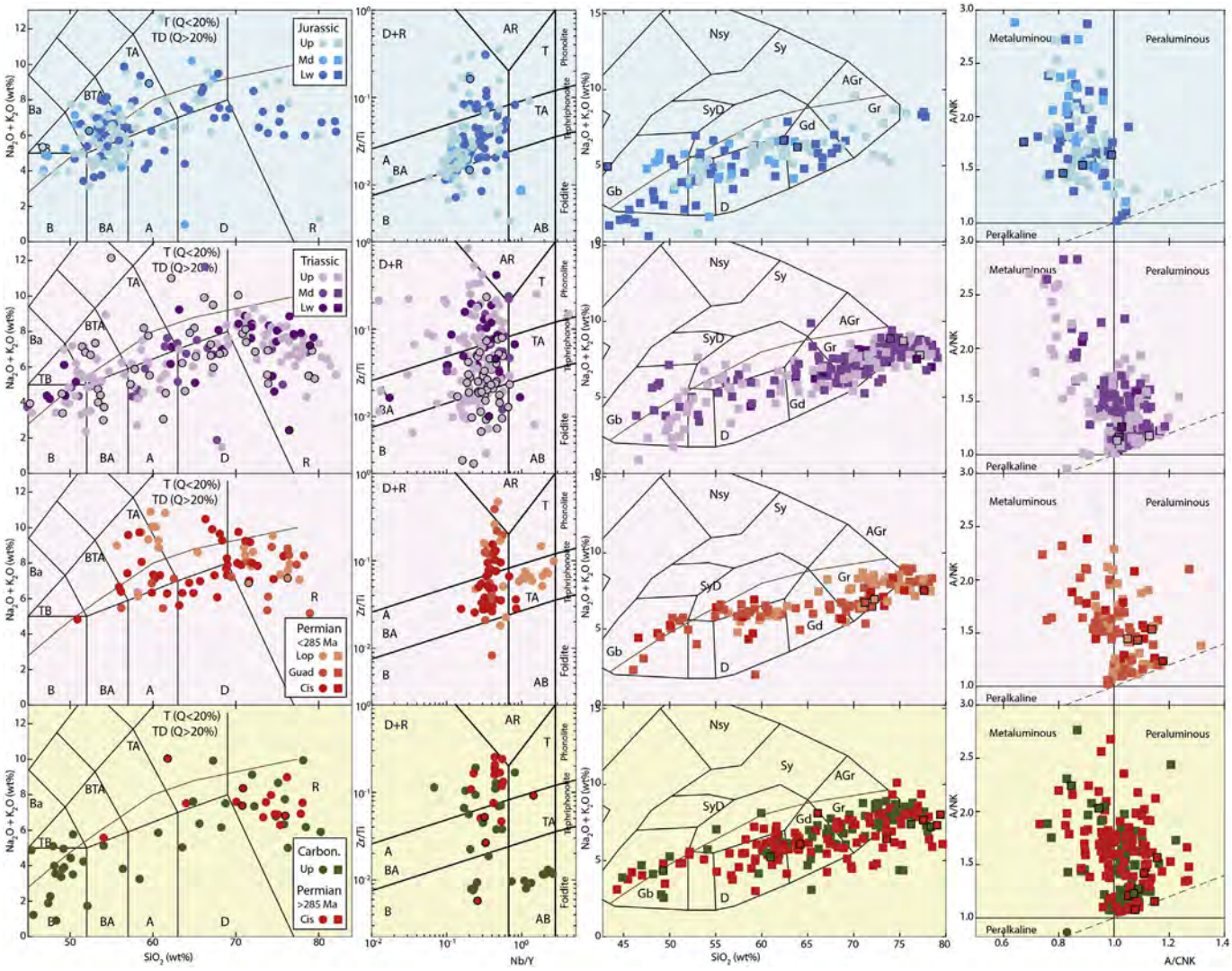

Fig. 5. Irvine and Baragar (1971) TAS diagram (first column from left to right) for volcanic rocks, Sr/Ti vs Nb/Y diagram (second column) for altered volcanic rocks (Pearce, 1996, after Winchester and Floyd, 1977); TAS (third column) (Cox et al., 1979) and Shand's index diagram (Shand, 1943) (fourth column) for plutonic rocks. Circles correspond to volcanic rocks and squares to plutonic rocks, symbols with black stroke correspond to samples analyzed for this study. Carbon.: Carboniferous; Cis >285 Ma: Cisuralian older than 285 Ma; Cis <285 Ma: Cisuralian younger than 285 Ma; Guad: Guadalupian; Lop: Lopingian; Up: Upper, Md: Middle; Lw: Lower. Series age limits are from (Cohen et al., 2013). Background colors are as in Fig. 3 and refer to the Gondwana, Pre-Andean, and Andean cycles. Ba: Basanite; TB: Trachybasalt; B: Basalt; AB: Alkali Basalt; BTA: Basaltic Trachyandesite; TA: Trachyandesite; A: Andesite; T: Trachyte; TD: Trachydacite; D: Dacite; R: Rhyolite; AR: Alkali Rhyolite; Q: Quartz; Gb: Grabbro: SD: Syenodiorite; D: Diorite; GD: Graniodiorite/Quartz-diorite; Sy: Syenite; Gr: Granite; A-Gr: Alkali Granite; NSy: Nepheline syenite.

grained porphyritic basaltic andesites with small plagioclase, clinopyroxene or olivine phenocrysts in an intersestal groundmass with plagioclase microliths, altered mafics, opaque minerals and devitrified glass. The only sample from the Pastos Blancos Formation (27°00′-31°00′S) is a porphyritic andesite with plagioclase, scarce biotite and undetermined mafic phenocrysts in and intersertal groundmass with plagioclase microliths, altered mafics, opaque minerals and devitrified glass.

Three volcanic units, the Canto del Agua, Agua Chica and Cifuncho formations, were sampled near the coastline (Fig. 2). The single sample of the Canto del Agua Formation (28°15′S) is a lithic tuff with andesitic fragments, plagioclase and minor quartz phenocrysts and an ash (mainly glassy) matrix. The samples from Agua Chica Formation (26°05′S) are one andesitic lava flow and one crystalline tuff with plagioclase and minor biotite and amphibole phenocrysts, instersticial groundmass or glassy matrix. The Cifuncho formation (25°20′-26°00′S) samples are porphyritic and dacitic lavas or subvolcanic bodies, with plagioclase and quartz as the most abundant phenocrysts, and minor biotite and/or amphibole, the groundmass is intergranular (andesite) of felsitic (dacite) with scarce mafics.

4.3. Early Andean cycle

The Jurassic intrusives are very common in the Coastal Cordillera (Coastal Batholith) but absent in the Frontal and Domeyko Cordilleras, the two units sampled for this study are the Lower Jurassic: Sierra Esmeralda Plutonic Complex (25°55′S), medium grained biotite- amphibole monzodiorite and amphibole-muscovite tonalite; and Quebrada la Vaca Granodiorite (29°05′S), a medium grained biotite-clinopyroxene grandiorite with (and one aphanitic equivalent). The Upper Jurassic-Lower Cretaceous volcanic Algarrobal Formation (29°00′-31°S) was also sampled in the Frontal Cordillera, the collected rocks correspond to porphyritic basaltic andesites.

5. Elemental and Sr-Nd-Pb isotope geochemistry

Elemental and Sr-Nd-Pb isotopic compositions of the analyzed samples are listed in Table 2 and Table 3, respectively. Additional data on elemental composition, concerning samples with isotope results in this

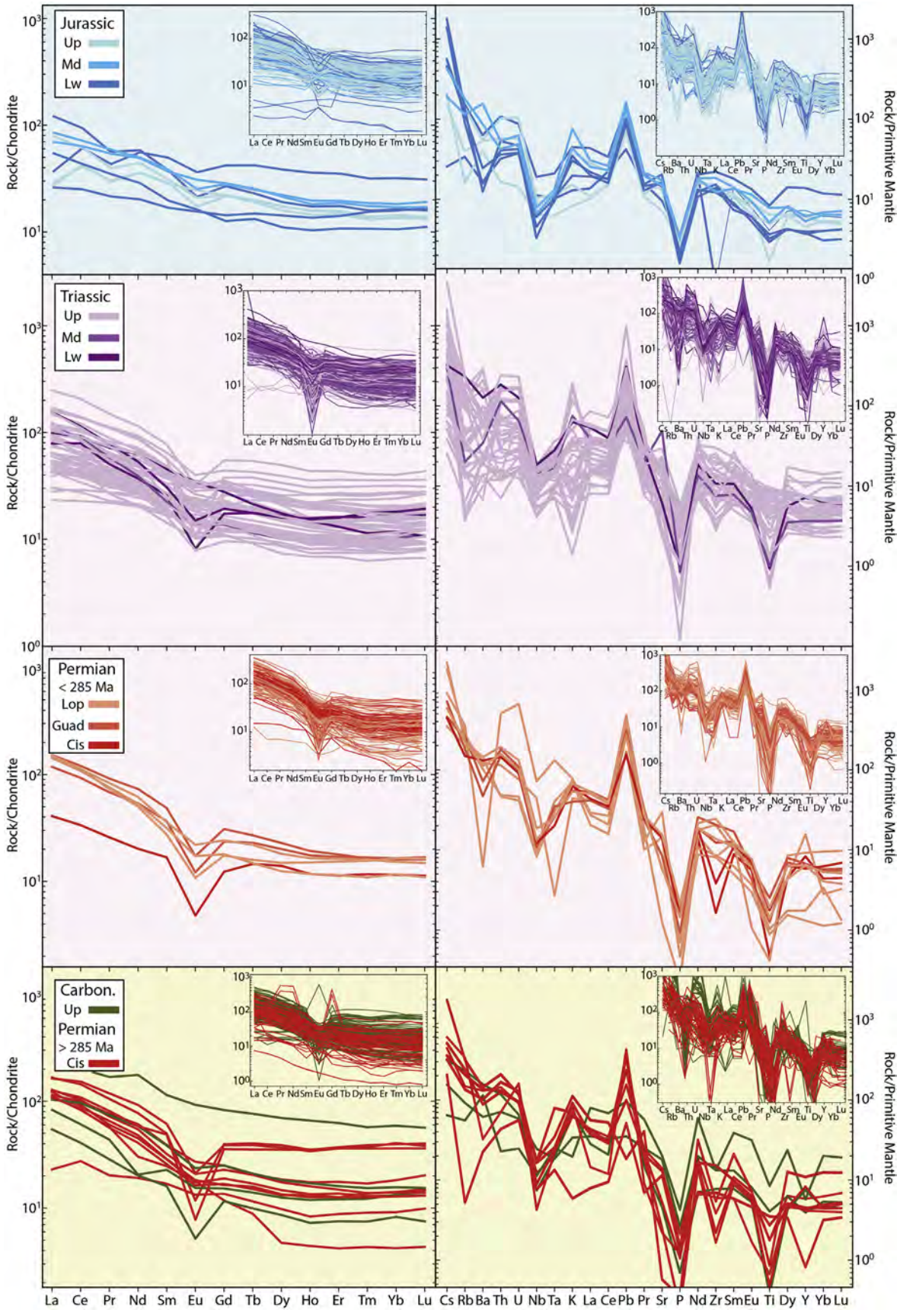

Fig. 6. Chondrite-normalized REE (left column diagrams) and primitive mantle normalized trace elements composition of analyzed rocks (right column diagrams). Inset in each diagram correspond to published data. Legends are as in Fig. 5. Chondrite and primitive mantle composition are from Sun and McDonough (1989). Background colors are as in Fig. 3 and refer to the Gondwana, Pre-Andean, and Andean cycles.

work, are Supplementary Material 3. The ages used for the calculation of initial isotopic ratios and for εNd initial are given in the Supplementary Material 2.

The normalized SiO_2 content (wt% free of volatile phase) of the analyzed samples and published data exhibit a mixed distribution with two pronounced peaks at the 51.0–56.5% (~basaltic andesite) and 62.1–70.0% (~dacite) intervals (Fig. 4). In the Carboniferous to Permian and in many Triassic rocks there is a strong dominance of intermediate to silicic compositions although the Triassic suites have a slightly higher proportion of ~basaltic andesite compositions. The Jurassic rocks are different with a large population below 60% SiO_2. According to the TAS classification diagrams volcanic rocks range from basalts to rhyolite and plutonic rocks from gabbro to granite; the samples plot within or close to the subalkaline field (Fig. 5).

In the case of volcanic rocks, when using the classification diagram for altered rocks, all but three samples plot in the subalkaline field (Fig. 5), suggesting that the moderate to strong alteration degree observed in the studied volcanic units (see Table 1 and Supplementary Material) may have induced a Na—K metasomatism in the rocks. Intrusive rocks are mostly peraluminous but plot close to the metaluminous field. Carboniferous to Permian rocks and, to a minor extent Triassic rocks, are mostly peraluminous, whereas Jurassic intrusion are mostly metaluminous; only two samples of the late Triassic Montegrande Granite plot in the peralkaline field (Fig. 5).

The chondrite normalized REE patterns of the samples are relatively flat, with the exception of some Permian and Triassic samples, the La_N/Yb_N range from 1.08 to 16.50 (with two Permian samples as outliers at 38 and 40). The highest REE contents are for Carboniferous and Permian samples, whereas the lowest are for Upper Triassic and Jurassic rocks (Fig. 6). Negative Eu anomalies are observed in the majority of the samples, but much less pronounced for the Jurassic rocks; thus Eu/Eu* ranges from 0.19 to 1.10 in all samples and from 0.67 to 1.03 in the Jurassic samples. The Primitive Mantle-normalized spider diagrams for trace elements show similar patterns for all the studied samples (Fig. 6). Although there is a significant dispersion among LILE (large-ion lithophile elements), these elements are systematically enriched over HFSE (high field strength elements), for which the contents are similar to depleted mantle sources. Marked troughs in Nb, Ta, Ti and Zr, along with prominent peaks in K and Pb are also shared features in all samples (Fig. 6).

The isotopic composition of the samples is moderately variable for Nd and Pb and more scattered for Sr. Most of the analyzed samples plot along or near the mantle array, but units representing the Gondwana cycle plot closer to the continental crust than those representing the Early Andean cycle (Fig. 7a). Samples representing the Pre-Andean stage plot roughly in between the other two groups (Fig. 7a). The Pb isotopic composition is close to the enriched mantle field for the samples of the Gondwana, Pre-Andean and Early Andean units (Fig. 7b).

6. Discussion

6.1. A geochemical perspective for the evolution of the SW Gondwana margin: continuous subduction from Carboniferous to Jurassic?

It has long been proposed that the composition of the igneous rocks of the Gondwana cycle and Pre-Andean stage is highly variable in response to tectonic reorganization that changed the sources and generation conditions of magmatism (Mpodozis and Kay, 1992). The new and compiled data however, do not completely support that idea. The available geochemical data suggest that some patterns of regional magmatism changed from the late Paleozoic to Mesozoic but others remained constant throughout the period.

Whereas rocks of the Gondwana cycle have higher SiO_2 contents than Jurassic rocks (Fig. 4) as it would be expected from continental- and oceanic-type arc magmatism, the Pre-Andean units do not exhibit the rhyolite-basalt bimodal distribution that has previously been interpreted as the product of continental rift processes (Parada et al., 1999; Ramos and Kay, 1991). SiO_2 contents akin to rhyolites are the dominant composition, but the volume of ~dacites (SiO_2 60–70%) is very similar to that of basalts and basaltic-andesites (SiO_2 50 to 55%). Moreover, a compilation of reported lithologies of all Triassic igneous outcrops in northern Chile indicate that basaltic andesite and andesites are the dominant petrographic type for volcanic rocks (>50% total area of Triassic volcanic rocks) and diorite-tonalite-granodiorite represent 40% to 55% of the exposed intrusions (Oliveros et al., 2018). Additionally, although the Permian Pre-Andean magmatism (Choiyoi) has been interpreted as the result of extensive crustal melting (Kay et al., 1989; Kleiman and Japas, 2009; Llambías and Sato, 1995) and its composition is strongly dominated by the rhyolite-granite types, the fact is that the

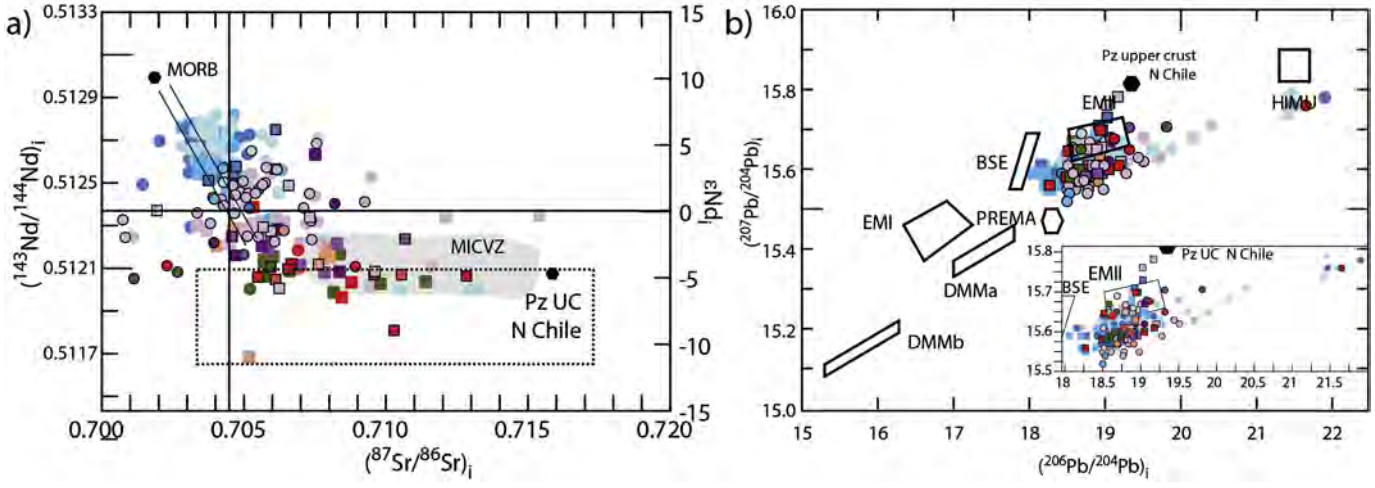

Fig. 7. Initial a) $^{87}Sr/^{86}Sr$ versus $^{143}Nd/^{144}Nd$ (εNd) and b) $^{206}Pb/^{204}Pb$ versus $^{207}Pb/^{204}Pb$ diagrams for the analyzed samples and published data. Ages for the calculation are in the Supplementary Material. Symbols are as in Fig. 5. Inset shows the field where the majority of the samples plot. Average Paleozoic Upper Crust in northern Chile is from Lucassen et al. (2006). Dotted line represents the range of Sr—Nd isotopic values of the continental crust (White, 2015). Bulk Silicate Earth (BSE) and mantle reservoirs (EMI, EMII, PREMA, DMMa, DMMb and HIMU) in b) are from Zindler and Hart (1986), not recalculated. MORB and BSE in a) are recalculated at 200 Ma (compilation of Vásquez et al., 2011), MICVZ: Miocene ignimbrites of the Central Andean Volcanic Zone (compilation of De Silva et al., 2006).

most silicic compositions are found in Triassic rocks (Figs. 4 and 5). Such feature has been observed for continental arcs and attributed to variation in crustal thickness: in arcs emplaced on thinned crust, the thermal lifespan of the magma chambers may equal the time of melt segregation, allowing a rather small volume of very silicic magmas to reach upper crustal levels, whereas arcs on a thick crust allow extensive differentiation that leads to larger volumes of intermediate magmatism (Farner and Lee, 2017). The progressive thinning of the crust after the San Rafael orogeny may have had an influence in the generation of very silicic magmas.

Another way to produce high volumes of intermediate-silicic magmatism in a continental arc setting, such as those observed in the Pre-Andean stage (Permian), is the lithospheric melting of the slab following its vertical detachment due to collision, a phenomenon known as slab failure (Hildebrand et al., 2018). The rocks generated in this context would have a clear subduction signature but with more silicic composition that normal arcs and trace element composition akin to deep magma sources (Hildebrand et al. 2018). According to the tectonic discrimination diagrams of Whalen and Hildebrand (2014), the silicic Permian and Triassic (and also Carboniferous) rocks plot both in the range of typical slab failure magmatism and of normal arc magmatism (Supplementary Material 4), not allowing to distinguish if this process may have taken place during the Pre-Andean stage.

The majority of the volcanic and all the plutonic rocks are subalkaline (Fig. 5); minor volumes of volcanic alkaline rocks are found in every period, but particularly in the Pre-Andean stage (for example,

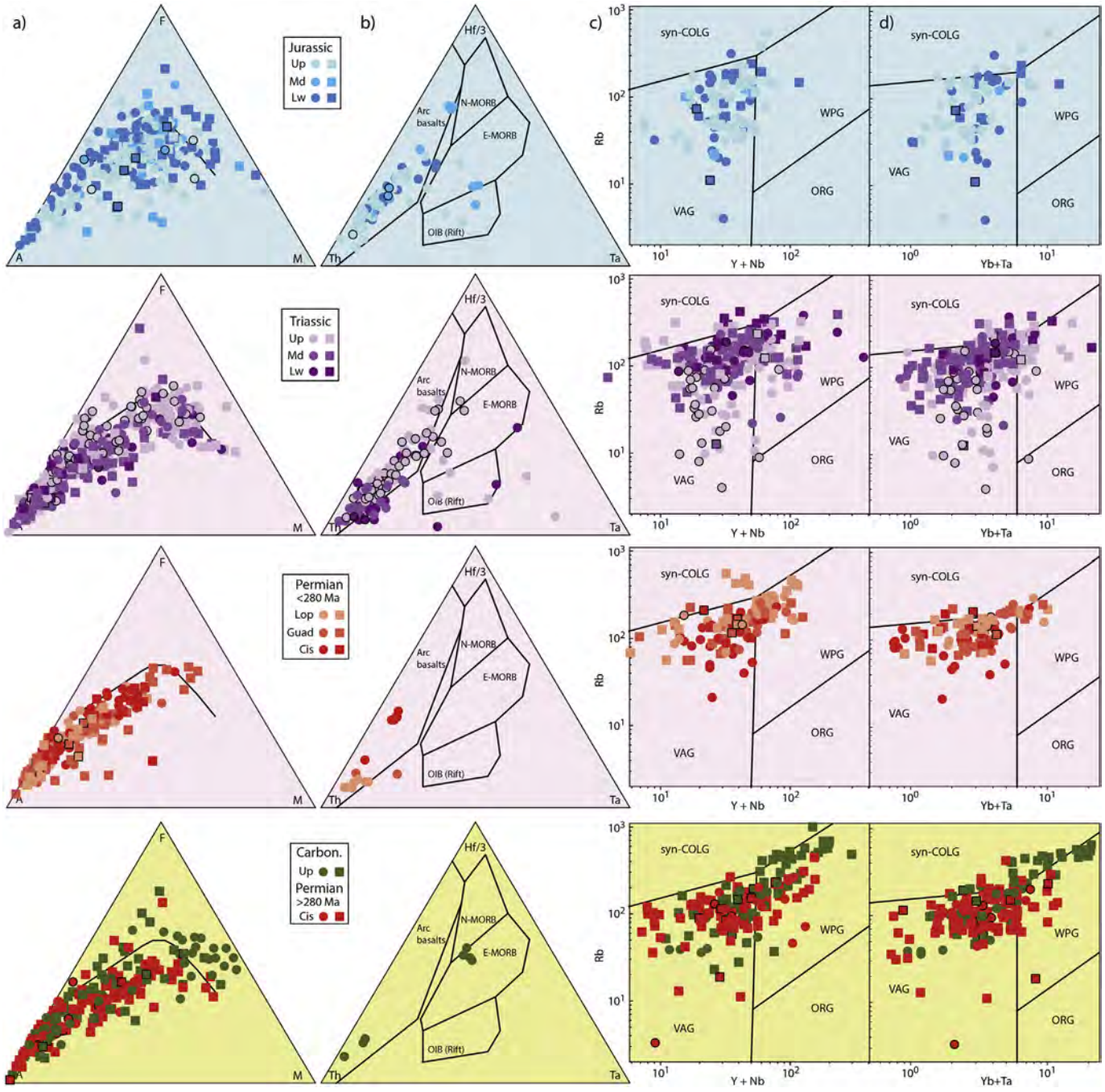

Fig. 8. a) AFM diagrams (Irvine and Baragar, 1971) and b) basalts Th-Ta-Hf/3 (Wood, 1980) and granites c) Rb-Y-Nb, d) Rb-Yb-Ta (Pearce 1984), tectonic discrimination diagrams for Carboniferous to Jurassic igneous rocks. Legends and symbols are as in Fig. 5. Background colors are as in Fig. 3 and refer to the Gondwana, Pre-Andean, and Andean cycles.

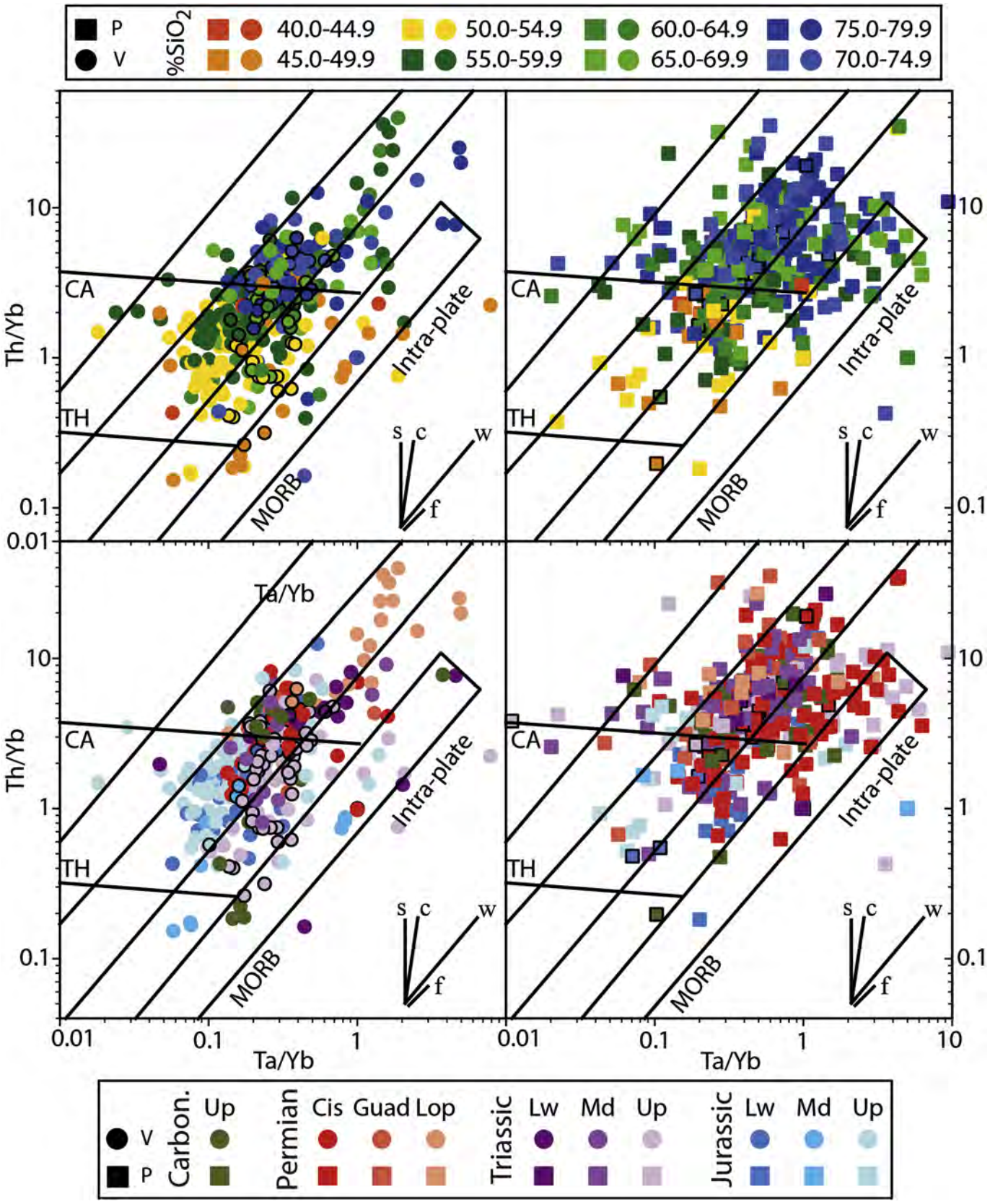

Fig. 9. Th/Yb vs Ta/Yb diagrams (Pearce, 1982), for Carboniferous to Jurassic igneous rocks. Ranges of SiO_2 content are delimited in the upper plots. Legends and symbols in the lower plots are as in Fig. 5.

the Lopingian Choyoi volcanics and partly the Norian Pastos Blancos Fm in the Frontal Cordillera, Fig. 5). Although the alteration degree of the rocks is moderate to high, the AFM diagram suggest that the igneous rocks are largely calc-alkaline, with minor tholeiitic volcanism restricted to the Jurassic period (Fig. 6a) (Lucassen et al., 2006; Lucassen and Franz, 1994). The Al-Ca-alkalis composition of plutonic rocks varies

from mixed but peraluminous dominated in the Gondwana cycle and Pre-Andean stage (with the former slightly more peraluminous), to dominantly metaluminous in the Early Andean cycle. This suggests a continuous shifting from S-type to I-type plutonism with time, typical of Cordilleran arcs (Ducea et al., 2015), but the majority of the intrusions have a transitional character and do not correspond to the S or I end members. Moreover, cordierite- or muscovite-bearing, or ilmenite dominated granitoids are only reported as relatively restricted volume intrusions of Lopingian and Norian ages in the Frontal Cordillera between 28° and 30°30′S (Hervé et al., 2014; Llambías and Sato, 1995; Mpodozis and Cornejo, 1988; Nasi et al., 1990; Parada, 1988), whereas biotite- or hornblende-bearing or magnetite dominated granitoids are the most common plutonic lithology in the three stages (Oliveros et al., 2018 and references therein).

In terms of their trace elements content, the rocks of the three stages exhibit ubiquitous enrichment in LILE over HFSE, with characteristic troughs in Nb—Ta, Ti, and P compared to primitive mantle (Fig. 6). In the tectonic discriminations diagrams for basaltic and granitic rocks most of the samples plot either on the arc basalts (Fig. 8b) or volcanic arc granites field, with a minor number of samples (Late Permian, Late Triassic and Jurassic) falling on the within plate or syn-collisional fields for granitoids (Fig. 8c,d). The involvement of fluids in the source of the Gondwana cycle, Pre-Andean stage and Early Andean Cycle magmas can also be inferred from the Th-Ta-Yb contents of the studied rocks (Fig. 9), which indicate that even the most primitive samples correspond to magmas dominated by a subduction (fluid-induced melting of a depleted mantle) component (Fig. 9). The magmas may have been oxidized, implying the involvement of fluids in their sources, because even for strongly fractionated REE compositions and high contents of light REE, the Eu anomalies are not so pronounced (Fig. 10a,b).

The isotope composition of Carboniferous and Permian rocks suggest that magmas were evolved (i.e. radiogenic Sr and Pb and unradiogenic Nd) yet less than expected for a magmatism with high degree of continental crust assimilation or for crust-derived melts, as it would be the case for the Gondwana cycle and Pre-Andean stage magmatism, respectively. For example, the Gondwana cycle magmas, thought to represent a continent-ocean subduction setting with a thick continental crust (Mpodozis and Ramos, 1989), have lower $^{87}Sr/^{86}Sr$ and higher $^{206}Pb/^{204}Pb$, εNd and εHf (del Rey et al., 2016) than the rocks of the modern Central Andean Volcanic Zone (εNd: −2 to −5 versus −4 to −9, $^{87}Sr/^{86}Sr_i$: 0.702 to 0.708 versus 0.705 to 0.709, $^{206}Pb/^{204}Pb_i$: 18.20 to 19.20 versus 17.75 to 18.75, Mamani et al., 2010; Scott et al. 2018). In a similar way, the isotope compositions of Pre-Andean Permian intrusions and volcanics, emplaced not only over the Gondwana arc but also on the metasedimentary cover of the margin (Coloma et al., 2017; González et al., 2018; Hervé et al., 2014; Llambías and Sato, 1995), are far from the average of Paleozoic crust for Nd, Sr and Pb (Fig. 7a,b). Hf isotopic composition (initial εHf) for zircons of the Gondwana cycle range from −5 to +2 and for zircons of the Pre-Andean stage from −4 to +7 (Willner et al., 2008; Bahlburg et al., 2009; Deckart et al., 2014; Hervé et al., 2014; del Rey et al., 2016); indicating that the latter are less evolved and the Pre-Andean magmatism would not have had a large input of Carboniferous curst or older.

This suggest that the crust cannot be the sole source of Pre-Andean Permian magmatism but, as much as for Gondwana and Early Andean igneous rocks, the measured isotopic ratios are better explained by the variable mixing of two magmatic sources: a somewhat depleted mantle and the continental crust. A similar conclusion has been advocated for Carboniferous to Triassic batholiths in the High Andes and Coastal Cordillera of central Chile (Parada et al., 1999; Deckart et al., 2014; del Rey et al., 2016; Hervé et al., 2014; Vásquez et al., 2009). Deviations from the mantle array in the Sr isotopic composition of Triassic Pre-Andean and Early Andean rocks with positive εNd (Fig. 7a) may be in part due to fluid remobilization by extensive, post-magmatic, seawater or hydrothermal alteration (Rogers and Hawkesworth, 1989; Kramer et al., 2005; Lucassen et al., 2006; Rossel et al., 2013), which is a common feature for the rocks exposed in the modern forearc of northern Chile (Oliveros et al., 2006, 2007).

Thus, the dominant lithological types in the Gondwana, Pre-Andean and Early Andean magmatism, the systematic chemical signature of a source compatible with a flux-melting of the depleted mantle, and the isotope composition that is best explained by mixture of mantle and continental crust sources are independent evidence that point out to subduction-related processes.

7. Tectonic evolution of the Andean convergent margin between 18° and 40°S

The magmatism that characterizes the Gondwana cycle, represents a period bracketed in between the onset of subduction somewhere after ca. 330 Ma and the ca. 280–270 Ma San Rafael orogenic phase (Astini et al., 2009; Bahlburg et al., 2009; Hervé et al., 2014; Mpodozis and Kay, 1992). This magmatism would have started after the emplacement of Mississipian plutons interpreted as anorogenic (Fig. 8) and the extrusion of minor volumes N/E-MORB type volcanism (Fig. 9) interpreted as an ensialic basin to the east and farther inland of what would later be the Gonwana arc (Astini et al., 2009; Dahlquist et al., 2010; Koukharsky et al., 2014; Alasino et al., 2012, 2017). The Coastal (south of 31°S) and the Frontal (north of 31°S) Cordillera batholiths are composed of plutons emplaced in a progressively thickened crust and have a significant crustal component in their source with protracted lithospheric residence (Fig. 11a) (Deckart et al., 2014; Hervé et al., 2014; Martin et al., 1999; Mpodozis and Kay, 1992; Tomezzoli, 2009). The end of this cycle is marked by the San Rafael Orogenic Phase that deformed the 330–280 Ma batholiths and sedimentary units in the Frontal Cordillera (Kleiman and Japas, 2009) and exhumed the arc roots north of the Domeyko Cordillera (Tommlison et al., 2012). This orogenic phase was initially attributed to collision of a continental mass during the Cisuralian (Mpodozis and Kay, 1992) but more recently it has been suggested that it could be related to flat-slab subduction, that resulted in the diachronic deformation advance in fold-and-thrust belts (Rapalini and Astini, 2005) and migration of the magmatism towards the foreland (Kleiman and Japas, 2009). A local limitation to the flat-slab model for the end of the Gondwana cycle is the magmatic activity within the accretionary prism, for example the Cisuralian Cifuncho Plutonic Complex emplaced shortly after the metamorphism in the prism took place (Contreras et al., 2013). These particular conditions suggest that not the entire margin would have been under a flat-slab scenario, although this regime could have dominated the margin evolution ot the end of the orogenic cycle. Taking into account the characteristic of its magmatism and the compressive structural setting, it is likely that the margin acted as an advancing orogen (Cawood and Buchan, 2007) during the Gonwdana cycle.

The Pre-Andean Choiyoi Group (ca. 285–248 Ma) comprises several magmatic units that crop out along ca. 2000 km in western Argentina and northeastern Chile (Fig. 2), with an estimated volume of 1,260,000 km^3 (Fig. 1) and it is interpreted as the gravitational collapse of the previous orogeny (Kleiman and Japas, 2009; Llambías et al., 2003, 1993; Llambías and Sato, 1995; Rocher et al., 2015; Sato et al., 2015; Spalletti and Limarino, 2017). The vast majority of the rocks are acid in composition, having magmatic affinities that define a temporal trend from calk-alkaline to anorogenic (Llambías and Sato, 1995) and they are interpreted as magmatism due to crustal melting or extensive recycling, triggered by basaltic underplating (that provided the heat) in an extensional tectonic regime (Hervé et al., 2014; Llambías and Sato, 1995; Mpodozis and Kay, 1990; Ramos and Kay, 1991; Rapela and Llambías, 1985). The database complied in this work contains most of the reported chemical data for the Choiyoi magmatism in Argentina and Chile and yet the composition the analyzed samples is largely consistent with a straightforward subduction-related origin (see above) (Fig. 11b).

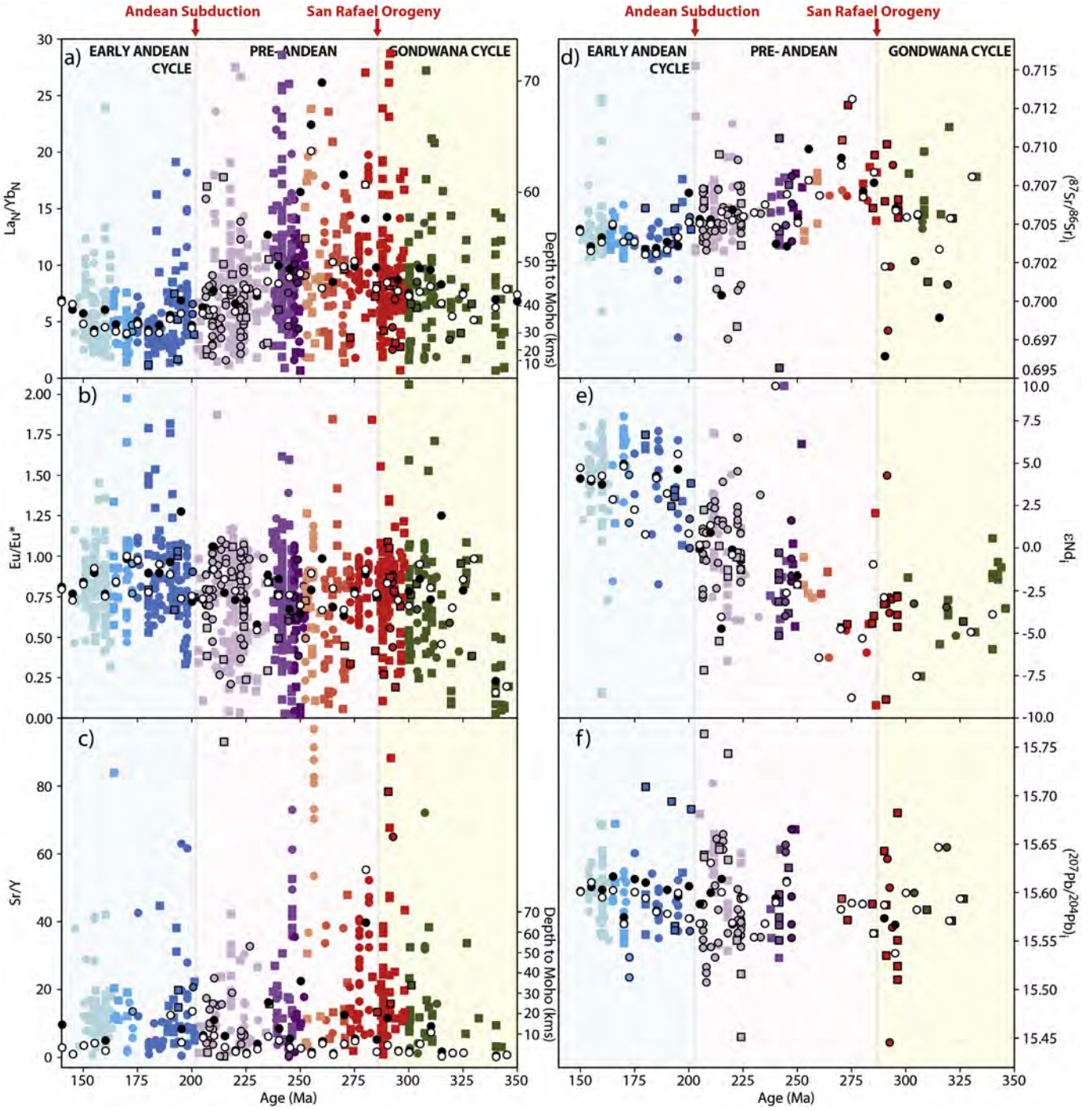

Fig. 10. Age versus a) chondrite-normalized La/Yb and b) Eu/Eu* (Eu* = Eu/(Sm*Gd)^{½}), and c) Sr/Y for analyzed and published samples with 55 < SiO_2 < 70%wt and MgO <6 wt%. Age versus d) initial $^{87}Sr/^{86}Sr$, e) initial $^{143}Nd/^{144}Nd$ (εNd) and f) initial $^{207}Pb/^{204}Pb$ for all analyzed and published samples. Chondrite values from Sun and McDonough (1989). Ages without errors for each sample were assigned from data in Supplementary Material 2 and 3, using the following criteria: radiometric age reported in literature for the very same sample, or age reported for the nearest sample of the same unit or sub-unit, or mean value of the age range reported for the entire unit, or mean absolute value for the numerical range of the stratigraphic age assigned to the entire unit (age limits for stratigraphic stages from Cohen et al., 2013). Black and white dots represent mean and median values, excluding outliers, for each 5 Myr interval, respectively. Symbols and legends are as in Fig. 5. Background colors are as in Fig. 3 and refer to the Gondwana, Pre-Andean, and Andean cycles.

An alternative explanation to the systematic subduction signature is that melting affected only the more mafic and less evolved lower crust, that was in turn generated in a previous subduction setting during the Upper Carboniferous or Ordovician (Alasino et al., 2012, 2017; Coira et al., 2016; Ducea et al., 2015; Martina et al., 2011; Otamendi et al., 2010; Walker et al., 2015). However, no inherited zircons of that age range or lower crustal xenoliths in the plutonic units of the Choiyoi province have been reported, and only local metasedimentary enclaves of the host rocks are found (Llambías and Sato, 1995). Furthermore, there is lack of >280 Ma inherited zircons in the Permian-Triassic (Choiyoi) samples dated by the in-situ U—Pb method (del Rey et al., 2016; Hervé et al., 2014; Sato et al., 2015), even though Mesoproterozoic model ages have been reported for the crustal component in some of them (del Rey et al., 2016). Therefore, even though anorogenic or crustal-derived signatures have been identified in some of the Choiyoi intrusions in Argentina (Llambías and Sato, 1995) and

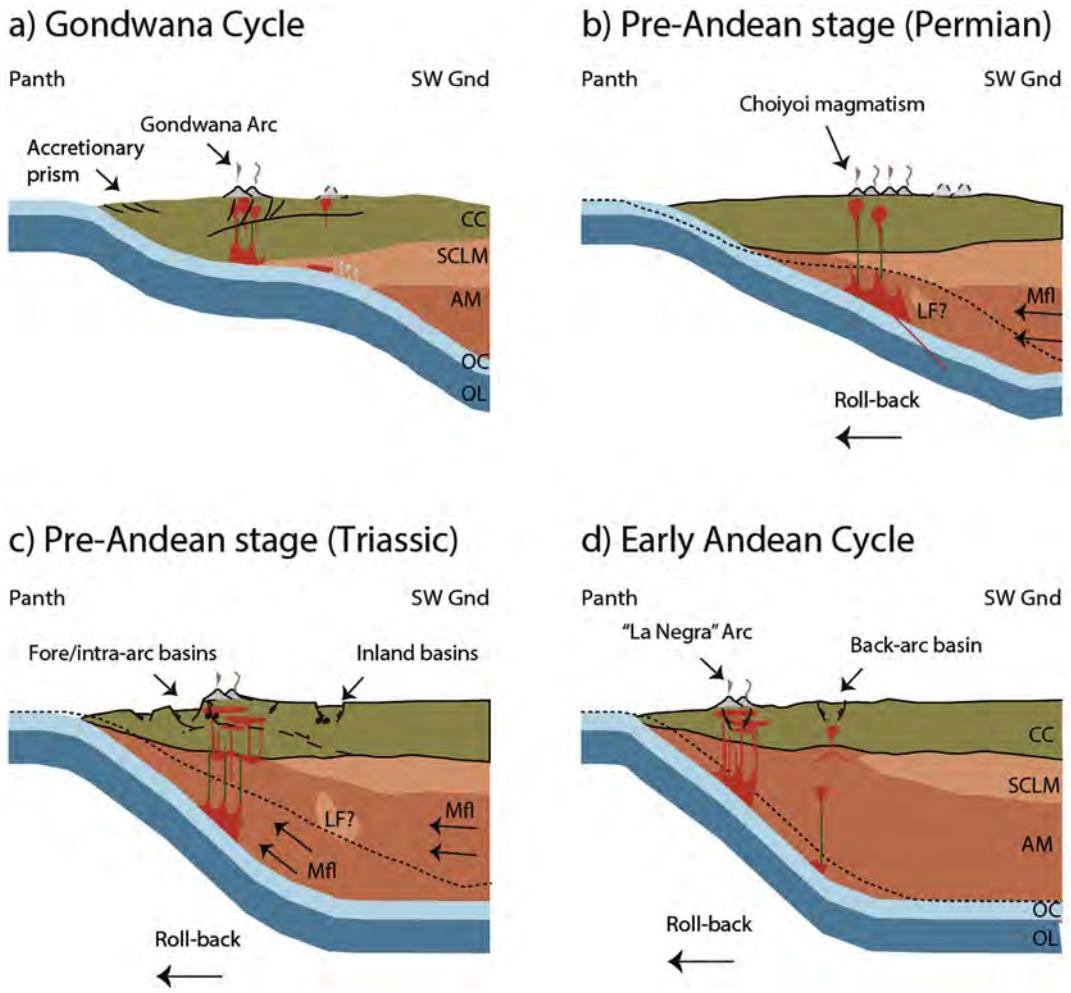

Fig. 11. Proposed tectonic and paleogeographic configuration for the Proto- and Early-Andean margin of SW Gondwana at a) the end of the Gondwana cycle, during the Latest Carboniferous and Early Permian, where the San Rafael Orogeny took place, likely due to flat slab subduction, inducing hydroweakening of the lithospheric mantle; b) the Permian Pre-Andean stage where slab roll-back induced lithospheric loss (either through foundering of the lithospheric roots or thermal erosion due to asthenospheric mantle flow) c) the Triassic Pre-Andean stage where increased roll-back and mantle flow caused generalized extension in the upper crust and the development of fore-arc, intra-arc and inland basins; and d) during the Early Andean cycle, where the arc was emplaced westward of the former magmatic fronts. Panth: Panthalassa Ocean (and oceanic plate), SW Gnd: Southwestern Gondwana continental interior; Mfl: asthenospheric mantle flow; LF: lithospheric foundering. OC: Oceanic crust, OL: Oceanic lithospheric mantle; CC: Continental Crust; SCLM: Subcontinental lithospheric mantle; AM: Asthenospheric mantle.Dotted line represent the upper limit of the slab from the previous stage.

equivalents units in Chile (Mpodozis and Kay, 1992; del Rey et al., 2019), the case for the generation of the Choiyoi magmatism solely through crustal melting or reworking seems rather unlikely.

Continuous subduction during the entire Pre-Andean Permian period is then a plausible scenario for the SW margin of Gondwana, although this process could have had a restricted contribution to crustal growth, implying a significant amount of recycling through assimilation, as it has been observed for southern Perú (Garzione et al., 2017; Mišković and Schaltegger, 2009) or Patagonia (Castillo et al., 2017)

By the end of the magmatic activity of the Choiyoi province another episode of magmatism during the Early-Middle Triassic preceded the rifting of large-scale intracontinental basins, in which restricted volumes of basaltic flows with intraplate signatures extruded (de Machuca et al., 2019; Martínez, 2004; Ramos and Kay, 1991; Sommer et al., 2018), suggesting a passive margin configuration. These large-scale basins (Ichigualasto and Cuyo) were located farther inland with respect to position of the main magmatic axis (Fig. 1) that was closer to the margin's edge. On the other hand, the units cropping out in the Frontal and Domeyko Cordilleras that represent marine and continental depocenters, and their related igneous rocks, have been interpreted as subduction-related rifting basins (Suarez and Bell, 1992), located either in forearc (San Felix basin, Salazar et al., 2019), or back-arc (Domeyko basin, Espinoza et al., 2019) positions (Fig. 11c). This variety of contradicting interpretations implies there is no consensus regarding the tectonic configuration of the Pre-Andean stage for the Triassic. Furthermore, the volumetrically most significant magmatism at the time was not bimodal, as expected for continental rift settings. This magmatism has an arc-related signature and less crustal contribution than the Permian counterparts (Figs. 7, 8, 9). Thus, the Pre-Andean Triassic record of magmatism and the architecture of the rift basins in the continent margin (northern Chile) suggest that this stage represents a subduction setting, whereas the magmatism and depocenters in the inner part of the continent (northwestern Argentina) may have developed through continental rifting with NW orientation (de Machuca et al., 2019; Giambiagi et al., 2011).

Nonetheless, transitional (calk-alkaline) to alkaline magmatism did occur during the Pre-Andean stage in the Late Triassic (Norian), as it is attested by the chemistry of some of the basaltic lava flows and syenogranites in the Frontal Cordillera (Quebrada del Salitre, La Ternera and Pastos Blancos formations, Colorado granites, Coloma et al., 2017; González et al., 2018). Samples with such signatures do not represent the entire magmatic record of each unit and their volume of rocks is rather restricted compared to the units that bear a clear calc-alkaline subduction-related chemical composition (Ortiz and Merino, 2015;

Salazar and Coloma, 2016; Murillo et al., 2017; González et al., 2018). Coloma et al. (2017) have interpreted this transitional magmatism as a potential precursor of the ultimate emplacement of the Andean arc along the present-day Coastal Cordillera. This tectonic setting is likely given that some of the Pre-Andean Norian-Rhaetian volcanic units represent the early stages of the Jurassic back-arc basin (Espinoza et al., 2019) located to the east of the Jurassic Andean arc (Oliveros et al., 2006), as an analogue to the Rhaetian-Hettangian Pre-Cuyo group that preceded the development of the Jurassic Neuquén back-arc basin in the southern Andes (D'Elia et al., 2012). In fact, during the main activity of the Early Andean arc, alkaline to transitional volcanism occurred in the eastern (inner continent) edge of the back-arc basin and it is interpreted in the context of the extensional tectonic that dominated during the early stages of the Andean arc (Rossel et al., 2015, 2013). Therefore, the presence of alkaline igneous rocks in the Pre-Andean Triassic record cannot be directly attributed to passive margin within plate magmatism (Ramos and Kay, 1991; Charrier et al., 2007), but rather to back-arc depocenters (Rossel et al., 2013).

Subduction of an oceanic (Panthalassa-related) plate under the SW Gondwana margin might have then persisted throughout the Permian and Triassic periods (Fig. 11) but the dynamics of this process must have undergone significant changes. If the Carboniferous to Jurassic magmatism of the SW Gondwana margin is considered as the product of a continental-type margin, the La_N/Yb_N and Sr/Y ratios of the studied and published samples may be related to crustal thickness (Chapman et al., 2015; Profeta et al., 2015), with a maximum at ca. 280 Ma, right after the San Rafael Orogeny (Kleiman and Japas, 2009; Sato et al., 2015) and then a steady decrease until the end of the Jurassic (Fig. 10a,c). In a similar way, crustal contribution to magma sources also decreased from ca 280 Ma to 150 Ma (Fig. 10d,e). This is in very good agreement with the overall extensional setting proposed for the continental margin at the same time span (del Rey et al., 2016; Grocott and Taylor, 2002; Hervé et al., 2014; Llambías and Sato, 1995; Mpodozis and Kay, 1992; Mpodozis and Ramos, 1989; Sato et al., 2015). Recent models of the plate configuration suggest that the continental margin of SW Gondwana was active and overriding an oceanic plate with spreading centers (Müller et al., 2016; Riel et al., 2018; Torsvik and Cocks, 2013; Young et al., 2019) at least since the Late Carboniferous and until the Late Jurassic. This reinforces the idea that magmatism along the SW Gondwana margin must has been generated by subduction.

Sr/Y and La_N/Yb_N peaks towards the end of the Lopingian to the Middle Triassic (~255–240 Ma) escape from the more general trend of decreasing ratios (Fig. 10 a, c) and are not coupled to $^{87}Sr/^{86}Sr$ positive or εNd_i negative peaks (Fig. 10 d,e), nor with εHf negative peaks (del Rey et al., 2019). The model of kinematic evolution of Young et al. (2019) proposes a shift in the absolute motion of the.

continental plate, from northeastward to southwestward (oceanic plate maintained its northeastward motion), that roughly coincides with the high Sr/Y- La_N/Yb_N magmatism. It is possible that compression or increasing convergence took place during this time span, resulting in a thickened crust, perhaps via slab shallowing (Huangfu et al., 2016), that did not imply increased crustal contribution to magmatism. The model also suggests that shortly after, at ~240–225 Ma, the convergence shifted from dextral to sinistral and again the absolute motion of the continental plate change to northeastward, diminishing the convergence with the oceanic plate (Matthews et al., 2016; Young et al., 2019). This time frame coincides with the inception and development of the NW-oriented rift basins, both close to the continental the margin (Cifuncho, Domeyko, La Ternera and San Félix basins, Suarez and Bell, 1992; Espinoza et al., 2019; Salazar et al., 2019) and farther into the foreland (Ichigualasto and Cuyo basins, Giambiagi et al., 2011). Thus, the conditions for plates convergence, and not only the far field stresses related to the Pangea break-up (Charrier et al., 2007), may have played a role in the generation and evolution of the Triassic rift basins.

A sinistral regime with practically no absolute convergence component has been proposed for the SW Gondwana margin between 220 and 220 Ma (Young et al., 2019), however the potential magmatic and tectonic responses to such scenario (for example Aragón et al., 2013) is not supported by our data. This suggest that global reconstructions with large extrapolations would benefit more detailed studies that link the geological and geochemical record with the motion of recycled oceanic plates.

In contrast to what the geochemistry and geologic evidence suggest for the evolution of the present-day Andean region of Chile and Argentina, extensive alkaline magmatism of the Triassic Mitu Group and continental anatectites have been linked to continental rifting due to Pangea disassembly without penecontemporaneous subduction (Spikings et al., 2016). The margin should have then been significantly segmented if simultaneous passive and active zones were developed along it.

Variation in the geometry and physics of the subducting plate are the most probable control on tectonic segmentation but it is difficult to identify in the geological record at the temporal scales of this study. The continental margin may have been interacting an active ridge in the Panthalassa ocean with during the Pre-Andean stage (Matthews et al., 2016; Young et al., 2019). Although there is no direct evidence of ridge subduction in the Carboniferous to Jurassic record, the passage of this plate boundary could have induced differential deformation and magmatism along the margin and it is an hypothesis that should be tested.

Aside from changes in the geometry and rheology of the subducting oceanic plate which is for example the main factor for modern Andean segmentation (Stern, 2004), the Pre-Andean stage segmentation could have been the result of heterogeneities in the upper South American plate (Ramos, 1994) or differential response to Pangea realm reorganization as proposed by Riel et al. (2018). Given that the distribution of Triassic rift basins would have been controlled by the location of boundary zones of terrains accreted to South America (Giambiagi et al., 2011) it is possible that such heterogeneities would have in part influenced the response of the margin to convergence.

Steepening of the oceanic plate and roll-back would have triggered the dominant extensional tectonics of the margin after the San Rafael phase, and would have been responsible for a more significant mantle signature of the Triassic magmas. The temporal and spatial variation of the subduction angle however, did not affected the locus of magmatism which continued to develop mainly in the present day High Andes with minor expressions in the Coastal Cordillera (Fig. 1). It was not until 210 Ma that a major shift of the magmatic axis took place from south Peru to Central Chile, where more voluminous magmatism was emplaced along the present-day Coastal Cordillera (Figs. 1–3)(Parada

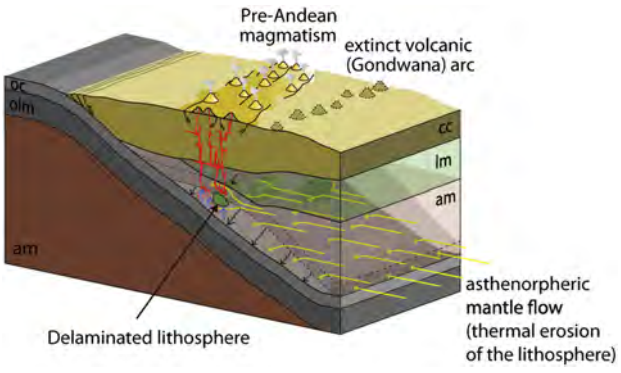

Fig. 12. Conceptual model of potential mechanisms of lithospheric removal during the Pre-Andean stage in northern Chile. Segmented line represent the position of the slab by the end of the Gondwana cycle. Yellow arrows represent the asthenospheric flow In response to slab steepening (small black arrow denote the slab movement). oc: Oceanic crust, olm: Oceanic lithospheric mantle; cc: Continental Crust; lm: Sub-continental lithospheric mantle; am: Asthenospheric mantle.

et al., 1999; Boekhout et al., 2012; F. Coloma et al., 2017; Vásquez et al., 2011) and continued throughout the Jurassic with no counterpart in the High Andes until ca. 160 Ma (Rossel et al., 2013). Whatever the reason for this important spatial migration of the magmatic loci, it does not relate to any detectable break in the geochemical evolution of the Pre-Andean rocks analyzed so far (Fig. 10). The post-210 Ma magmatism of the Coastal Cordillera is widely known as the first stage of the Andean subduction dominated by the development of the "La Negra" Arc (Fig. 11d)(Oliveros et al., 2006; Charrier et al., 2007). The arc produced voluminous magmatism with variable composition but dominantly intermediate and calc-alkaline to tholeiitic affinities (Fig. 5), over a thinned crust that underwent sinistral transtention due to the stress partitioning of an oblique subduction of the Phoenix (or Panthalassa) plate (Scheuber and Gonzalez, 1999; Grocott and Taylor, 2002; Lucassen et al., 2006). The overall extensional setting and the development of a marine back-arc region is consistent with a model of retreating orogen (Cawood and Buchan, 2007) for the Early Andean cycle.

8. Lithospheric evolution of the Early Andes

The chemistry of Late Carboniferous to the Late Jurassic igneous rocks strongly suggest that magmatism was dominantly of subduction-related nature. Although it is possible to explain the geological and tectonic changes that took place along the margin during this period in the context of continuous plate convergence, an evolutionary model that accounts for the systematic increase in the sub-arc mantle component of magmas is still needed. The formation of prevailing magmatic crust in longstanding immobile arcs may induce the increase of the sub-arc mantle component, but this process would not explain the extension that occurred in the Pre-Andean stage. Another process that may account for the geochemical evolution in magmatism is the foundering of subcontinental lithospheric mantle (Figs. 11b,c, and 12). Most long lived Phanerozoic arcs have a cyclic geochemical and isotopic behavior that is partly related to lithospheric delamination. (DeCelles et al. 2009; Ducea and Barton, 2007). Loss of the lithospheric roots of Cordilleran-type arcs through delamination or foundering has been well documented in the Andes and the North American Mesozoic arc (e.g. Ducea and Saleeby, 1998; Ducea et al., 2013; Kay and Kay, 1993; Zandt et al., 2004). It is a process that results both in magmatism with an asthenospheric mantle source in regions of thick crust and asthenosphere upwelling-driven exhumation of the crust and development of plain elevated areas such as the Puna in northwestern Argentina (Ducea et al., 2013; Kay and Kay, 1993).

The spatial and temporal scales in which delamination has been reported vary between 20 and 100 km and ca. 5 to 40 Myr (Ducea, 2011; Gutiérrez-Alonso et al., 2011). Although increasing mantle signature and exhumation are characteristics of the Pre-Andean stage magmatism and tectonic evolution, they are observed along ca. 2000 km of the margin and from ca. 270 to 200 Ma, which is far in excess of what can be a single delamination process. Multiple-stages delamination has been suggested in some tectonic models (DeCelles et al., 2009) but it is a process unlikely to have taken place wholesale at the thousand-kms-long scale needed for explaining the observed features of the pre-Andean margin.

Another process that may result in loss of lithosphere and its replacement by fertile asthenospheric mantle is "decratonization" (Kusky et al., 2014; Spencer et al., 2017) (Fig. 12), which would have taken place in North China craton during the Cretaceous in response to slab roll-back. Mesozoic magmastim in this area transitioned from calc-alkaline, adakitic rocks mainly derived from thickened ancient lower continental crust (negative εNd) to extensive magmatism including A-type granites, alkaline to calc-alkaline composition and increased contribution of a depleted mantle source (less negative to positive εNd), during the peak of decratonization (Zhang et al., 2014). This change in the petrography of the magmatism would be similar to the changes in the magmatic chemistry from the Gonwana cycle to the Pre-Andean stage, although the subduction component is much more intense in the latter. The thermal erosion of the cratonic lithosphere due to asthenospehric upwelling in the space left by a retreating lid that triggers slab roll-back induces both more juvenile magmatism and extensional tectonics and exhumation on the upper continental plate. As much as lithospheric foundering, decratonization is intrinsically associated to continent-oceanic subduction, but it has been documented in much larger spatial and temporal scales (Spencer et al., 2017) and could take place along an entire margin without the need of shortening/compression events and phase changes in the lower crust to induce delamination.

In the case of the Pre-Andean stage, the San Rafael orogenic phase would have provided the fluids from a dehydrating flat slab, when slab roll-back started to act after the orogenic collapse (del Rey et al., 2016), the space left by the retreating slab may have been filled by asthenospheric mantle, which melted in the presence of those fluids. The melted asthenosphere could have thermochemically eroded the continental lithosphere, and at the same time generated the extension that prevailed during the Permian and Triassic along the margin (Fig. 11). The persistent signal of evolution from lithospheric-dominated to asthenosphere-dominated sources of magmatism, coupled to protracted extensional regime and the large spatio-temporal scales of such evolution suggest that decratonization might have occurred along the proto-Andean margin, prior to the establishment of the Andean arc in the very edge of the continental plate.

9. Conclusions

The elemental and isotopic composition of 86 samples of volcanic and plutonic rocks spanning ca. 330 to 150 Ma analyzed for this study, along with 1054 geochemical data of Carboniferous to Jurassic igneous rocks, representing the Gondwana cycle, Pre-Andean stage and Early Andean cycle magmatism, from the Chilean and Argentinean Andes provide a first order record of magmatic evolution along the South American margin during Pangea's life and break-off. In spite of previous tectonic models that proposed arrested subduction during the supercontinent disassembly, the magmatism along the proto-Andean margin is consistently of subduction-related nature throughout the period. Typical features of arc magmatism are found in most of the analyzed and reported samples: calc-alkaline affinities, LILE enrichment over HFSE, Nb—Ta troughs and moderate to small Eu negative anomalies. SiO_2 content of the Pre-Andean rocks is higher than expected for arc rocks and the compositional bimodality that had been attributed to Triassic magmatism is not observed in the compiled record. Sr-Nd-Pb isotope composition of the samples analyzed for this study and published data suggests that magma sources included depleted mantle reservoir and continental crust. Although the Pre-Andean magmatism had been previously interpreted as the result of crustal melting, this seems unlikely given the less evolved isotopic signatures of volcanic and plutonic rocks compared to the Paleozoic basement.

The temporal evolution of the magmatism from the Gondwana to Early Andean cycle suggests an increase of the sub-arc mantle component in the latter. This shift in the magmatic composition was accompanied by prevailing extensional tectonics both in the continental margin and foreland. Loss of the lithospheric roots of the arc or thermal erosion of the lithosphere after a flat subduction event are proposed as the most likely scenarios for the geodynamic evolution of the Pre-Andean margin.

Supplementary data to this article can be found online at https://doi.org/10.1016/j.gr.2019.11.002.

Declaration of competing interest

The authors declare that they have no known competing financial interests or personal relationships that could have appeared to influence the work reported in this paper.

Acknowledgements

This research was funded through the Fondecyt grant 1120715, the "Plan Nacional de Geología" of the National Geological and Mining Service (SERNAGEOMIN), the ENLACE 218.040.025-1.0 (Universidad de Concepción) and the Conicyt doctoral grants 21140774 (ME) and 21150502 (JG). M.N.D. acknowledges support from US National Science Foundation grant EAR 1725002 and the Romanian Executive Agency for Higher Education, Research, Development and Innovation Funding projects PN-III-P4-ID-PCE-2016-0127 and PN-III-P4-ID-PCCF-2016-0014. Natalia Astudillo, Rodolfo Ferrando, Rodrigo González, Diego Montecino, Miguel Ortiz, Roberto Merino, Ismael Murillo and Ricardo Velásquez are thanked for the fruitful discussions on the updated geological mapping in northern Chile. Florencia Bechis, Amancay Martínez, Laura Giambiagi are thanked for collaborations in the field work. Two anonymous reviewers are thanked for their constructive comments that greatly improved an earlier version of this manuscript. M. Santosh is thanked for editorial handling.

References

Alasino, P.H., Dahlquist, J., Pankhurst, R.J., Galindo, C., Casquet, C., Rapela, C.W., Larrovere, M., Fanning, C.M., 2012. Early Carboniferous sub- to mid-alkaline magmatism in the Eastern Sierras Pampeanas, NW Argentina: A record of crustal growth by the incorporation of mantle-derived material in an extensional setting. Gondwana Research 22, 992–1008. https://doi.org/10.1016/j.gr.2011.12.011.

Alasino, P.H., Larrovere, M.A., Rocher, S., Dahlquist, J.A., Basei, M.A.S., Memeti, V., Paterson, S., Galindo, C., Macchioli, M., Campos, C., 2017. Incremental growth of an upper crustal, A-type pluton, Argentina: evidence of a re-used magma pathway. Lithos 284–285, 347–366. https://doi.org/10.1016/j.lithos.2017.04.013.

Aragón, E., Pinotti, L., Fernando, D., Castro, A., Rabbia, O., Coniglio, J., Aguilera, Y.E., 2013. The Farallon-Aluk ridge collision with South America: Implications for the geochemical changes of slab window magmas from fore-to back-arc. Geoscience Frontiers 4, 377–388. https://doi.org/10.1016/j.gsf.2012.12.004.

Ardill, J., Flint, S., Chong, G., Wilke, H., 1998. Sequence stratigraphy of the Mesozoic Domeyko Basin, northern Chile. Journal of the Geological Society of London 155, 71–88.

Arriagada, C., Roperch, P., Mpodozis, C., Fernandez, R., 2006. Paleomagnetism and tectonics of the southern Atacama Desert (25-28°S), northern Chile. Tectonics 25, 1–26. https://doi.org/10.1029/2005TC001923.

Astini, R., Martina, F., Ezpeleta, M., Dávila, F.M., Cawood, P., 2009. Chronology from rifting to foreland basin in the Paganzo Basin (Argentina), and a reappraisal on the "Eo- and Neohercynian" tectonics along Western Gondwana. XII Congr. Geológico Chil. 1–4.

Bahlburg, H., Vervoort, J.D., Du Frane, S.A., Bock, B., Augustsson, C., Reimann, C., 2009. Timing of crust formation and recycling in accretionary orogens: Insights learned from the western margin of South America. Earth Science Reviews 9, 215–241. https://doi.org/10.1016/j.earscirev.2009.10.006.

Bell, C.M., 1987. The origin of the Upper Palaeozoic Chanaral mélange of N Chile. Journal of the Geological Society of London 144, 599–610.

Bissig, T., Clark, A.H., Lee, J.K.W., von Quadt, A., 2003. Petrogenetic and metallogenetic responses to Miocene slab flattening: new constraints from the El Indio-Pascua Au–Ag–Cu belt. Chile/Argentina. Miner. Depos. 38, 844–862. https://doi.org/10.1007/s00126-003-0375-y.

Boekhout, F., Spikings, R., Sempere, T., Chiaradia, M., Ulianov, A., Schaltegger, U., 2012. Mesozoic arc magmatism along the southern Peruvian margin during Gondwana breakup and dispersal. Lithos 146–147, 48–64. https://doi.org/10.1016/j.lithos.2012.04.015.

Breitkreuz, C., Bahlburg, H., Delakowitz, B., Pichowiak, S., 1989. Paleozoic volcanic events in the Central Andes. Journal of South American Earth Sciences 2, 171–189. https://doi.org/10.1016/0895-9811(89)90045-X.

Brown, M., 1991. Comparative geochemical interpretation of Permian–Triassic plutonic complexes of the Coastal Range and Altiplano (25°30′ to 26°30′ S), northern Chile. Geological Society of America Special Papers 265, 157–171. https://doi.org/10.1130/SPE265-p157.

Castillo, P., Fanning, C.M., Pankhurst, R.J., Hervé, F., Rapela, C.W., 2017. Zircon O- and Hf-isotope constraints on the genesis and tectonic significance of Permian magmatism in Patagonia. Journal of the Geological Society of London 174. https://doi.org/10.1144/jgs2016-152 (jgs2016-152).

Cawood, P.A., Buchan, C., 2007. Linking accretionary orogenesis with supercontinent assembly. Earth-Science Reviews 82 (3–4), 217–256. https://doi.org/10.1016/j.earscirev.2007.03.003.

Cembrano, J., Lavenu, A., Reynolds, P., Arancibia, G., López, G., Sanhueza, A., 2002. Late Cenozoic transpressional ductile deformation north of the Nazca – South America – Antarctica triple junction. Tectonophysics 354, 289–314. https://doi.org/10.1016/S0040-1951(02)00388-8.

Chapman, J.B., Ducea, M.N., Decelles, P.G., Profeta, L., 2015. Tracking Changes in Crustal Thickness During Orogenic Evolution With Sr/Y: an Example From the North American Cordillera Tracking Changes in Crustal Thickness During Orogenic Evolution With Sr/Y; an Example From the North American Cordillera. https://doi.org/10.1130/G36996.1.

Charrier, R., Pinto, L., Rodríguez, M.P., 2007. Tectonostratigraphic evolution of the Andean Orogen in Chile. In: Moreno, T., Gibbons, W. (Eds.), The Geology of Chile. The Geological Society, London, pp. 21–114. https://doi.org/10.1144/GOCH.3.

Charrier, R., Ramos, V., Tapia, F., Sagripanti, L., 2014. Tectono-stratigraphic evolution of the Andean Orogen between 31 and 37 S (Chile and Western Argentina). Geol. Soc. London. Spec. Publ. 399, 13–61. https://doi.org/10.1144/SP399.20.

Cohen, K.M., Finney, S.C., Gibbard, P.L., Fan, J.-X., 2013. The ICS international chronostratigraphic chart. Episodes 36, 199–204. https://doi.org/10.1111/j.1502-3931.1980.tb01026.x (updated).

Coira, B., Davidson, J., Mpodozis, C., Ramos, V., 1982. Tectonic and magmatic evolution of the Andes of northern Argentina and Chile. Earth-Science Reviews 18 (3-4), 303–332.

Coira, B., Cisterna, C.E., Ulbrich, H.H., Cordani, U.G., 2016. Extensional Carboniferous magmatism at the western margin of Gondwana: Las Lozas valley, Catamarca. Argentina. Andean Geol. 43, 105–126. https://doi.org/10.5027/andgeoV43n1-a06.

Coloma, F., Valin, X., Oliveros, V., Vásquez, P., Creixell, C., Salazar, E., Ducea, M.N., 2017. Geochemistry of permian to triassic igneous rocks from northern Chile (28°-30°15'S): Implications on the dynamics of the proto-Andean margin. Andean Geology 44, 147–148. https://doi.org/10.5027/andgeoV44n2-a03.

Cornejo, P., Mpodozis, C., Rivera, O., Matthews, S.J., 2009. Carta Exploradora, Regiones de Antofagasta y Atacama. Servicio Nacional de Geología y Minería, Santiago.

Cox, K.J., Bell, J.D., Pankhurst, R.J., 1979. The Interpretation of Igneous Rocks. First. ed. Springer, Dordrecht.

Creixell, C., Oliveros, V., Vásquez, P., Navarro, J., Vallejos, D., Valin, X., Godoy, E., Ducea, N., 2016. Geodynamics of Late Carboniferous–Early Permian forearc in north Chile (28°30′–29°30′S). Journal of the Geological Society of London 173. https://doi.org/10.1144/jgs2016-010 (jgs2016-010).

D'Elia, L., Muravchik, M., Franzese, J.R., Bilmes, A., 2012. Volcanismo de sin-riftde la Cuenca Neuquina, Argentina: Relación con la evolución Triásico Tardía-Jurásico Temprano del margen Andino. Andean Geology 39, 106–132.

Dahlquist, J.A., Alasino, P.H., Eby, G.N., Galindo, C., Casquet, C., 2010. Fault controlled Carboniferous A-type magmatism in the proto-Andean foreland (Sierras Pampeanas, Argentina): Geochemical constraints and petrogenesis. Lithos 115, 65–81.

De Silva, S., Zandt, G., Trumbull, R., Viramonte, J.G., Salas, G., Jiménez, N., 2006. Large ignimbrite eruptions and volcano-tectonic depressions in the Central Andes: a thermomechanical perspective. Geological Society of London, Special Publication 269, 47–63.

de Machuca, B.C., López, M.G., Morata, D., Fuentes, M.G., 2019. Geochemical constraints on the petrogenesis of Triassic alkaline basalts of Sierra de Valle Fértil, Western Sierras Pampeanas, Argentina: implications for their origin, evolution and tectonic setting. Journal of South American Earth Sciences 95, 102297.

Deckart, K., Hervé, F., Fanning, C.M., Ramírez, V., Calderón, M., Godoy, E., 2014. U-Pb Geochronology and Hf-O Isotopes of zircons from the Pennsylvanian Coastal Batholith. South-Central Chile. Andean Geol. 41, 49–82. https://doi.org/10.5027/andgeoV41n1-a03.

Drew, S.T., Ducea, M.N., Schoenbohm, L.M., 2009. Mafic volcanism on the Puna Plateau, NW Argentina: Implications for lithospheric composition and evolution with an emphasis on lithospheric foundering. Lithosphere 1 (5), 305–318.

Ducea, M.N., 2011. Fingerprinting orogenic delamination. Geology 39, 191–192. https://doi.org/10.1130/focus022011.1.

Ducea, M., Saleeby, J., 1998. A case for delamination of the deep batholithic crust beneath the Sierra Nevada, California. International Geology Review 40, 78–93. https://doi.org/10.1080/00206819809465199.

Ducea, M.N., Seclaman, A.C., Murray, K.E., Jianu, D., Schoenbohm, L.M., 2013. Mantle-drip magmatism beneath the Altiplano-Puna plateau, Central Andes. Geology 41, 915–918. https://doi.org/10.1130/G34509.1.

Ducea, M.N., Otamendi, J.E., Bergantz, G.W., Jianu, D., Petrescu, L., 2015. The Ordovician Famatinian-Puna arc. GSA Mem. 212, 125–138. https://doi.org/10.1130/2015.1212(07).

Espinoza, M., Oliveros, V., Vásquez, P., Bechis, F., 2015. U-Pb Geochronology and Kinematic Preliminary Analyses of Late Triassic-Early Jurassic Basins in Northern Chile (24.5°-26°S). XIV Congreso Geológico Chileno, La Serena, Chile.

Escayola, M.P., Pimentel, M.M., Armstrong, R., 2007. Neoproterozoic backarc basin: Sensitive high-resolution ion microprobe U-Pb and Sm-Nd isotopic evidence from the Eastern Pampean Ranges, Argentina. Geology 35, 495–498. https://doi.org/10.1130/G23549A.1.

Espinoza, M., Montecino, D., Oliveros, V., Astudillo, N., Vásquez, P., Reyes, R., Celis, C., González, R., Contreras, J., Creixell, C., Martínez, A., 2019. The synrift phase of the early Domeyko Basin (Triassic, northern Chile): sedimentary, volcanic and tectonic interplay in the evolution of an ancient subduction-related rift basin. Basin Research 31, 4–32. https://doi.org/10.1111/bre.12305.

Farner, M.J., Lee, C.-T.A., 2017. Effects of crustal thickness on magmatic differentiation in subduction zone volcanism: a global study. Earth and Planetary Science Letters 470, 96–107. https://doi.org/10.1016/j.epsl.2017.04.025.

Fosdick, J.C., Carrapa, B., Ortíz, G., 2015. Faulting and erosion in the Argentine Precordillera during changes in subduction regime: reconciling bedrock cooling and detrital records. Earth and Planetary Science Letters 432, 73–83. https://doi.org/10.1016/j.epsl.2015.09.041.

Fuentes, P., Fernández, C., Díaz-Alvarado, J., Díaz-Azpiroz, M., 2019. Using 3D kinematic models in subduction channels. The case of the Chañaral tectonic mélange, Coastal Cordillera, northern Chile. Gondwana Research 74, 251–270. https://doi.org/10.1016/j.gr.2018.12.009.

Giambiagi, L., Martinez, A.N., 2008. Permo-Triassic oblique extension in thePotrerillos-Uspallata area, western Argentina. Journal of South American Earth Sciences 26, 252–260. https://doi.org/10.1016/j.jsames.2008.08.008.

Giambiagi, L., Mescua, J., Bechis, F., Martinez, a., Folguera, a., 2011. Pre-Andean deformation of the Precordillera southern sector, southern Central Andes. Geosphere 7, 219–239. https://doi.org/10.1130/GES00572.1.

González, J., Oliveros, V., Creixell, C., Velásquez, R., Vásquez, P., Lucassen, F., 2018. The Triassic magmatism and its relation with the Pre-Andean tectonic evolution: Geochemical and petrographic constrains from the High Andes of north Central Chile (29°30′ - 30°S). Journal of South American Earth Sciences 87, 95–112. https://doi.org/10.1016/j.jsames.2017.12.009.

Grocott, J., Taylor, G.K., 2002. Magmatic arc fault systems, deformation partitioning and emplacement of granitic complexes in the Coastal Cordillera, north Chilean Andes (25°30'S to 27°00'S). Journal of the Geological Society of London 159, 425–442. https://doi.org/10.1144/0016-764901-124.

Grocott, J., Arévalo, C., Welkner, D., Cruden, A., Sciences, E., Kt, K., Valley, M., Limited, E., Street, W.G., Survey, G., Mar, S., Nacional, S., Street, R., Arevalo, C., 2009. Fault-assisted vertical pluton growth: Coastal Cordillera, north Chilean Andes. Journal of the Geological Society of London 166, 295–301. https://doi.org/10.1144/0016-76492007-165.

Gutiérrez-Alonso, G., Murphy, J.B., Fernández-Suárez, J., Weil, A.B., Franco, M.P., Gonzalo, J.C., 2011. Lithospheric delamination in the core of Pangea: Sm-Nd insights from the Iberian mantle. Geology 39, 155–158. https://doi.org/10.1130/G31468.1.

Hervé, F., Fanning, C.M., Calderón, M., Mpodozis, C., 2014. Early Permian to late Triassic batholiths of the Chilean Frontal Cordillera (28°-31°S): SHRIMP U-Pb zircon ages and Lu-Hf and O isotope systematics. Lithos 184–187, 436–446. https://doi.org/10.1016/j.lithos.2013.10.018.

Hildebrand, R.S., Whalen, J.B., Bowring, S.A., 2018. Resolving the crustal composition paradox by 3.8 billion years of slab failure magmatism and collisional recycling of continental crust. Tectonophysics 734, 69–88.

Howell, J.A., Schwarz, E., Spalletti, L.A., Veiga, G.D., 2005. The Neuquén Basin: an overview. Geol. Soc. London. Spec. Publ. 252, 1–14. https://doi.org/10.1144/GSL.SP.2005.252.01.01.

Irvine, T.N., Baragar, W.R., 1971. A Guide to the Chemical Classification of the Common Volcanic Rocks. Can. Journal of Earth Science 8, 523–548. https://doi.org/10.1139/e71-055.

Kay, R.W., Kay, S.M., 1993. Delamination and delamination magmatism. Tectonophysics 219, 177–189. https://doi.org/10.1016/0040-1951(93)90295-U.

Kay, S.M., Mpodozis, C., 2001. Central Andean Ore deposits linked to evolving shallow subduction systems and thickening crust. GSA Today 11, 4–9. https://doi.org/10.1017/CBO9781107415324.004.

Kay, S.M., Ramos, V.A., Mpodozis, C., Sruoga, P., 1989. Late Paleozoic to Jurassic silicic magmatism at the Gondwana margin: analogy to the Middle Proterozoic in North America? Geology. https://doi.org/10.1130/0091-7613(1989)017<0324:LPTJSM>2.3.CO;2.

Kleiman, L.E., Japas, M.S., 2009. The Choiyoi volcanic province at 34°S-36°S (San Rafael, Mendoza, Argentina): Implications for the late Palaeozoic evolution of the southwestern margin of Gondwana. Tectonophysics 473, 283–299. https://doi.org/10.1016/j.tecto.2009.02.046.

Kramer, W., Siebel, W., Romer, R.L., Haase, G., Zimmer, M., Ehrlichmann, R., 2005. Geochemical and isotopic characteristics and evolution of the Jurassic volcanic arc between Arica (18 30′ S) and Tocopilla (22 S), North Chilean Coastal Cordillera. Chemie der Erde-Geochemistry 65 (1), 47–78.

Kusky, T.M., Windley, B.F., Wang, L., Wang, Z., Li, X., Zhu, P., 2014. Flat slab subduction, trench suction, and craton destruction: Comparison of the North China, Wyoming, and Brazilian cratons. Tectonophysics 630, 208–221. https://doi.org/10.1016/j.tecto.2014.05.028.

Llambías, E.J., Sato, A.M., 1995. El batolito Colanguil transicion entre orogenesis y anorogenesis 50, 111–131.

Llambías, E.J., Quenardelle, S., Montenegro, T., 2003. The Choiyoi Group from Central Argentina: a subalkaline transitionalto alkaline association in the craton adjacent to the active marginof the Gondwana continent. Journal of South American Earth Sciences 16, 243–257. https://doi.org/10.1016/S0895-9811(03)00070-1.

Llambías, E.J., Kleiman, L.E., Salvarredi, J.A., 1993. El Magmatismo Gondwanico. Ramos, V.A., (Ed.), Geol. y Recur. Nat. Mendoza, Relat. XII Congr. Geológico Argentino y II Congr. Explor. Hidrocarburos. 1, 53–64.

Lossada, A.C., Giambiagi, L., Hoke, G.D., Fitzgerald, P.G., Creixell, C., Murillo, I., Mardonez, D., Velásquez, R., Suriano, J., 2017. Thermochronologic evidence for late Eocene Andean Mountain Building at 30°S. Tectonics 36, 2693–2713. https://doi.org/10.1002/2017TC004674.

Lucassen, F., Franz, G., 1994. Arc related Jurassic igneous and meta-igneous rocks in the Coastal Cordillera of northern Chile/Region Antofagasta. Lithos 32, 273–298. https://doi.org/10.1016/0024-4937(94)90044-2.

Lucassen, F., Franz, G., Thirlwall, M.F., Mezger, K., 1999. Crustal Recycling of Metamorphic Basement: late Palaeozoic Granitoids of Northern Chile (22 S). Implications for the Composition of the Andean Crust. Journal of Petrology 40, 1527–1551. https://doi.org/10.1093/petroj/40.10.1527.

Lucassen, F., Kramer, W., Bartsch, V., Wilke, H.G., Franz, G., Romer, R.L., Dulski, P., 2006. Nd, Pb, and Sr isotope composition of juvenile magmatism in the Mesozoic large magmatic province of northern Chile (18-27??S): Indications for a uniform subarc mantle. Contributions to Mineralogy and Petrology 152, 571–589. https://doi.org/10.1007/s00410-006-0119-y.

Maksaev, V., Munizaga, F., Tassinari, C., 2014. Temporalidad del magmatismo del borde paleo-Pacífico de Gondwana: Geocronología U-Pb de rocas ígneas del Paleozoico tardío a Mesozoico temprano de los Andes del norte de Chile entre los 20° y 31°S. Andean Geology 41, 447–506. https://doi.org/10.5027/andgeoV41n3-a01.

Mamani, M., Wörner, G., Sempere, T., 2010. Geochemical variations in igneous rocks of the Central Andean orocline (13°S to 18°S): Tracing crustal thickening and magma generation through time and space. Bulletin Geological Society of America 122, 162–182. https://doi.org/10.1130/B26538.1.

Martin, M.W., Kato, T.T., Rodriguez, C., Godoy, E., Duhart, P., McDonough, M., Campos, A., 1999. Evolution of the late Paleozoic accretionary complex and overlying forearc-magmatic arc, south Central Chile (38°–41°S): Constraints for the tectonic setting along the southwestern margin of Gondwana. Tectonics 18, 582. https://doi.org/10.1029/1999TC900021.

Martina, F., Viramonte, J.M., Astini, R.A., Pimentel, M.M., Dantas, E., 2011. Mississippian volcanism in the south-Central Andes: New U-Pb SHRIMP zircon geochronology and whole-rock geochemistry. Gondwana Research 19, 524–534. https://doi.org/10.1016/j.gr.2010.07.004.

Martínez, A.N., 2004. Secuencias volcánicas permo-triásicas de los cordones del Portillo y del Plata, Cordillera Frontal, Mendoza: su interpretación tectónica. Universida de Buenos Aires.

Martínez, F., Peña, M., Arriagada, C., 2015. Geología de las áreas Iglesia Colorada - Cerro del Potro y Cerro Mondaquita, Región de Atacama. Servicio Nacional de Geología y Minería, Carta Geológica de Chile, Serie Geología Básica 179–180. Minería, Santiago, Servicio Nacional de Geología y.

Matthews, K.J., Maloney, K.T., Zahirovic, S., Williams, S.E., Seton, M., Mueller, R.D., 2016. Global plate boundary evolution and kinematics since the late Paleozoic. Global and Planetary Change 146, 226–250.

Mišković, A., Schaltegger, U., 2009. Crustal growth along a non-collisional cratonic margin: a Lu-Hf isotopic survey of the Eastern Cordilleran granitoids of Peru. Earth and Planetary Science Letters 279, 303–315. https://doi.org/10.1016/j.epsl.2009.01.002.

Mpodozis, C., Cornejo, P., 1988. Hoja Pisco Elqui. IV Región de Coquimbo., Servicio Nacional de Geología y Minería. Carta Geológica de Chile 68. map scale 1:250.000.

Mpodozis, C., Kay, S.M., 1990. Provincias magmáticas ácidas y evolución tectónica de Gondwana: Andes Chilenos (28-31oS). Rev. Geológica Chile 17, 153–180.

Mpodozis, C., Kay, S.M., 1992. Late Paleozoic to Triassic evolution of the Gondwana margin: evidence from Chilean Frontal Cordilleran batholiths (28°S to 31°S). Geological Society of America Bulletin 104, 999–1014. https://doi.org/10.1130/0016-7606(1992)104<0999:LPTTEO>2.3.CO;2.

Mpodozis, C., Ramos, V.A., 1989. The Andes of Chile and Argentina. Geology of the Andes and its Relation to Hydrocarbon and Mineral Resources 11, 59–90.

Müller, R.D., Seton, M., Zahirovic, S., Williams, S.E., Matthews, K.J., Wright, N.M., Shephard, G.E., Maloney, K.T., Barnett-moore, N., Bower, D.J., Cannon, J., 2016. Ocean basin evolution and global-scale reorganization events since Pangea breakup. Annu. Rev. Earth Planet. Sci. Lett., 107–138 https://doi.org/10.1146/annurev-earth-060115-012211.

Murillo, I., Velásquez, R., Creixell, C., 2017. Geología de la Áreas Guanta - Los Cuartitos y Paso de Vacas Heladas, Regiones de Atacama y Coquimbo. Servicio Nacional de Geología y Minería, Carta Geológica de Chile, Serie Geología Básica 192–193.

Nasi, C., Moscoso, R., Maksaev, V.J., 1990. Hoja Guanta, Región de Coquimbo. Servicio Nacional de Geología y Minería, Carta Geológica de Chile, Serie Geología Básica 67.

Oliveros, V., Féraud, G., Aguirre, L., Fornari, M., Morata, D., 2006. The early Andean Magmatic Province (EAMP): 40Ar/39Ar dating on Mesozoic volcanic and plutonic rocks from the Coastal Cordillera, northern Chile. Journal of Volcanology and Geothermal Research 157, 311–330.

Oliveros, V., Morata, D., Aguire, L., Féraud, G., Fornari, M., 2007. Jurassic to early cretaceous subduction-related magmatism in the Coastal Cordillera of northern Chile (18°30–24°S): Geochemistry and petrogenesis. Revista Geologica de Chile 34.

Oliveros, V., Labbé, M., Rossel, P., Charrier, R., Encinas, A., 2012. Late Jurassic paleogeographic evolution of the Andean back-arc basin: New constrains from the Lagunillas Formation, northern Chile (27°30′–28°30'S). Journal of South American Earth Sciences 37, 25–40.

Oliveros, V., González, J., Espinoza, M., Vásquez, P., Rossel, P., Creixell, C., Sepúlveda, F., Bastías, F., 2018. The early stages of the volcanic arc in the Southern Central Andes. In: Folguera, A., Contreras-Reyes, E., Heredia, N., Encinas, A., Iannelli, S., Oliveros, V., Dávila, F.M., Collo, G., Giambiagi, L.B., Maksymowicz, A., Iglesia Llanos, M.P., Turienzo, M.M., Naipauer, M., Orts, D., Litvak, V.D., Alvarez, O., Arriagada, C. (Eds.), The Evolution of the Chilean-Argentinean Andes. Springer International Publishing, Berlin Heidelberg, pp. 185–212. https://doi.org/10.1007/978-3-319-67774-3.

Ortiz, M., Merino, R.N., 2015. Geología de las áreas Río-Chollay y Matancillas y Cajón del Encierro, Regiones de Atacama y Coquimbo. Servicio Nacional de Geología y Minería, Carta Geológica de Cile, Serie Geología Básica 175–176.

Otamendi, J.E., Ducea, M.N., Tibaldi, A.M., Bergantz, G.W., de la Rosa, J.D., Vujovich, G.I., 2009. Generation of tonalitic and dioritic magmas by coupled partial melting of gabbroic and metasedimentary rocks within the deep crust of the Famatinian magmatic arc, Argentina. Journal of Petrology 50 (5), 841–873.

Otamendi, J.E., Pinotti, L.P., Basei, M.A.S., Tibaldi, A.M., 2010. Evaluation of petrogenetic models for intermediate and silicic plutonic rocks from the Sierra de Valle Fértil-La Huerta, Argentina: Petrologic constraints on the origin of igneous rocks in the Ordovician Famatinian-Puna paleoarc. Journal of South American Earth Sciences 30, 29–45. https://doi.org/10.1016/j.jsames.2010.07.004.

Pankhurst, R., Millar, I., Hervé, F., 1996. A Permo-Carboniferous U-Pb age for part of the Guanta Unit of the Elqui-Limari Batholith at Rio del Transito, Northern Chile. Rev. Geol. Chile 23. 35–42 ST–A Permo–Carboniferous U–Pb Age for Par.

Parada, M.A., 1988. Pre-Andean peraluminous and metaluminous leucogranitoid suites in the High Andes of Central Chile. Journal of South American Earth Sciences 1, 211–221. https://doi.org/10.1016/0895-9811(88)90039-9.

Parada, M.A., Nyström, J.O., Levi, B., 1999. Multiple sources for the Coastal Batholith of Central Chile (31-34°S): Geochemical and Sr-Nd isotopic evidence and tectonic implications. Lithos 46, 505–521. https://doi.org/10.1016/S0024-4937(98)00080-2.

Pearce, J.A., 1982. Trace element characteristics of lavas from destructive plate boundaries. In: Thorps, R.S. (Ed.), Andesites. John Wiley and Sons, New York, pp. 525–548.

Pearce, J.A., 1996. Pearce_1996_A Users Guide to Basalt Discrimination Diagrams.pdf.

Peña, M., Becerra, J., Martínez, F., Arriagada, C., 2013. Geología del Área Yerbas Buenas-Tres Morros, Región de Atacama. Servicio Nacional de Geología y Minería, Carta Geológica de Chile, Serie Geología Básica 155. Minería, Santiago, Servicio Nacional de Geología y.

Pichowiak, S., Buchelt, M., Damm, K.W., 1990. Magmatic activity and tectonic setting of the early stages of the Andean cycle in northern Chile. Plutonism from Antarctica to Alaska. Geological Society of America Special Publication 241, 127–144.

Prinz, P., Wilke, H.G., von Hillebrandt, A., 1994. Sediment accumulation and subsidence history in the Mesozoic marginal basin of northern Chile. Tectonics South. Cent. Andes Struct. Evol. an Act. Cont. Margin 219–232.

Profeta, L., Ducea, M.N., Chapman, J.B., Paterson, S.R., Gonzales, S.M.H., Kirsch, M., Petrescu, L., DeCelles, P.G., 2015. Quantifying crustal thickness over time in magmatic arcs. Scientific Reports 5, 17786. https://doi.org/10.1038/srep17786.

Ramos, V.A., 1994. Terranes of Southern Gondwanaland and their Control in the Andean Structure (30°-33° S Latitude). Tectonics South. Cent. Andes, 249–261 https://doi.org/10.1007/978-3-642-77353-2_18.

Ramos, V.A., Folguera, A., 2009. Andean flat-slab subduction through time. Geological Society of London, Special Publication 327, 31–54.

Ramos, V.A., Kay, S.M., 1991. Triassic rifting and associated basalts in the Cuyo basin, central Argentina. Andean Magmat. Its Tecton. Setting 79–92. https://doi.org/10.1130/SPE265-p79.

Rapalini, A.E., Astini, R.A., 2005. La remagnetización sanrafaélica de la Precordillera en el Pérmico: nuevas evidencias. Rev. Asoc. Geol. Argen. 60, 290–300.

Rapela, C.W., Llambías, E.J., 1985. Evolución magmática y relaciones regionales de los complejos eruptivos de La Esperanza, provincia de Río Negro. Revista de la Asociación Geológica Argentina 40, 4–25.

Rebolledo, S., Charrier, R., 1994. Evolución del basamento paleozoico en el área de Punta Claditas, Región de Coquimbo, Chile (31-32°S). Revista Geologica de Chile 21, 55–69. https://doi.org/10.5027/andgeoV21n1-a03.

del Rey, A., Deckart, K., Arriagada, C., Martínez, F., 2016. Resolving the paradigm of the late Paleozoic-Triassic Chilean magmatism: Isotopic approach. Gondwana Research 37, 172–181. https://doi.org/10.1016/j.gr.2016.06.008.

del Rey, A., Deckart, K., Planavsky, N., Arriagada, C., Martínez, F., 2019. Tectonic evolution of the southwestern margin of Pangea and its global implications: evidence from the mid Permian–Triassic magmatism along the Chilean-argentine border. Gondwana Research 76, 303–321. https://doi.org/10.1016/j.gr.2019.05.007.

Ribba, L., Mpodozis, C., Hervé, F., Nasi, C., Moscoso, R., 1988. El Basamento del Valle del Tránsito, Cordillera de Vallenar: Eventos magmáticos y metamórficos y su relación con la evolución de los Andes Chileno-Argentinos. Rev. Geológica Chile 15, 129–149. https://doi.org/10.5027/andgeoV15n2-a03.

Riel, N., Jaillard, E., Martelat, J., Braun, J., 2018. Journal of South American Earth Sciences Permian-Triassic Tethyan realm reorganization : Implications for the outward Pangea. margin 81, 78–86. https://doi.org/10.1016/j.jsames.2017.11.007.

Rocher, S., Vallecillo, G., Castro, B., Machuca, D., Alasino, P., 2015. El Grupo Choiyoi (Pérmico temprano-medio) en la Cordillera Frontal de Calingasta, San Juan, Argentina: volcanismo de arco asociado a extensión 32. pp. 415–432.

Rossel, P., Oliveros, V., Ducea, M.N., Charrier, R., Scaillet, S., Retamal, L., Figueroa, O., 2013. The Early Andean subduction system as an analog to island arcs: evidence from across-arc geochemical variations in northern Chile. Lithos 179, 211–230.

Rossel, P., Oliveros, V., Ducea, M.N., Hernandez, L., 2015. Across and along arc geochemical variations in altered volcanic rocks: evidence from mineral chemistry of Jurassic lavas in northern Chile, and tectonic implications. Lithos 239. https://doi.org/10.1016/j.lithos.2015.10.002.

Ruiz, C., Aguirre, L., Corvalán, J., Klohn, C., Klohn, E., Levi, B., 1965. Geología y yacimientos metalíferos de Chile. Instituto de Investigaciones Geológicas, Chile, p. 305.

Salazar, E., Coloma, F., 2016. Geología del área Cerros de Cantaritos-Laguna Chica, Región de Atacama. Servicio Nacional de Geología y Minería. Carta Geológica de Chile, Serie Geología Básica, p. 181. https://doi.org/10.13140/RG.2.2.30000.56327.

Salazar, E., Coloma, F., Creixell, C., 2013. Geología del Área El Tránsito-Lagunillas, Servicio Nacional de Geología y Minería-Gobierno Regional de Atacama. 1 Mapa escala 1: 100.000. Santiago 1–113.

Salazar, E., Vásquez, P., Vallejos, D., Creixell, C., Oliveros, V., Ducea, M.N., 2019. Stratigraphic and provenance analysis of Triassic units between 28-29°S, northern Chile: implications on the tectonic and paleogeographic evolution of the southwestern margin of Gondwana. Andean Geology (in press).

Sato, A.M., Llambias, E.J., Basei, M.A.S., Castro, C.E., 2015. Three stages in the Late Paleozoic to Triassic magmatism of southwestern Gondwana, and the relationships with the volcanogenic events in coeval basins. Journal of South American Earth Sciences 63, 48–69. https://doi.org/10.1016/j.jsames.2015.07.005.

Scheuber, E., Gonzalez, G., 1999. Tectonics of the Jurassic-Early Cretaceous magmatic arc of the north Chilean Coastal Cordillera (22°–26° S): A story of crustal deformation along a convergent plate boundary. Tectonics 18 (5), 895–910.

Scheuber, E., Bogdanic, T., Jensen, a., Reutter, K., 1994. Tectonic development of the north Chilean Andes in relation to plate convergence and magmatism since the Jurassic. Tectonics South. Cent. Andes, 121–139 https://doi.org/10.1007/978-3-642-77353-2_9.

Shand, S., 1943. Eruptive Rocks: Their Genesis, Composition, and Classification, with a Chapter on Meteorites. John Wiley Sons, Inc [444 p].

Sommer, C.A., Barreto, C.J.S., Lafon, J.M., Fernandes de Lima, E., Alexandre, F.M., Chemale Jr., F., Koester, E., 2018. Pb isotope geochemistry and reappraisal of Sr-Nd isotopes of the Cerro Morado basic magmatism (Ischigualasto-Villa Union Triassic basin, NW Argentina): implications for the mantle sources. Braz. J. Geol. 48, 115–126.

Spalletti, L.A., Limarino, C.O., 2017. The choiyoi magmatism in south western gondwana: implications for the end-permian mass extinction - a review. Andean Geology 44, 328–338. https://doi.org/10.5027/andgeoV44n3-a05.

Spencer, C.J., Roberts, N.M.W., Santosh, M., 2017. Growth, destruction, and preservation of Earth's continental crust. Earth-Science Reviews 172, 87–106. https://doi.org/10.1016/j.earscirev.2017.07.013.

Spikings, R., Reitsma, M.J., Boekhout, F., Miskovic, A., Ulianov, A., Chiaradia, M., Gerdes, A., Schaltegger, U., 2016. Characterisation of Triassic rifting in Peru and implications for the early disassembly of western Pangaea. Gondwana Research 35, 124–143. https://doi.org/10.1016/j.gr.2016.02.008.

Stern, C.R., 2004. Active Andean volcanism, its geologic and tectonic setting.pdf. Revista Geologica de Chile 31, 161–206.

Stern, R.J., Reagan, M., Ishizuka, O., Ohara, Y., Whattam, S., 2012. To understand subduction initiation, study forearc crust: to understand forearc crust, study ophiolites. Lithosphere 4, 469–483. https://doi.org/10.1130/L183.1.

Suarez, M., Bell, C.M., 1992. Triassic rift-related sedimentary basins in northern Chile (24°-29°S). Journal of South American Earth Sciences 6, 109–121. https://doi.org/10.1016/0895-9811(92)90001-F.

Sun, S., McDonough, W.F., 1989. Chemical and isotopic systematics of oceanic basalts: implications for mantle composition and processes. Geological Society of London, Special Publication 42, 313–345. https://doi.org/10.1144/GSL.SP.1989.042.01.19.

Thiele, R., Hervé, F., 1984. Tectonica de ante arco en los terrenos preandinos del norte chico, Chile. Revista Geologica de Chile, 61–75 https://doi.org/10.5027/andgeoV11n2-a06.

Tomezzoli, R.N., 2009. The Apparent Polar Wander Path for South America during the Permian-Triassic. Gondwana Research 15, 209–215. https://doi.org/10.1016/j.gr.2008.10.005.

Tomlinson, A.J., Blanco, N., García, M., Baeza, L., Alcota, H., Ladino, M., Pérez de Arce, C., Fanning, C.M., Martin, M.W., 2012. Permian exhumation of metamorphic complexes in the Calama area: evidence for flat-slab subduction in northern Chile during the San Rafael tectonic phase and origin of the Central Andean Gravity High. XIII Congreso Geologico Chileno, Antofagasta, Abstracts 1, 209–211.

Tomlison, A.J., Cornejo, P., Mpodozis, C., 1999. Hoja Potrerillos, Región de Atacama. Servicio Nacional de Geología y Minería, Mapas Geológicos 14.

Torsvik, T.H., Cocks, L.R.M., 2013. Gondwana from top to base in space and time. Gondwana Research 24, 999–1030. https://doi.org/10.1016/j.gr.2013.06.012.

Vásquez, P., Glodny, J., Franz, G., Romer, R.L., Gerdes, A., 2009. Origin of fayalite granitoids: new insights from the Cobquecura Pluton, Chile, and its metapelitic xenoliths. Lithos 110, 181–198. https://doi.org/10.1016/j.lithos.2009.01.001.

Vásquez, P., Glodny, J., Franz, G., Frei, D., Romer, R.L., 2011. Early Mesozoic plutonism of the Cordillera de la Costa (34°–37°S), Chile: constraints on the onset of the Andean Orogeny. Journal of Geology 119, 159–184. https://doi.org/10.1086/658296.

Walker, B.A., Bergantz, G.W., Otamendi, J.E., Ducea, M.N., Cristofolini, E.A., 2015. A MASH zone revealed: the mafic complex of the Sierra Valle Fértil. Journal of Petrology 56, 1863–1896. https://doi.org/10.1093/petrology/egv057.

Huangfu, P., Wang, Y., Cawood, P.A., Li, Z.-H., Fan, W., Gerya, T.V., 2016. Thermomechanical controls of flat subduction: Insights from numerical modeling. Gondwana Research 40, 170–183. https://doi.org/10.1016/j.gr.2016.08.012.

Vicente, J-C., 1975. El Jurásico marino de la Alta Cordillera de San Juan y Mendoza (31°30' a 33° Sur): Cambios de facies y paleogeografía. 6° Congreso Geológico Argentino (Bahía Blanca). Actas 1, 21–22.

Welkner, D., Arévalo, C., Godoy, E., 2006. Geología de la Carta Freirina-El Morado, Región de Atacama. Servicio Nacional de Geología y Minería, Carta Geológica de Chile, Serie Geología Básica 100.

Whattam, S.A., Stern, R.J., 2011. The 'subduction-initiation rule': a key for linking ophiolites, intra-oceanic forearcs and subduction initiation: Contrib. to. Mineralogy and Petrology 162 (5), 1031–1045. https://doi.org/10.1007/s00410-011-0638-z.

White, W., 2015. Isotope Geochemistry. John Wiley & Sons (478 p).

Willner, A.P., Gerdes, A., Massonne, H.J., 2008. History of crustal growth and recycling at the Pacific convergent margin of South America at latitudes 29°-36° S revealed by a U-Pb and Lu-Hf isotope study of detrital zircon from late Paleozoic accretionary systems. Chemical Geology 253, 114–129. https://doi.org/10.1016/j.chemgeo.2008.04.016.

Winchester, J.A., Floyd, P.A., 1977. Geochemical discrimination of different magma series and their differentiation products using immobile elements. Chemical Geology 20, 325–343. https://doi.org/10.1016/0009-2541(77)90057-2.

Wood, D.A., 1980. The application of a Th-Hf-Ta diagram to problems of tectonomagmatic classification and to establishing the nature of crustal contamination of basaltic lavas of the British Tertiary Volcanic Province. Earth and Planetary Science Letters 50, 11–30. https://doi.org/10.1016/0012-821X(80)90116-8.

Young, A., Flament, N., Maloney, K., Williams, S., Matthews, K., Zahirovi, K., Müller, R.D., 2019. Global kinematics of tectonic plates and subduction zones since the late Paleozoic Era. Geoscience Frontiers https://doi.org/10.1016/j.gsf.2018.05.011 (In press).

Zandt, G., Gilbert, H., Owens, T.J., Ducea, M., Saleeby, J., Jones, C.H., 2004. Active foundering of a continental arc root beneath the southern Sierra Nevada in California. Nature 431, 41–46. https://doi.org/10.1038/nature02847.

Zhang, S.H., Zhao, Y., Davis, G.A., Ye, H., Wu, F., 2014. Temporal and spatial variations of Mesozoic magmatism and deformation in the North China Craton: implications for lithospheric thinning and decratonization. Earth Science Reviews 131, 49–87. https://doi.org/10.1016/j.earscirev.2013.12.004.
Zindler, A., Hart, S., 1986. Chemical geodynamics. Annual Review of Earth and Planetary Sciences 14, 493–571.

Verónica Oliveros is Associate Professor at the Earth Sciences Department of the University of Concepción, Chile. She received a doctorate from the University of Chile and University of Nice-Sophia Antipolis, and after a short stage as post-doc at the University of Chile she joint her current institution, where she helped to establish the doctoral program on Geological Sciences. Her research focuses on the Paleozoic and Mesozoic evolution of the Andes and SW South American margin, integrating field geology, petrology and isotope geochemistry. She also works with evolution of the continental crust, planetary formation and isotopic tools for evaluating the impact of native forests on water quality.

Paulina Vásquez obtained her doctoral degree from the Technische Universität Berlin. Her thesis discusses the petrology of Triassic plutons in South Central Chile and its implications on the Mesozoic evolution of the Andes. Since then she has worked at the Regional Geology Section of the National Geology and Mining Service (SERNAGEOMIN) where she has contributed to the updating of the geological maps in northernmost Chile. Her research focuses on petrology, structural geology and geochemistry of the geological record in the fore arc region, covering topics such as Paleozoic evolution of the SW Gondwana margin, Early Andean magmatism, Neogene evolution of the Atacama Desert, among others.

Christian Creixell graduated in geology at the University of Concepción in 2001, and obtained a PhD in Sciences at the University of Chile in 2007, studying the structural geology, paleomagnetism and composition of mafic dike swarms of central Chile. From 2008 to present, he has developed his career in regional geology at the National Geology and Mining Service (SERNAGEOMIN), where currently is in charge of the Regional Geology Section. Most of his research since 2008 has been focused in the tectonic evolution of Paleozoic to Cretaceous basins and magmatic arcs of north Chile

Friedrich Lucassen works as a scientist in the Isotope Geochemistry Group at the University of Bremen, Germany. He received a doctorate in Geology from Technische Universität Berlin in 1992. Since then he worked during numerous 'post-doc' positions on the chemical and isotopic composition of continental lithosphere in the Andes and NE-Africa, but also on experimental petrology.

Mihai N. Ducea is a professor of Geology at the University of Arizona and also holds a courtesy appointment at the University of Bucharest, Romania. He received a BS from the University of Bucharest, followed by a PhD at Caltech. Ducea's research is primarily aimed at understanding links between igneous and metamorphic petrologic processes and the tectonic evolution of continents. He is primarily interested in continental margin processes and conducts fieldwork at various field locations in the western North American Cordillera, the central Andes, the Carpathians, and southern Tibet. He runs a geochemical and radiogenic isotopic laboratory at Arizona.

Isabella Ciocca graduated in geology at the University of Concepción in 2018 and is currently finishing her Master degree in geography at the same institution. She works on wildfires hazard at south-central Chile and glacial geomorphology in the Mountain Geoscience Group, and has collaborated as a lecturer at the University of Concepción (Geography Department) and University of Santísima Concepción (History and Geography Department).

Javiera González obtained her bachelor degree in Geology from the University of Concepción (awarded best undergraduate student of her generation) and is currently finishing her doctoral thesis at the same institution. She works with the Triassic magmatism in the High Andes of north-central Chile, studying the construction of batholiths in active continental margins under extensional regimes. She also works actively in outreach to primary school students.

Mauricio Espinoza graduated in geology at the University of Chile in 2012. He worked for two years in the National Geology and Mining Service (SERNAGEOMIN) focused on the regional geology of northern Chile. He obtained a PhD from the Universidad de Concepción in 2019 studying the evolution of Triassic basins and its relationship with the Cenozoic Andean building in northern Chile. His research has focused on the tectonic and stratigraphy of rift basins, coupling fieldwork basis with U—Pb, and Ar—Ar geochronometers.

Esteban Salazar obtained his geology and Masters degrees at the University of Chile in 2013 studying the Mesozoic tectonostratigraphic evolution on the Chilean-Pampean flat slab segment in the southern Central Andes. Since then he has been working on geological mapping for the National Geology and Mining Service (SERNAGEOMIN) in the same area, also collaborating on specific collaborative studies involving Paleozoic and Mesozoic stratigraphy, facies analysis, structural geology, geomorphology and thermochronology. He also works on stratigraphic and structural geology studies in Tierra del Fuego.

Felipe Coloma graduated in Geology at the University of Chile in 2010. He worked in geotechnics in that year, and later, in 2011, started to work in the National Geology and Mining Service (SERNAGEOMIN), in Regional Geology. He contributed with the geological mapping of the Vallenar mountain range, and actually he is working on the mapping of the coast and Cordillera in the north of Chile. He also worked in geochemistry of mainly intrusive rocks of northern Chile.

Simone A. Kasemann is Professor of Isotope Geochemistry at the University of Bremen (Germany). After her doctorate at TU Berlin, she joined the European Commission's Joint Research Centre in Belgium and worked at the Universities of Bristol and Edinburgh, focussing on developing analytical techniques to investigate processes in both the Earth's interior and surface. Her research expertise is in metal and metalloid stable isotope geochemistry to investigate past records of environmental changes and mass transfer processes at active margins.